Magnus Jervan

Improvement of an Autonomous Passenger Ferry Model Based on Multivariate Residual Modeling

Master's thesis in Cybernetics & Robotics
Supervisor: Morten Breivik & Bjørn-Olav H. Eriksen
June 2020

Master's thesis

NTNU
Norwegian University of
Science and Technology

Magnus Jervan

Improvement of an Autonomous Passenger Ferry Model Based on Multivariate Residual Modeling

Master's thesis in Cybernetics & Robotics
Supervisor: Morten Breivik & Bjørn-Olav H. Eriksen
June 2020

Norwegian University of Science and Technology
Faculty of Information Technology and Electrical Engineering
Department of Engineering Cybernetics

NTNU
Kunnskap for en bedre verden

Abstract

When developing an autonomous ferry intended to operate in confined areas it is important with an accurate and precise control system. The performance of the control system can be increased by utilizing a feedforward controller to give an estimate of the required control input to reach the reference. However, this requires an accurate model of the ferry. To achieve this it is common to derive an initial model based on first principles, however this model usually is not able to explain all of the dynamics. The model errors could be caused by assumptions that simplify the model or unique dynamics for this ferry depending on the size and shape. These model errors causes deviations between the estimates of the model and the true system, and by minimizing these deviations the estimations become more accurate and the ferry model is improved.

In this thesis a multivariate analysis is presented to model the lack-of-fit residual between the initial model and the true system. A partial least squares regression (PLSR) based method is used to derive the multivariate model, with a selection of basis functions as the input. A new method through surface analysis is presented to improve the selection of basis functions, by systematically removing basis functions that contribute the least and determines if this increases the model fit through cross validation. The multivariate model of the residual complements the initial model and is used in parallel with this to give a better representation of the ferry.

The multivariate analysis (MVA) is tested in simulations and on experimental data. In simulations the methods derived a good approximation of the residual, and by implementing this model in the controller the performance was improved significantly. The accuracy of the multivariate method is also evaluated by simulations inflicted by noise and a constant disturbance, where the method still gave good results. Path following of a desired trajectory comparing the performance of the controller with and without the multivariate model implemented, shows the benefit of modeling the residual with multivariate methods. This resulted in more accurate tracking, and especially reducing large deviations from the desired trajectory, in addition to a reduced energy consumption. The lack-of-fit residual from the experimental data was also reduced by using the multivariate method, which gave basis to two proposed models for different purposes. One model is intended for implementation in the controller to give a better approximation of the control input. This model accounts for some of the thruster dynamics in addition to the dynamics of the ferry. The other is proposed for simulation purposes, and only describes the dynamics of the ferry. Hence the multivariate method is able to analyse the lack-of-fit residual from the experimental data of the ferry, and derive an improved model of the ferry.

Sammendrag

Når man utvikler en autonom ferge beregnet til å operere i trange områder, er det viktig med et nøyaktig kontrollsystem. Presisjonen til kontrollsystemet kan forbedres ved å bruke en foroverkobling for å estimere det nødvendige pådraget, men dette krever en nøyaktig model av fergen. Det er vanlig å utlede en initiell model basert på fysiske betraktninger, men disse modellene pleier vanligvis ikke å være i stand til å forklare hele dynamikken. Modellfeilene medfører til et avvik mellom estimatene fra modellen og det virkelige fergesystemet, og ved å minimere disse avvikene vil estimatene bli mer nøyaktige og fergemodellen forbedres.

I denne master oppgaven presenteres det en multivariate analyse med mål om å modellere modellfeilen mellom en initiell model og den faktiske fergen. En metode basert på partiell minste kvadrat regresjon (PLSR) brukes til å finne modellen, med en seleksjon av passende basisfunksjoner som input. En ny metode er presentert som overflate-analyse som brukes til å utbedre seleksjonen av basisfunksjoner, ved å systematisk fjerne basisfunksjonene som bidrar minst til modellen og bruker kryssvalidering for å teste om modellen forbedres. Den multivariate modellen av modellfeilen implementeres med den initielle modellen for å gi en utbedret representasjon av fergedynamikken.

Denne metoden er tested gjennom simuleringer og på eksperimentell data. I simuleringene greide den multivariate analysen å estimere modellfeilen med god nøyaktighet, og ved å implementere denne modellen i kontrolleren ble ytelsen forbedret betraktelig. Presisjonen til den mutlivariate metoden er også evaluert ved simuleringer påført støy og med en konstant forstyrrelse, hvor metoden fortsatt ga gode resultater. Kontrolleren er testet med banefølging av en forutsbestemt rute for å sammenlikne forskjellene med og uten den multivariate modellen implementert. Her kom fordelene av å forbedre modellen tydelig fram ved at kontrolleren fulgte banen mer nøyaktig, samtidig som at energi forbruket minsket. Modellfeilen fra den eskperimentelle dataen ble også forbedret med multivariate metoder. Dette ga grunnlaget for to foreslåtte modeller med forskjellig formål. En model er beregnet for å implementeres i kontrolleren for å få et mer nøyaktig pådrag. I denne modellen er dynamikken til trusterene også inkludert i tillegg til fergen. Den andre modellen er beregnet for simueringsformål, og beskriver kun dynamikken til fergen. Dette viser at multivariate metoder kan benyttes til å analysere modellfeil fra experimentell data til en ferge, og lage en utbedret model av fergen.

Preface

This thesis is written as a part of a M.Sc. degree in Cybernetics and Robotics at the Department of Engineering Cybernetics, Norwegian University of Science and Technology (NTNU). I would like to express a special thanks to my supervisors Morten Breivik and Bjørn-Olav H. Eriksen for guidance and valuable discussions while working on this thesis. Over the course of this thesis, bi-weekly meetings have been held where the progress was followed and various subjects was discussed. I would also like to thank Damiano Varagnolo for insight and help with the theory and implementation of the multivariate methods. I would like to thank my family and friends for the support and motivation throughout the duration of my 5-year long master study.

The thesis is based on previous work done on the autonomous ferry milliAmpere, among others during the specialization project I wrote last semester which focused on online system identification (Jervan, 2019). The same background theory is used in this thesis, but the methods for system identifications are new. The goal of this thesis is to use multivariate methods to improve the model of the ferry. This has been implemented and tested through simulations done with MATLAB R2019a/Simulink and performed on collected data from the experimental vessel. This has given a rapid learning curve about the possibilities of multivariate modeling and analysis, which I am very grateful for.

<div align="center">
Magnus Jervan
June 8, 2020
Trondheim, Norway
</div>

Table of Contents

List of Tables

List of Figures

Abbreviations

Chapter 1

Introduction

1.1 Motivation

Autonomous control is being developed on many platforms, with a rapidly increasing application area. This ranges from autonomous ground vehicles (AGVs) to unmanned surface vehicles (USVs) and unmanned aerial vehicles (UAVs). By utilizing automated vehicles this can give benefits of optimized transportation, free human resources and increasing operational persistence, which results in reduced cost and could give more environmental friendly solutions. Such automated control systems has already been implemented and used in several applications like autonomous container ships and self-driving cars that can operate alongside humans on the road (Yara, 2020). The use of such vehicles could help cities in need of public transportation either for supplementing existing infrastructure or as an on-demand service in remote areas where it would not be cost efficient to have a person deployed.

An autonomous ferry can take advantage of the water ways and could help with the burden on trafficated roads. By being unmanned the operational cost is also reduced. With a fully electrical propulsion system it can serve as an environmental friendly and cost efficient addition to the infrastructure. To operate a ferry in trafficated waters there is not much room for error. An automated ferry therefore needs a precise and efficient controller that can steer the ferry in conditions that involve other human controlled vessels and perturbation from difficult wind and sea conditions. The ferry milliAmpere is a prototype of a planned autonomous ferry operating in Trondheim, and is used as an experimental platform. A model of what the planned autonomous ferry should look like is shown in Figure 1.1, and will be used for transporting passengers and cyclists. When transporting people the safety is the first priority and this requires the controller to keep the ferry at the desired position and follow the trajectory it is supposed to at all times. To improve the accuracy a model based controller is utilized. This requires a model of the ferry that explains the dynamics a good as possible. There are initial models that can be generalized to the ferry considering different physical assumptions, that can give a good estimation

of the ferry model. However there are other factors that will affect the ferry that is not captured by the initial model. The modeling errors between the initial model and the ferry system can be analysed further. By modeling this residual it can give a better estimation of the ferry dynamics and results in a more accurate model. This can contribute to a more precise and effective controller performance. This also enables experiments that are tested in simulations to give a better estimates of how the ferry will react. This could give useful information before the experiment is done on the ferry. The underlying structure of the residual is difficult to know, however by modeling the residual it can improve the ferry model.

Figure 1.1: A model of the planned autonomous ferry. Courtesy of Petter Mustvedt, department of Design, NTNU.

1.2 Previous work

There has already been done a lot of work on the ferry. On the experimental platform, different sensors are implemented like global navigation satellite system (GNSS), inertial measurement unit (IMU) and LiDAR, to get measurements of the movement of the ship and its surroundings. Previously, motion controllers have been implemented on the ferry, and an initial vessel model based on first principals has been derived. The vessel model is the basis for this thesis, and is improved with multivariate methods.

The use of multivariate methods has typically been used in chemometrics, bioinformatics and similar fields, where there are several variables with unknown correlations and structure (Boulesteix and Strimmer, 2006). These methods have seen little application in dynamical systems. These applications extend to identifying parameters in a predefined ship model (Yin et al., 2015) and through residual based modeling to improve a robot manipulator model (Gale et al., 2017). The residual based modeling is based on comparing an initial model with estimated parameters to the real system, and the estimation error leaves a residual. Unknown factors can affect the system is not necessarily accounted for when deriving the initial model. It is shown that these unanticipated effects can give erroneous model parameters, and by using multivariate analysis (MVA) the lack-of-fit residual can be described and corrected for (Martens, 2011).

1.3   Problem description

The objective of this thesis is to improve the initial model of the ferry using MVA. The model is improved by analysing a lack-of-fit residual, between the initial model and data from the real system, with multivariate methods. In simulation the "true" ferry system is altered to create a discrepancy from the "believed" ferry model. There are several combinations of basis functions that can be used in the analysis, so an appropriate selection of the input must be done. The accuracy of the multivariate model is compared to the initial model, and implemented in the controller to test how it affects the performance. The following objectives are to be achieved in this master thesis:

- Design a lack-of-fit residual that captures the discrepancies for the initial model.

- Find appropriate basis functions of the available measurement to be included in the analysis.

- Create a model discrepancy between the "believed" and "true" model in the simulations, and use multivariate methods to derive a model based on the residual.

- Evaluate the fit of the multivariate model, and simulate the effects of implementing it in the controller.

- Collect experimental data from the ferry and develop a multivariate model that improves the initial model based on the data.

1.4   Contributions

The contributions of this master thesis are:

- A lack-of-fit residual is derived capturing the discrepancies of the initial model. The model structure of the residual can be directly implemented with the initial model and correct for the discrepancies.

- A selection of basis functions is found to include in the analysis. These may have an effect on the dynamics of the ferry and are found suitable to use.

- Multivariate methods are used to analyse the simulated residual. Firstly, this is done in a case where there are limited basis functions included in the analysis. Secondly, this is compared to the multivariate model from using the selected basis functions. The performance of the multivariate modeling is also evaluated with noise and a constant disturbance.

- A method called surface analysis is derived to further improve the multivariate model. This is done by systematically removing basis functions to find better suited combinations of the basis functions, resulting in the selected multivariate model to give a better explanation of the residual.

- The derived multivariate model from the simulation results is evaluated and the effect of implementing this model in the controller is tested.

- An analysis is done on the collected experimental data. This derives into two proposed multivariate models, where the effect of utilizing them is evaluated. The first model is intended to be implemented in the controller, to increase the performance, and the second model focuses on giving a more accurate representation of the ferry dynamics for simulation purposes.

1.5 Outline

The master thesis is organized in the following manner. Chapter 2 describes the theoretical background of the initial ferry model and the controller that is used. In Chapter 3, the theory of the multivariate methods are presented. In addition, the lack-of-fit residual is derived and it is shown how the multivariate model can improve the current model. Chapter 4 contains the simulation results, which includes the multivariate analysis of the simulated residual, and the surface analysis. The multivariate methods are also tested with data inflicted by noise and constant disturbances. Chapter 5 presents the experimental results from the collected data, and the proposed model to reduce the residual. Finally, Chapter 6 concludes this thesis and gives suggestions for future work.

Chapter 2

Theoretical background

In this chapter the background theory is presented. This includes the modeling of the ferry and the implemented controllers. The relevant background theory of the vessel model and the controller was carried out in the specialization project preceding this thesis (Jervan, 2019). The presentation from the project report is included below with some added specifications that are relevant in this thesis.

2.1 Vessel modeling

The vessel is described by an initial model that is based on a six degree of freedom (DOF) rigid-body. It is simplified by neglecting heave, roll and pitch, by assuming they are small. This results in a 3 DOF model with the states surge, sway and yaw. The kinematics of the ferry is given by

$$\dot{\boldsymbol{\eta}} = \mathbf{R}(\psi)\boldsymbol{\nu}, \tag{2.1}$$

with the state vectors $\boldsymbol{\eta} = [x, y, \psi]^T \in \mathbb{R}^2 \times S^1$, $\boldsymbol{\nu} = [u, v, r]^T \in \mathbb{R}^3$ and the rotational matrix $\mathbf{R} \in \mathbb{R}^{3\times3}$. The pose vector $\boldsymbol{\eta}$ is represented in the north-east-down (NED) frame, where the x axis points to true north, y axis to the east and z pointing downwards. The NED coordinate system is a tangential plane from where the origin is placed, and does not take the earths curving into account. Since operation of the autonomous ferry is in a local area the affect of the earth curving can be neglected.
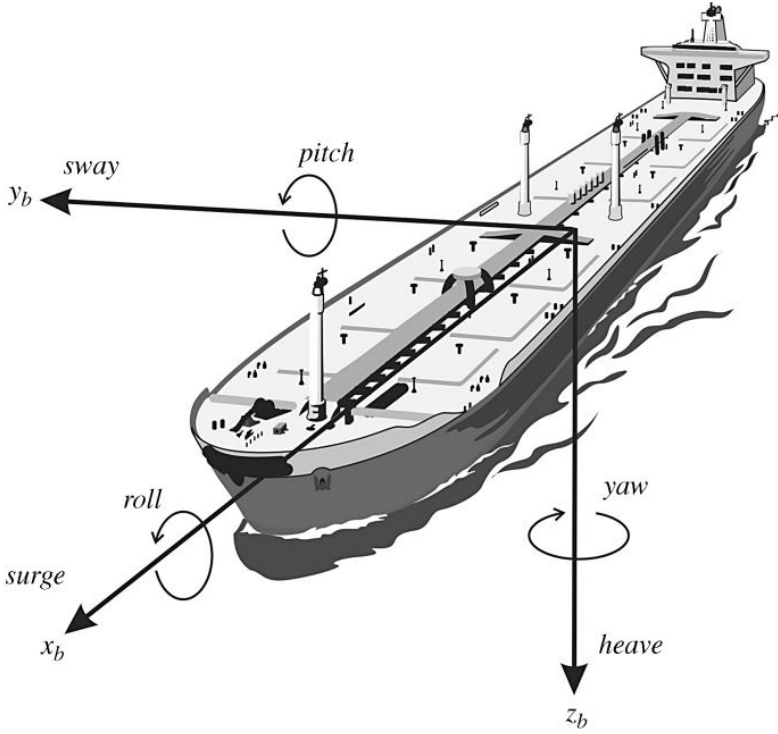
Figure 2.1: Illustration of the coordinate system in the body-fixed reference frame (Fossen, 2011).

The body frame is shown in Figure 2.1, where origin of the coordinate system is fixed to the ferry's position. The direction of the axises are fixed to the ships heading, with the x axis pointing in the longitudinal direction of the vessel, the y axis pointing in the transverse direction of the vessel and the z axis normal on x and y axis and pointing downwards. The rotation matrix rotates the coordinates from body to the NED frame, and is simplified to

$$\mathbf{R}(\psi) = \begin{bmatrix} cos(\psi) & -sin(\psi) & 0 \\ sin(\psi) & cos(\psi) & 0 \\ 0 & 0 & 1 \end{bmatrix} \tag{2.2}$$

The kinetics of the ferry is described in (Fossen, 2011), and is on the form

$$\mathbf{M}\dot{\boldsymbol{\nu}} + \mathbf{C}(\boldsymbol{\nu})\boldsymbol{\nu} + \mathbf{D}(\boldsymbol{\nu})\boldsymbol{\nu} = \boldsymbol{\tau}, \tag{2.3}$$

where $\boldsymbol{\tau} = [\tau_u, \tau_v, \tau_r]^T \in \mathbb{R}^3$ is the force and moment applied surge, sway and yaw. The matrices are given by

$$\mathbf{M} = \begin{bmatrix} m_{11} & m_{12} & m_{13} \\ m_{21} & m_{22} & m_{23} \\ m_{31} & m_{32} & m_{33} \end{bmatrix} \tag{2.4a}$$

$$\mathbf{C}(\boldsymbol{\nu}) = \begin{bmatrix} 0 & 0 & c_{13}(\boldsymbol{\nu}) \\ 0 & 0 & c_{23}(\boldsymbol{\nu}) \\ c_{31}(\boldsymbol{\nu}) & c_{32}(\boldsymbol{\nu}) & 0 \end{bmatrix} \tag{2.4b}$$

$$\mathbf{D}(\boldsymbol{\nu}) = \begin{bmatrix} d_{11}(\boldsymbol{\nu}) & d_{12} & d_{13} \\ d_{21} & d_{22}(\boldsymbol{\nu}) & d_{23}(\boldsymbol{\nu}) \\ d_{31} & d_{32}(\boldsymbol{\nu}) & d_{33}(\boldsymbol{\nu}) \end{bmatrix} \tag{2.4c}$$

where $\mathbf{C}(\boldsymbol{\nu})$ is dependent on the inertia matrix $\mathbf{M}$ as

$$c_{13}(\boldsymbol{\nu}) = -m_{12}u - m_{22}v - m_{23}r \tag{2.5a}$$

$$c_{23}(\boldsymbol{\nu}) = m_{11}u \tag{2.5b}$$

$$c_{31}(\boldsymbol{\nu}) = -c_{13}(\boldsymbol{\nu}) \tag{2.5c}$$

$$c_{32}(\boldsymbol{\nu}) = -c_{23}(\boldsymbol{\nu}) \tag{2.5d}$$

and the elements of $\mathbf{D}(\boldsymbol{\nu})$ are defined as

$$d_{11}(\boldsymbol{\nu}) = -X_u - X_{|u|u}|u| - X_{uuu}u^2 \tag{2.6a}$$

$$d_{12} = -X_v \tag{2.6b}$$

$$d_{13} = -X_r \tag{2.6c}$$

$$d_{21} = -Y_u \tag{2.6d}$$

$$d_{22}(\boldsymbol{\nu}) = -Y_v - Y_{|v|v}|v| - Y_{|r|v}|r| - Y_{vvv}v^2 \tag{2.6e}$$

$$d_{23}(\boldsymbol{\nu}) = -Y_r - Y_{|v|r}|v| - Y_{|r|r}|r| \tag{2.6f}$$

$$d_{31} = -N_u \tag{2.6g}$$

$$d_{32}(\boldsymbol{\nu}) = -N_v - N_{|v|v}|v| - N_{|r|v}|r| \tag{2.6h}$$

$$d_{33}(\boldsymbol{\nu}) = -N_r - N_{|v|r}|v| - N_{|r|r}|r| - N_{rrr}r^2 \tag{2.6i}$$

From (2.6), $\mathbf{D}(\boldsymbol{\nu})$ can be divided into a linear and nonlinear part, $\mathbf{D}(\boldsymbol{\nu}) = \mathbf{D}_L + \mathbf{D}_{NL}(\boldsymbol{\nu})$. In (Pedersen, 2019), the parameters of the initial model, shown in appendix A, was identified by an optimal control problem (OCP) formulated on the form

$$\min_{\mathbf{P}, \boldsymbol{x}} \quad \int_0^t \mathbf{L}(\boldsymbol{x}(t), \bar{\boldsymbol{x}}(t), \mathbf{P}) dt \tag{2.7a}$$

$$\text{s.t} \quad \dot{\boldsymbol{x}}(t) = \mathbf{f}(\boldsymbol{x}(t), \bar{\boldsymbol{u}}(t), \mathbf{P}) \forall t \in [0, t] \tag{2.7b}$$

$$h(\boldsymbol{x}(t)) \leq \mathbf{0} \forall t \in [0, t]. \tag{2.7c}$$

where the solution to the problem is a set of the parameters in $\mathbf{P}$ that minimizes the objective function. The objective function is a weighted least squares given by

$$\mathbf{L}(\boldsymbol{x}(t), \bar{\boldsymbol{x}}(t), \mathbf{P}) = (\boldsymbol{x}(t) - \bar{\boldsymbol{x}}(t))^T \mathbf{W}(\boldsymbol{x}(t) - \bar{\boldsymbol{x}}(t)), \tag{2.8}$$

where W is a weighting matrix. The solution gives the parameters resulting in the smallest error between the meassurements in $\boldsymbol{x}(t)$ and the estimated output from the model with these parmeters in $\bar{\boldsymbol{x}}(t)$. This has given the initial model based on the physical assumptions and the parameters in $\mathbf{M}, \mathbf{C}$ and $\mathbf{D}$.

2.2   Motion control

The goal with the model of the ferry is for it to be used in a feedforward (FF) controller, in addition to more exact simulations of the ferry. There are different controllers that can utilise the ferry model to improve the control. The proportional-integral-derivative (PID) controller is one of the simpler feedback (FB) controllers, and a FF can be added to predict the necessary control input based on the ferry model. The FB and FF works independent of each other in this controller, so it is easy to remove either part. This makes it possible to remove the FB part and compare how the model in the FF performs compared to the true system of the ferry. This controller will test the accuracy of the models that is given by the system identification.

The FF uses the desired velocity and acceleration to calculate the estimated control input $\boldsymbol{\tau}$ needed for the vessel to follow the reference. The feedforward uses a model of the ferry to estimate $\boldsymbol{\tau}$, so that

$$\boldsymbol{\tau}_{FF} = \mathbf{F}(\dot{\boldsymbol{\nu}}_d, \boldsymbol{\nu}_d), \tag{2.9}$$

where $\boldsymbol{\tau}_{FF} \in \mathbb{R}^3$ is the control input from the FF and $\boldsymbol{F} \in \mathbb{R}^3$ is the function for the ferry model, with $\dot{\boldsymbol{\nu}}_d$ and $\boldsymbol{\nu}_d$ being the desired acceleration and velocity respectively. The feedforward term from the initial model in (2.3) is given by

$$\boldsymbol{F}_0(\dot{\boldsymbol{\nu}}_d, \boldsymbol{\nu}_d) = \mathbf{M}\dot{\boldsymbol{\nu}}_d + \mathbf{C}(\boldsymbol{\nu}_d)\boldsymbol{\nu}_d + \mathbf{D}(\boldsymbol{\nu}_d)\boldsymbol{\nu}_d, \tag{2.10}$$

where the subscript in $\boldsymbol{F}_0$ refers to this being the original model, before any altercations are done to the model.

The FB controller is formulated in the body frame as a PID controller, where the error in the NED frame is rotated to body. This gives the control error

$$\boldsymbol{e} = \boldsymbol{R}^T(\psi)(\boldsymbol{\eta}_d - \boldsymbol{\eta}) \tag{2.11}$$
$$\dot{\boldsymbol{e}} = \boldsymbol{\nu}_d - \boldsymbol{\nu} \tag{2.12}$$

From this the FB controller derives to

$$\boldsymbol{\tau}_{FB} = \mathbf{K}_p\mathbf{e} + \mathbf{K}_i \int_0^t \mathbf{e}(\lambda)d\lambda + \mathbf{K}_d\dot{\mathbf{e}}, \tag{2.13}$$
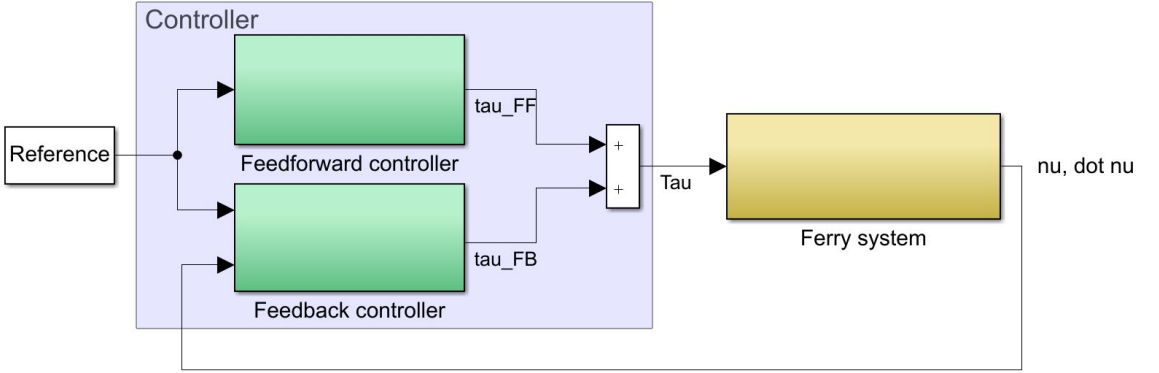
Figure 2.2: Block diagram of the setup between FB and the FF controller.

where $\mathbf{K}_p, \mathbf{K}_i, \mathbf{K}_d > 0 \in \mathbb{R}^{3 \times 3}$. The resulting control input is given from combining the FB and the FF controller to

$$\boldsymbol{\tau} = \boldsymbol{\tau}_{FB} + \boldsymbol{\tau}_{FF}. \tag{2.14}$$

A block diagram of the controller and how it interacts with the ferry is shown in Figure 2.2. The FF only utilizes the reference to give $\boldsymbol{\tau}_{FF}$, while $\boldsymbol{\tau}_{FB}$ reads the output of the ferry in a feedback loop to correct for the deviations.

2.2.1 Reference filter

The reference filter receives waypoint with the desired position and heading. A third order reference filter is implemented to ensure smooth an continuous signals for the desired position, velocity and acceleration. If a step on the desired position is given the reference filter gives a feasible signal for the ferry to follow. From the reference $\mathbf{r}$ to the desired position $\boldsymbol{\eta}_d$ the transformation is given in (Fossen, 2011) on the form

$$\boldsymbol{\eta}_d^{(3)} + (2\Delta + \mathbf{I})\Omega\ddot{\boldsymbol{\eta}}_d + (2\Delta + \mathbf{I})\Omega^2\dot{\boldsymbol{\eta}}_d + \Omega^3\boldsymbol{\eta}_d = \Omega^3\mathbf{r}, \tag{2.15}$$

where $\Omega = 0.5$ and represent the bandwidth of the filter, while $\Delta = 0.7$ serves as the damping term.

2.2.2 Line of sight guidance

To navigate through a set of waypoints, a line of sight (LOS) guidance system can be used to give a desired position and heading (Fossen, 2011). This enables path following for the ferry so that it can guide trough a set of waypoints. A LOS with enclosure based steering is used to reach the waypoints. This is done by following a straight line between the previous waypoint to the next. A circle of acceptance is created around the ferry and where it intercepts with the line between the waypoints gives the desired position, shown

in Figure 2.3. The desired heading is found from the angle of the LOS vector. When the next waypoint is within the circle of acceptance it navigates to the next waypoint.

The desired position and heading is given by

$$x_d = x_{los} \tag{2.16a}$$
$$y_d = y_{los} \tag{2.16b}$$
$$\psi_d = \text{atan2}(y_{los} - y(t), x_{los} - x(t)) \tag{2.16c}$$

where y_{los} and x_{los} are found by solving the equation set

$$R^2 = [x_{los} - x(t)]^2 + [y_{los} - y(t)]^2 \tag{2.17}$$
$$tan(\alpha_k) = \frac{y_{k+1} - y_k}{x_{k+1} - x_k} = \frac{y_{los} - y_k}{x_{los} - x_k} \tag{2.18}$$

The solution to these equations are found in (Fossen, 2011)(10.70 and 10.71), with conditions for which solution to the 2nd order equations to use depending on current and next waypoint.
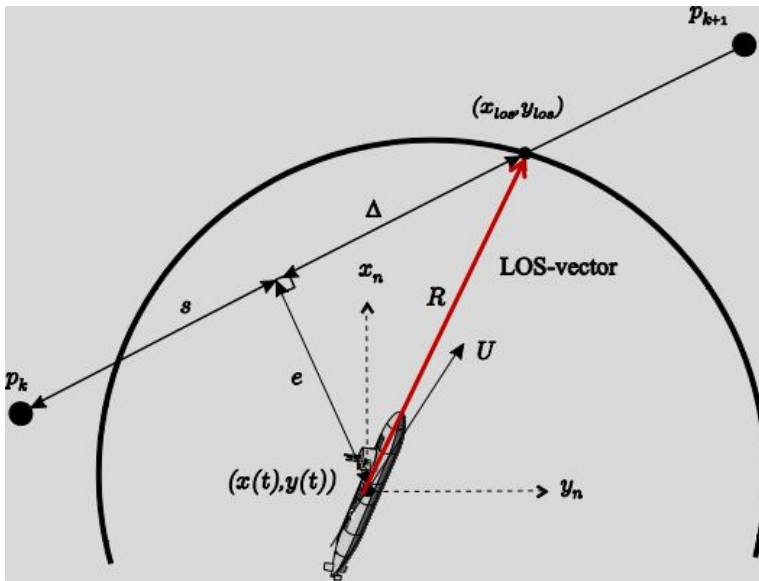
Figure 2.3: LOS vector from intersection between circle of acceptance and waypoint line. Courtesy of (Fossen, 2011).

Chapter 3

Multivariate modeling and analysis

The Multivariate analysis (MVA) is used to identify models and underlying structures. The MVA needs a set of inputs and outputs where it uses techniques to find correlations between the two. The output will be a residual that contains the discrepancies of the model, and by modeling the residual the ferry model is improved. A flowchart showing the process of finding a multivariate model is shown in Figure 3.1. The bigger picture of where the multivariate analysis is used for system identification is shown in Figure 3.2. A mechanistic model, as the initial model of the ferry, is fitted to the data, and the residual from the model is analysed to give an interpretable model with MVA. The uninterpretable residual could be analysed further with black box approaches, but this will not be done in this thesis. Ideally, the residual only contains white noise after being analysed, which means that there is no more information left in the data to extract.
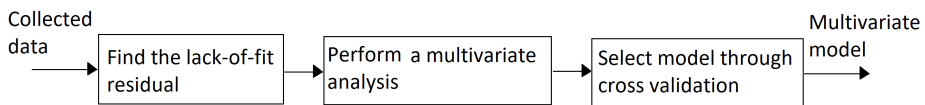
Figure 3.1: Flowchart showing the process of deriving a multivariate model from collected data.

With real measurements and experiments, all the dynamics may not be explainable with the data that is available, as for example wind and current will affect the movement of the ferry. It is also a mistake to overfit the data to the basis functions available, as this will give new modeling errors.
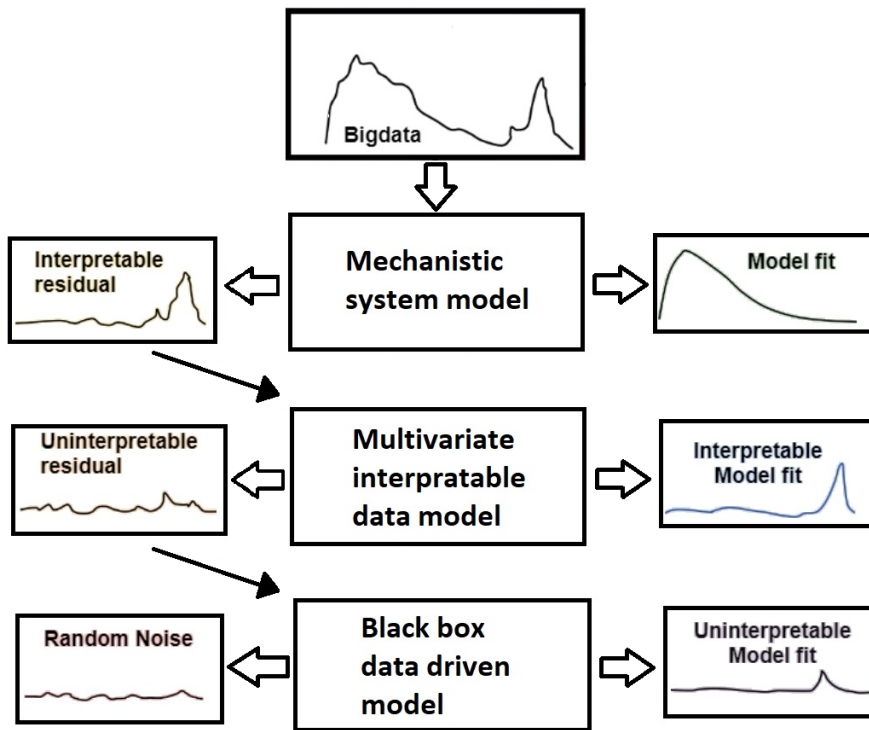
Figure 3.2: Pipeline for analysing data, with focus on the multivariate interpretable data model in this thesis. Inspired by Tekna seminar on big data cybernetics (Tekna, 2019)

3.1 Multivariate methods

Different MVA techniques can be used for analysing complex data set and identify underlying structures in the data (Esbensen et al., 2018). The methods and the theory that are used in this thesis are presented here.

3.2 Principal component analysis (PCA)

For analysing a single data set X, principal component analysis (PCA) is a method that can give insight to the data structure. Often, large parts of a data set can be explained with much fewer components and with a PCA the data can be reduced to a set containing less components. PCA can be realized with single value decomposition (SVD) where the first principal component (PC) is an axis through the data set that contains maximum variance. The next PC is orthogonal to the previous PC's with maximum variance. Since the PC's must be orthogonal there can be as many PC as there are dimensions. By plotting data in three dimensions it is possible to visualize the direction of the PC, as shown in Figure 3.3.
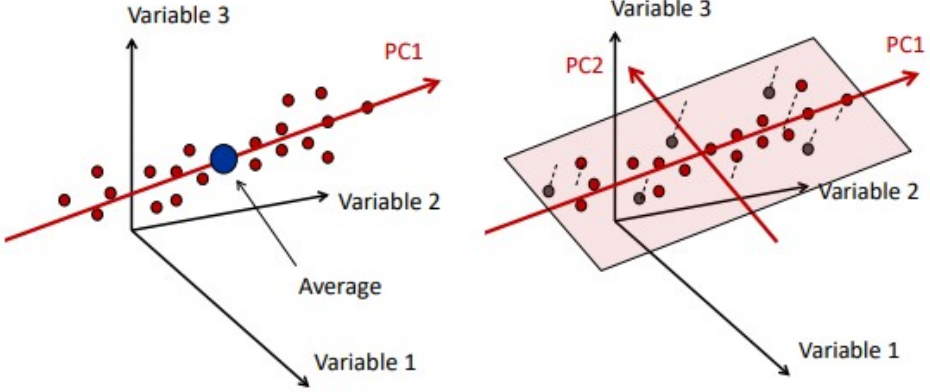
Figure 3.3: Visualization of the two first PC's from data in three dimensions (Esbensen et al., 2018).

With $\mathbf{X} \in \mathbb{R}^{N \times J}$ the PCA of the $j_{th} \in [1, 2, \ldots, J]$ order is

$$\boldsymbol{X} = \boldsymbol{T}_j \boldsymbol{P}_j^T + \boldsymbol{E}_j, \tag{3.1}$$

where $\boldsymbol{T}_j \in \mathbb{R}^{N \times j}$ is the scores, $\boldsymbol{P}_j \in \mathbb{R}^{J \times j}$ is the loadings and $\boldsymbol{E}_j \in \mathbb{R}^{N \times j}$ is the residual. The loading matrix gives the weight for the variable of each PC, and can be seen as the axis of the PC. The scores contains the original data rotated into the coordinate system of PC's. The residual $\boldsymbol{E}$ is the remaining data that is not explained by the PC's.

3.3 Partial least squares regression (PLSR)

For finding the correlation between two data set $\mathbf{X}$ and $\mathbf{Y}$, like input and output data, partial least squares regression (PLSR) is used. With PLSR the relationship between an input and output matrix is found. This method finds a linear regression model between $\boldsymbol{X}$ and $\boldsymbol{Y}$ by projecting the variables into a new space (Hastie et al., 2009). Instead of the PC maximizing the variance, it maximizes the covariance between the $\boldsymbol{X}$ scores and the scores from $\boldsymbol{Y}$. The PLSR is implemented with a power method called nonlinear iterative partial least squares (NIPALS) explained in the section below.

3.3.1 Nonlinear iterative partial least squares (NIPALS)

The NIPALS method finds correlations in the input matrix $\mathbf{X}$ and the output matrix $\mathbf{Y}$ to estimate the output in $\mathbf{Y}$ through PLSR. The data set is divided into two parts, one for training the NIPALS and the other half for testing. The model order is decided through cross validation with the test set. With J number of inputs and K number of outputs, the dimension of the input and output matrix will be: $\mathbf{X} \in \mathbb{R}^{N \times J}$ and $\mathbf{Y} \in \mathbb{R}^{N \times K}$, where

N is the number of data points. Each input and output variable has N samples, so that

$$\boldsymbol{X} = \begin{bmatrix} X_1(1) & X_2(1) & \ldots & X_J(1) \\ X_1(2) & X_2(2) & \ldots & X_J(2) \\ \vdots & \vdots & \vdots & \vdots \\ X_1(N) & X_2(N) & \ldots & X_J(N) \end{bmatrix} \tag{3.2a}$$

$$\boldsymbol{Y} = \begin{bmatrix} Y_1(1) & Y_2(1) & \ldots & Y_K(1) \\ Y_1(2) & Y_2(2) & \ldots & Y_K(2) \\ \vdots & \vdots & \vdots & \vdots \\ Y_1(N) & Y_2(N) & \ldots & Y_K(N) \end{bmatrix} \tag{3.2b}$$

This method iterates to find each PC, and the model order decides how many principal components should be included in the model. The algorithm iterates to find the scores and loadings with the following steps.

Step 1 is to scale and center the data to be zero mean by subtracting the mean of the variables and dividing each variable with its own standard deviation. This gives

$$\boldsymbol{E} = \frac{\boldsymbol{X} - \bar{\boldsymbol{x}}}{std(\boldsymbol{X})} \tag{3.3}$$

$$\boldsymbol{F} = \frac{\boldsymbol{Y} - \bar{\boldsymbol{y}}}{std(\boldsymbol{Y})}. \tag{3.4}$$

with $\boldsymbol{E} \in \mathbb{R}^{N \times J}$ and $\boldsymbol{F} \in \mathbb{R}^{N \times K}$, where $\bar{\boldsymbol{x}}$ is the mean of the variables in $\boldsymbol{X}$ and $\bar{\boldsymbol{y}}$ is the mean of the variables in $\boldsymbol{Y}$.

Step 2 is iterating through the data to find the scores and loadings of $\boldsymbol{E}$ and $\boldsymbol{F}$, and Loading weights $\boldsymbol{W} = [\boldsymbol{w}_1, \ldots, \boldsymbol{w}_j]$. These are used to determine the scores and loadings, and are found so that the PC maximizes the covariance between $\boldsymbol{E}$ and $\boldsymbol{F}$. The scores for the output $\boldsymbol{U}$ is chosen as the column with highest variance as an initial guess. If this is the first column in $\boldsymbol{Y}$ then $u_j = \boldsymbol{Y}_1$. For each factor of j the scores and loadings are found by

$$w_j^T = \frac{u_j E}{u_j^T u_j}, \qquad \text{Loading weights} \tag{3.5a}$$

$$w_j = \frac{w_j}{\sqrt{w_j^T w_j}} \qquad \text{Normalize loading weights to length 1} \tag{3.5b}$$

$$t_j = E w_j \qquad \text{Scores for } X \tag{3.5c}$$

$$p_j^T = \frac{t_j^T E}{t_j^T t_j} \qquad \text{Loadings for } X \tag{3.5d}$$

$$q_j^T = \frac{t_j^T F}{t_j^T t_j} \qquad \text{Loadings for } Y \tag{3.5e}$$

$$u_j = \frac{F q_j}{q_j^T q_j} \qquad \text{Scores for } Y \tag{3.5f}$$

These equations (3.5) are repeated until u_j converges. The current model is subtracted from the residuals, E and F. Step 2 is repeated with

$$E = E - t_j p_j^T \tag{3.6}$$

$$F = F - t_j q_j^T \tag{3.7}$$

$$j = j + 1, \tag{3.8}$$

until j reaches the desired model order.

Step 3 The model structure from NIPALS is given by

$$X = \bar{x} + T P^T + E \tag{3.9}$$

$$Y = \bar{y} + U Q^T + F, \tag{3.10}$$

where $T \in \mathbb{R}^{N \times j} = [t_1, \ldots, t_j]$, $P \in \mathbb{R}^{J \times j} = [p_1, \ldots, p_j]$, $U \in \mathbb{R}^{N \times j} = [u_1, \ldots, u_j]$ and $Q \in \mathbb{R}^{K \times j} = [q_1, \ldots, q_j]$. Regression coefficients are found from

$$\Theta_{pre} = W (P^T W)^{-1} Q^T \tag{3.11}$$

$$\Theta_{post} = \Theta_{pre} \frac{std(Y)}{2 std(X)} \tag{3.12}$$

$$\bar{\Theta} = \bar{y} - \bar{x} \Theta_{post} \tag{3.13}$$

$$\Theta^T = [\bar{\Theta}^T, \Theta_{post}^T] \tag{3.14}$$

with $\Theta_{pre}, \Theta_{post} \in \mathbb{R}^{J \times K}$, $\Theta \in \mathbb{R}^{(J+1) \times K}$ and $\bar{\Theta} \in \mathbb{R}^{1 \times K}$, where Θ_{pre} contains the parameters for the scaled variables. An estimation of the output, $\hat{Y}$, can be found from

$$\hat{Y} = \Theta \Phi^T \tag{3.15}$$

where $\Phi = [1, X]$.

3.4 Cross validation

Cross validation is important to perform on the models that are derived by the PLSR. Some models may fit perfectly well for some parts of the data, but are not generalizable to the rest of the set. This could be if input coincidentally matches the covariance of the output in some cases, or that the PLSR has only captured some parts of the model. Cross validation is therefore used to test how well the data driven model can predict the output. This is done by leaving out some of the data of the analysis, and compare the estimate of the model with the data (Bro et al., 2008). The deviation gives an indication of how good the model is. This is used when comparing the models from the PLSR and selecting what model order that explains the data best.

The cross validation is done by dividing the data set in two parts, a training set and a test set. The training set is for finding the models, and the models are validated with the test set by looking at the deviations from the estimates. There are different ways to select the model from an MVA. Cross validation is a safe method where the human understanding can help select the model that fits best from visual inspection. In addition there are automated methods that can select a model, however since all systems are different these criteria are not guaranteed to find the best suited model for all cases(Stoica and Selen, 2004).

3.5 Performance metrics

The performance metrics that are defined help compare the models that are derived and how they perform in the controller. In many estimations large deviations are more undesirable than small errors. With the mean squared error (MSE) larger errors are penalized more. The MSE is a performance metric that is well suited to evaluate how good an estimator is and is given by

$$MSE = \frac{1}{N} \sum_{i=1}^{N} e^2. \tag{3.16}$$

where e is the error of the measurements. When both small deviations are equally weighted as large deviations the more suited metric is the mean absolute error (MAE). This does not punish large errors by squaring the error, and simply evaluates the average deviation. The MAE is derived by

$$MAE = \frac{1}{N} \sum_{i=1}^{N} |e|. \tag{3.17}$$

While the above metrics can give a good indication to the accuracy of a controller, the performance can also be evaluated from their energy use (Sørensen and Breivik, 2015). Hence the integral absolute error and work (IAEW) metric is added where the performance of the controller is differed by the error and the work done. Especially for fully electric

ferries the energy consumption is important, a small improvement of the accuracy may not be beneficial if the energy is increased excessively. the IAEW is given by

$$IAEW = \int_0^t |e(t)|dt \int_0^t P(t)dt, \tag{3.18}$$

where $P = |\boldsymbol{\tau}^T \boldsymbol{\nu}|$ is the power.

3.6 The lack-of-fit residual
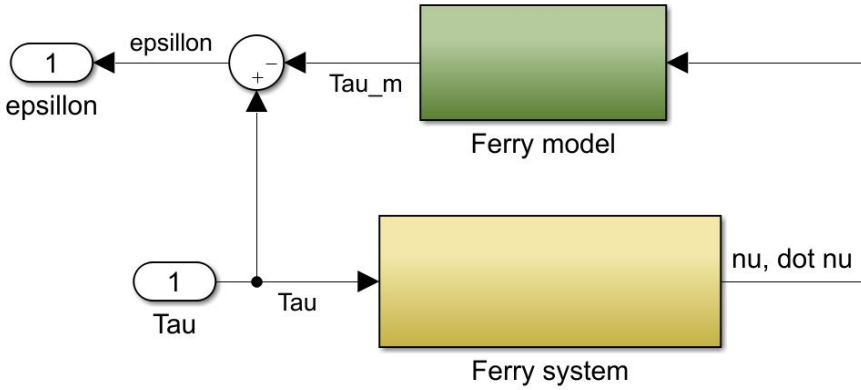
Figure 3.4: Block diagram of how the residual is found.

The initial model is a good approximation of the ferry, but is not perfect. To capture the discrepancies of the ferry model, it is compared to the real system to find the lack-of-fit residual. This is done by running the model with the outputs of the ferry, $\dot{\nu}$ and ν. The spesific velocity and acceleration gives basis for the model to estimate the control input that was used. The estimated control input $\tau_{m_0} = [\tau_{m_0,u}, \tau_{m_0,v}, \tau_{m_0,r}]^T \in \mathbb{R}^3$ is given as

$$\boldsymbol{F}_0(\dot{\boldsymbol{\nu}}, \boldsymbol{\nu}) = \boldsymbol{\tau}_{m_0}. \tag{3.19}$$

The estimated control input is compared to the real control input $\boldsymbol{\tau}$ by calculating the residual

$$\epsilon_0 = \boldsymbol{\tau} - \boldsymbol{\tau}_{m_0}, \tag{3.20}$$

where $\epsilon_0 = [\epsilon_{0,u}, \epsilon_{0,v}, \epsilon_{0,r}]^T \in \mathbb{R}^3$. If the model perfectly captures the ferry, the residual will be zero. Otherwise, it describes the discrepancies in the model. In Figure 3.4 the block diagram shows how the residual is found from the model and the ferry system. The goal is to analyse and find a model of the residual that can improve the initial model. The first proposal for finding a suited lack-of-fit residual was to use the residual from an

estimated acceleration and the measured acceleration, and use the control input as an input variable. The problem with this design was that to use the multivariate model in the FF the regression coefficients for the control input had to be inverted. This caused singularity issues that gave bad estimates. In addition acceleration measurements are not necessarily that accurate and by basing the residual on comparing the acceleration this could cause more uncertainties.

3.7 Updating the model
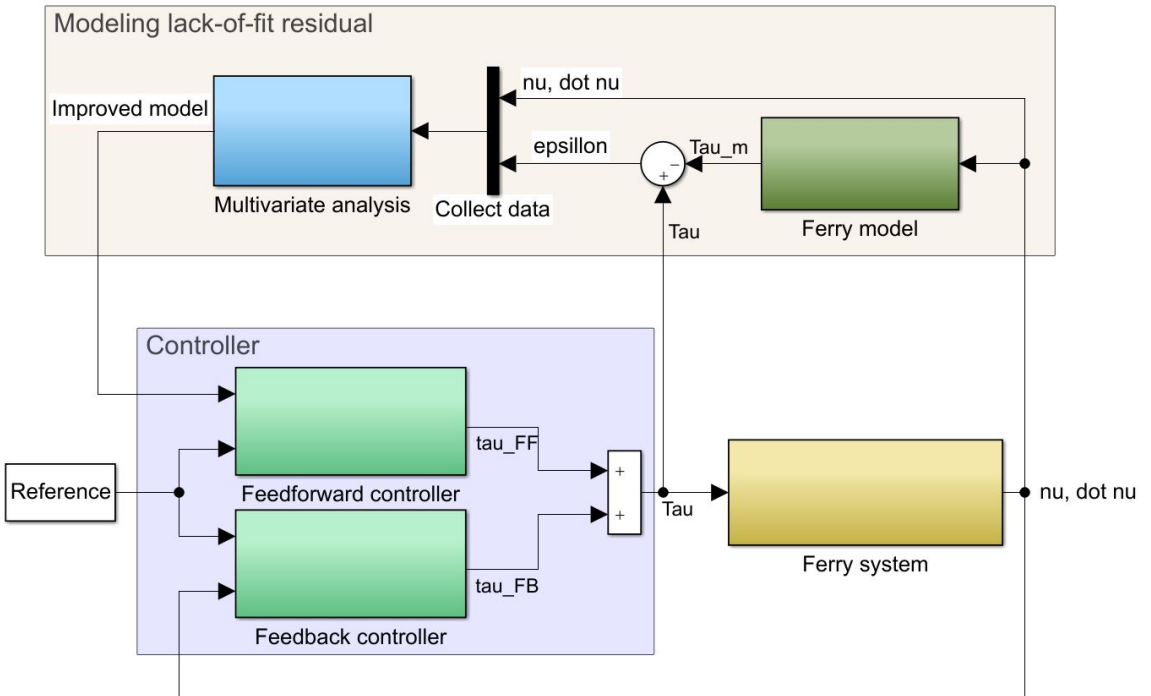
Figure 3.5: Block diagram of the system.

The controller of the ferry works online, giving commands to the ferry system. While the ferry is in operation the residual found in (3.20) is logged together with measurements of the states of the ferry. When the model in the FF needs improvement the collected data is analysed. Different methods that could trigger this could be an increasing inaccuracy in the model, triggered by a large residual or the feedback controller having to compensate more. The batch of collected data is analysed to find a model of the residual from MVA. The whole system is shown in Figure 3.5. The residual ϵ_0 from the initial model is modeled by $\boldsymbol{\tau}_{\epsilon_0} \in \mathbb{R}^3$ on the form

$$\boldsymbol{\Theta}_0 \boldsymbol{\Phi}_0^T(\dot{\boldsymbol{\nu}}, \boldsymbol{\nu}) = \boldsymbol{\tau}_{\epsilon_0} \tag{3.21}$$

where $\boldsymbol{\Theta}_0$ is a parameter vector with regression coefficients and $\boldsymbol{\Phi}_0$ is a vector containing basis functions of the state variables $\dot{\boldsymbol{\nu}}$ and $\boldsymbol{\nu}$. The goal for $\boldsymbol{\tau}_{\epsilon_0}$ is to give the most accurate model of ϵ_0, that can improve the current model of the ferry. This results in the improved model given as

$$\boldsymbol{F}_1(\dot{\boldsymbol{\nu}}, \boldsymbol{\nu}) = \boldsymbol{F}_0(\dot{\boldsymbol{\nu}}, \boldsymbol{\nu}) + \boldsymbol{\Theta}_0 \boldsymbol{\Phi}_0^T(\dot{\boldsymbol{\nu}}, \boldsymbol{\nu}) \tag{3.22}$$

$$\boldsymbol{F}_1(\dot{\boldsymbol{\nu}}, \boldsymbol{\nu}) = \boldsymbol{\tau}_{m_1}. \tag{3.23}$$

The coefficients of $\boldsymbol{\Theta}_0$ and the basis functions in $\boldsymbol{\Phi}_0^T(\dot{\boldsymbol{\nu}}, \boldsymbol{\nu})$ are found through MVA. The improved model is used in the FF giving a better estimation of the control input $\boldsymbol{\tau}$ needed to perform desired movement. The model in (3.22) is implemented in the FF by substituting $\dot{\boldsymbol{\nu}}$ and $\boldsymbol{\nu}$ to the desired trajectories from the reference filter, $\dot{\boldsymbol{\nu}}_d$ and $\boldsymbol{\nu}_d$. This gives a FF containing the initial model and the model of the residual $\boldsymbol{\tau}_{\epsilon_0}$. The improved FF is given by

$$\boldsymbol{\tau}_{FF} = \boldsymbol{F}_1(\dot{\boldsymbol{\nu}}_d, \boldsymbol{\nu}_d). \tag{3.24}$$

The model in (3.23) is now the new model of the ferry. The remaining residual after implementing the improved model is found by

$$\epsilon_1 = \boldsymbol{\tau} - \boldsymbol{\tau}_{m_1}, \tag{3.25}$$

with $\epsilon_1 \in \mathbb{R}^3$. The residual ϵ_1 gives an overview of the parts of the residual that the analysis is not able to model, and shows the remaining discrepancies of the model. This can give a good indication of how good the improvement is from implementing $\boldsymbol{\tau}_{\epsilon_0}$ in the model.

If desired further analysis of the data can be done to give a better estimate of the ferry model. This can be done by performing additional MVA with more advanced basis functions or by utilizing other methods like deep neural networks. The scalability of improving the model further is shown by the possibility of analysing and modeling the new residual ϵ_1. Further models can be added by

$$\boldsymbol{F}_k(\dot{\boldsymbol{\nu}}, \boldsymbol{\nu}) = \boldsymbol{F}_{k-1}(\dot{\boldsymbol{\nu}}, \boldsymbol{\nu}) + \boldsymbol{\Theta}_{k-1} \boldsymbol{\Phi}_{k-1}^T(\dot{\boldsymbol{\nu}}, \boldsymbol{\nu}) \tag{3.26}$$

$$\boldsymbol{F}_k(\dot{\boldsymbol{\nu}}, \boldsymbol{\nu}) = \boldsymbol{\tau}_{m_k}. \tag{3.27}$$

where k is the model iteration. If desired the model can be continuously improved with different methods until satisfied. This process can in theory continue until the residual only is left with white noise and all the dynamics are accounted for.

3.8 Possible model variables

There are some different input types that can be created from the data gathered from the ferry. There are measurements of $\dot{\nu}, \dot{\nu}, \tau$ and η. The position of the ferry, η, is normally not included when describing the movement of a ship, as the dynamics should be unaffected by where a ship is located. In some cases it can be useful with the heading of the ferry like when the wind speed and direction is measured, to find the correlation with the wind force. This is not implemented on the ferry, hence the positional and heading data is not included in the analysis, as the data is more misguiding than helpful. With the other variables there are multiple combinations possible that can be included in an analysis. In the initial model based on first principals the damping term contains variables from ν raised to the power of 2 and 3. Each variable in $\nu = [u, v, r]$ can be raised to the power of n, where $n = 1, 2, 3....$ The problem with this method is that when n is odd numbers the sign is included to the value, while when n is even numbers the value is an absolute value with the magnitude. Both the magnitude and the value with direction can be interesting to analyse. This gives two sets of variables raised to the power of n, showing the direction and the absolute value. A set of possible variables for u is given by

$$\text{Signed variables:} \quad u^{n_o}, \quad |u|u^{n_o} \tag{3.28}$$
$$\text{Magnitude variables:} \quad |u|^{n} \tag{3.29}$$

where $n_o = [1, 3, 5, ...]$ and $n = [1, 2, 3, ...]$. In addition there are cross-coupled terms with combinations of surge, sway and yaw movement that can be interesting to analyse. The initial model has terms depending on the magnitude of a state multiplied with an other, making it reasonably to assume these variables can affect the other states. This gives the variables

$$\text{Cross variables:} \quad uv, \quad ur, \quad vr \tag{3.30}$$
$$\text{single state signed cross variables:} \quad |u|v, \quad |u|r, \quad |v|u, \quad |v|r, \quad |r|u, \quad |r|v \tag{3.31}$$
$$\text{Magnitude of cross variables:} \quad |u||v|, \quad |u||r|, \quad |v||r| \tag{3.32}$$

The same number of variables can be found for $\dot{\nu}$. Measurements for $\dot{\nu}$ are more unreliable but when analysing collected data an accurate estimation can be found together with measurements for ν. Then there is a possibility to add variables of $\dot{\nu}\nu$, although it does not necessarily make sence to multiply acceleration and velocity from a physical perspective, they could be affecting the dynamics of the ferry.

Chapter 4

Simulation results

In this chapter the simulation results are presented. The simulations include a case to show how the MVA can be used, then the basis functions for the analysis is selected and used to identify the model under different conditions. All of the simulations are done in MATLAB/Simulink.

4.1 Design of experiment

It is important to design the experiments so that the data contains the information that is needed. This is achieved by pre-planning systematic variations in the experiment to induce different responses to the system (Antony, 2014). For the ferry this is done with the planned trajectory so that the data contains information about how different movements affect the ferry. The experiments that are done in the simulations are designed to give realistic testing of what the MVA can achieve. This includes the model to be identified, thruster dynamics and the trajectory the ferry runs. The trajectory that is designed is also used for the experiment on the ocean.

4.1.1 Model changes

An altercation is done to the model ferry, to create a discrepancy between the believed model and the true model in the simulations. The goal of the MVA is to identify this discrepancy and improve the believed model. The model parameters of the actual ferry system has been multiplied with 0.5, so the model in the controller is not accurate. The structure of the initial model is kept, as there are different complexity to the different states. Surge is decoupled from the other states, and is the least complex model. Sway and yaw are coupled, with yaw being dependent on the most basis functions and is the most complex state to identify. This gives different challenges for the MVA. The true model of the ferry used in the simulations are given by

$$\mathbf{M}_s \dot{\boldsymbol{\nu}} + \mathbf{C}_s(\boldsymbol{\nu})\boldsymbol{\nu} + \mathbf{D}_s(\boldsymbol{\nu})\boldsymbol{\nu} = \boldsymbol{\tau}, \tag{4.1}$$

where

$$\mathbf{M}_s = \mathbf{M}\delta \tag{4.2a}$$
$$\mathbf{C}_s = \mathbf{C}\delta \tag{4.2b}$$
$$\mathbf{D}_s = \mathbf{D}\delta, \tag{4.2c}$$

with $\delta = 0.5$. The model used in the controller, which is the model believed to be the correct model of the ferry, is given by $\boldsymbol{\tau}_m$. The initial model is the believed model before any further analysis, represented by $\boldsymbol{\tau}_{m_0}$ in (3.19).

The remaining residual between the believed model and the true model is also given by (4.1) with opposite sign in the parameters. This is the model to be identified with MVA. It is a complex model with surge decoupled from sway and yaw, instability in yaw and several coupling terms between sway and yaw.

4.1.2 Thruster dynamics

The thruster dynamics are implemented between the control input and the ferry model to represent the movement of the thrusters. It takes time to change the motor speed, so a rapid change in the control input does not give instant response from the thrusters. The thruster dynamics used in the simulations is modeled by

$$\boldsymbol{\tau} = \frac{4}{s^2 + 3.2s + 4}\boldsymbol{\tau}_c, \tag{4.3}$$

where $\boldsymbol{\tau}_c$ is the actual force from the thrusters. This selection of thruster dynamics is a little quicker than the identified model in (Pedersen, 2019), so the thrusters have a little less affect on the control input.

4.1.3 Trajectory
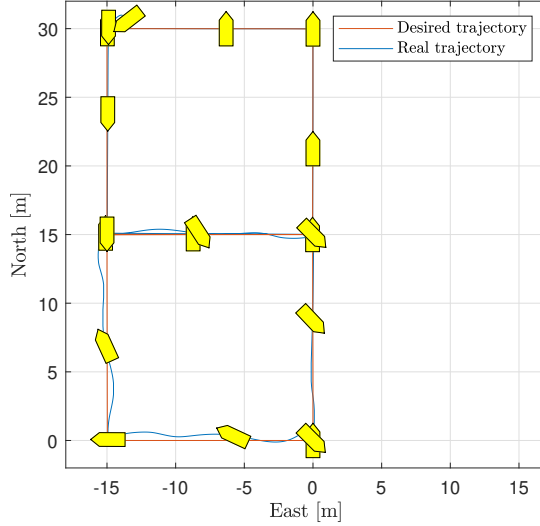
Figure 4.1: Desired trajectory and real trajectory used for the MVA.

The trajectory is selected so that the collected data is as rich as possbile. To achieve a rich signal all states must be excited by it self and coupled with the other states to distinguish the effect they have on each other. The 4-corner test is designed to get information of each state and how they are coupled (Skjetne et al., 2017). A modified version of the 4-corner test is chosen so that the trajectory turns and moves both ways and no symmetry is assumed in any direction. A trajectory of 12 segments is put together giving the trajectory shown in Figure 4.1, with the corresponding coordinates and heading in Table 4.1. This trajectory consists of movement in $surge$, $sway$, yaw, $surge/sway$ and $surge/sway/yaw$. Since a movement in yaw while changing the position excites both surge and sway, yaw can not be actuated alone with only surge or sway. All of the movements are done in both directions, so that for example the $surge/sway/yaw$ movement is done with change in yaw both clockwise (CW) and counterclockwise (CCW). A breakdown of the segments with the movement is shown in Figure 4.2. The trajectory starts and ends in $\boldsymbol{\eta} = [0, 0, 0]$, and segment 7 starts where segment 6 ends. A new waypoint is given every 60 second, and $\boldsymbol{\tau}$ from following the desired trajectory is shown in Figure 4.3. The control input $\boldsymbol{\tau}$ is the output of the controller, and not the exact thruster output from the thruster dynamics. The exact trust could be used, as the angle and the velocity of the propeller is measured, but the aim is to improve the controller, hence the model is compared to the controller output.

Table 4.1: The points of the desired trajectory giving the 12 segments in NED

x [m]	y [m]	ψ [deg]
0	-15	-90
15	-15	0
15	0	0
30	0	0
30	-15	0
30	-15	180
15	-15	180
15	0	135
0	0	135
0	0	-45
0	-15	-45
0	0	0
0	-15	-90
15	-15	0
15	0	0
0	30	0
30	-15	0
30	-15	180
15	-15	180
15	0	135
0	0	135
0	0	-45
0	-15	-45
0	0	0
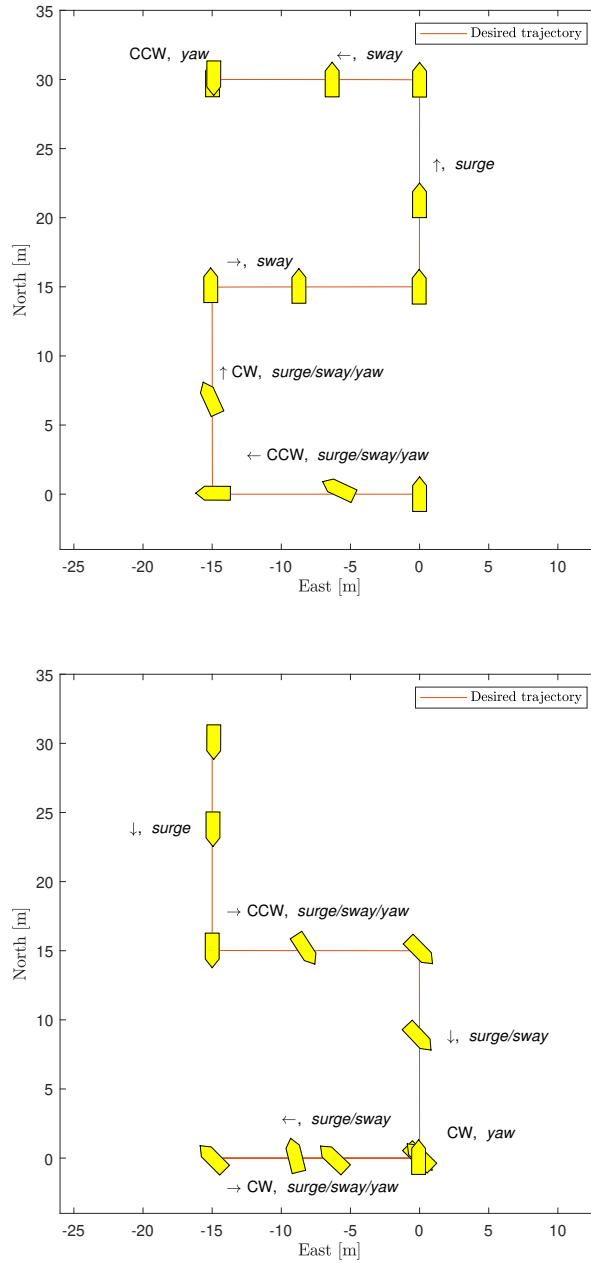
Figure 4.2: The movement of each segment in the trajectory. Segment 1 to 6 is showed above and segment 7 to 12 is showed below.
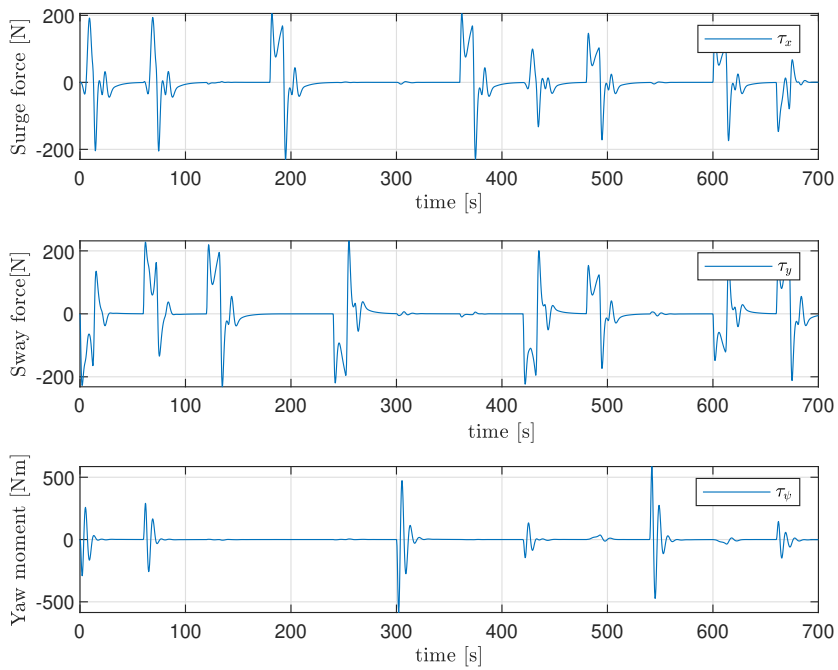
Figure 4.3: Control input τ when following the desired trajectory.

4.2 Case study of PLSR with velocity and acceleration as input variables

This case study is to get insight in the PLSR model that is found. The case is done with the following $\mathbf{X}$ and $\mathbf{Y}$ matrix:

$$\mathbf{X} = \begin{bmatrix} \dot{\boldsymbol{\nu}}^T(1) & \boldsymbol{\nu}^T(1) \\ \vdots & \vdots \\ \dot{\boldsymbol{\nu}}^T(N) & \boldsymbol{\nu}^T(N) \end{bmatrix}, \qquad \mathbf{Y} = \begin{bmatrix} {\boldsymbol{\epsilon_0}}^T(1) \\ \vdots \\ {\boldsymbol{\epsilon_0}}^T(N) \end{bmatrix}, \tag{4.4}$$

with the goal of identifying the error model. The error model contains multiple other terms that is not included in this analysis, hence the PLSR has parts of the residual it should not be able to explain. The trajectory for the case is the path shown in Figure 4.1, where the utilized controller for the ferry is a PID with the FF containing the initial model, (2.10), and a FB term, (2.13), correcting for the discrepancies in the FF.
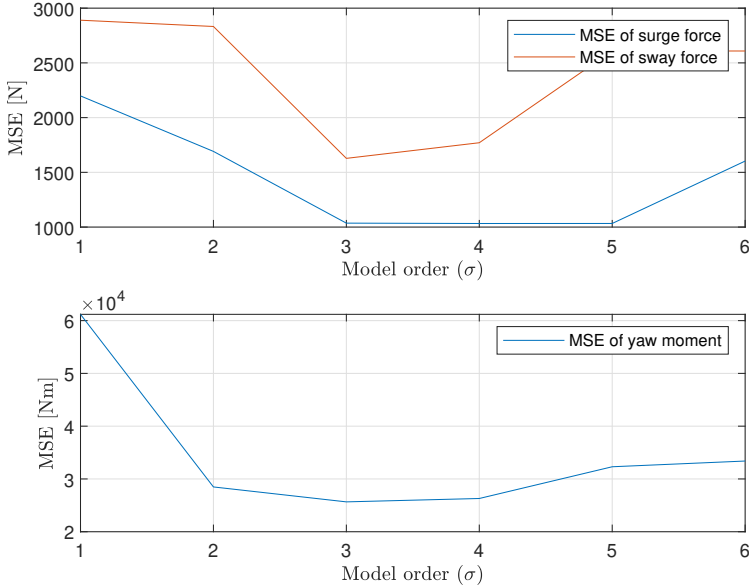
Figure 4.4: The MSE with the different model orders in the case.

The model from the case PLSR can maximum have an order equal to the number of basis functions in $\mathbf{X}$. In this case $\mathbf{X}$ has 6 basis functions, and the models from the different model orders(σ) are compared in the test set. The test set is the second half of the data, and the difference between the residual and the model gives a MSE, which is plotted in Figure 4.4. At $\sigma = 3$ the MSE is least for all states. With the higher order models from

the PLSR the MSE increases in the test set due covarinaces found in the training set that does not correspond to the test set. The MSE for surge force is almost equal for order 3, 4 and 5. Since the test set can not include all possible scenarios, there is always a chance that the model is overfitted to the data. In the case where the MSE is equal or slightly better for higher order models, it is preferable to choose the lowest order, as the chance of overfitting the model is reduced. The chosen order for further testing is therefore $\sigma = 3$. In Figure 4.5 a comparison of the residual, ϵ_0, and the model estimate, τ_{ϵ_0}, from the PLSR is compared.
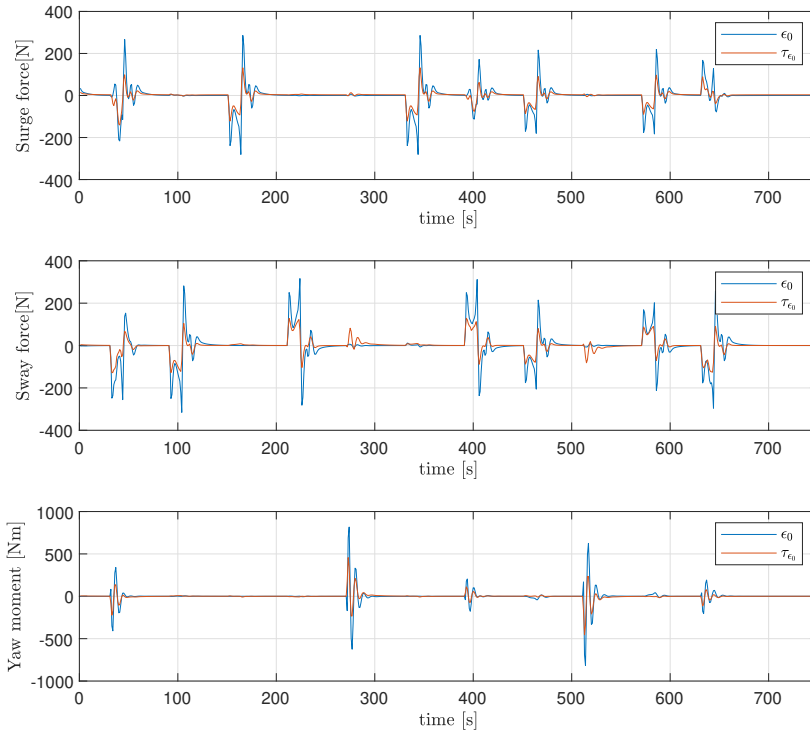
Figure 4.5: The residual, ϵ_{ϵ_0}, and the model estimate, τ_{ϵ_0} compared, with model order $\sigma = 3$.

To get more insight to which basis functions that influences the model, Θ_{pre} gives a good indication of this. In Θ_{pre} the parameters are still scaled down, and can be compared to each other. The magnitude of the parameters of Θ_{pre} are shown in Figure 4.6. This shows what basis functions that are weighted the most in the model. From the basis functions used in this case it is accurate that surge is mostly influenced by $\dot{u}$ and u, while sway, which is coupled with yaw, is influence by r, in addition to its own states $\dot{v}$ and v. The PLSR found less coupling for yaw as $\dot{r}$ and r is heavily weighted, although it is effected a little from v.
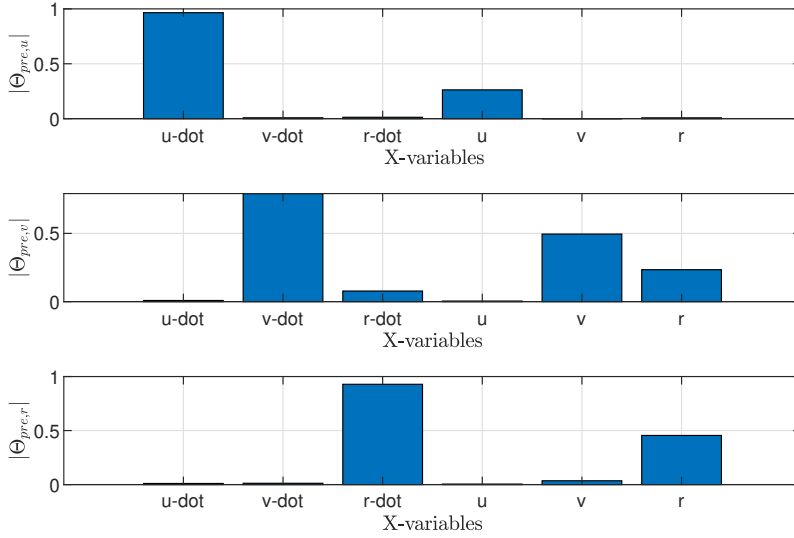
Figure 4.6: $|\mathbf{\Theta}_{pre}|$ showing the effect of each basis function in the model.

The case PLSR model is given by

$$\boldsymbol{\tau}_{\epsilon_0} = \mathbf{\Theta}_0 \mathbf{\Phi}_0(\dot{\boldsymbol{\nu}}, \boldsymbol{\nu}) \tag{4.5}$$

with $\mathbf{\Phi}_0(\dot{\boldsymbol{\nu}}_d, \boldsymbol{\nu}_d) = [1, \dot{u}, \dot{v}, \dot{r}, u, v, r]^T$ and $\mathbf{\Theta}_0 \in \mathbb{R}^{3 \times 7}$. By implementing (4.5) with the initial model, the improvement is shown by comparing ϵ_0 and the new residual, ϵ_1. This is done in Figure 4.7. The residual has been reduced with a PLSR of $\dot{\boldsymbol{\nu}}$ and $\boldsymbol{\nu}$, but the highest spikes are still not explained by the model. The improvement of the MSE with this PLSR model is shown in Table 4.2.

Table 4.2: The MSE of the residual with and without the case PLSR model.

The residual ϵ	MSE of surge force	MSE of sway force	MSE of yaw force
Without PLSR model	2757.4 N^2	4337.7 N^2	7260.8 Nm^2
With case PLSR model	**1036.0** N^2	**1627.8** N^2	**2565.8** Nm^2
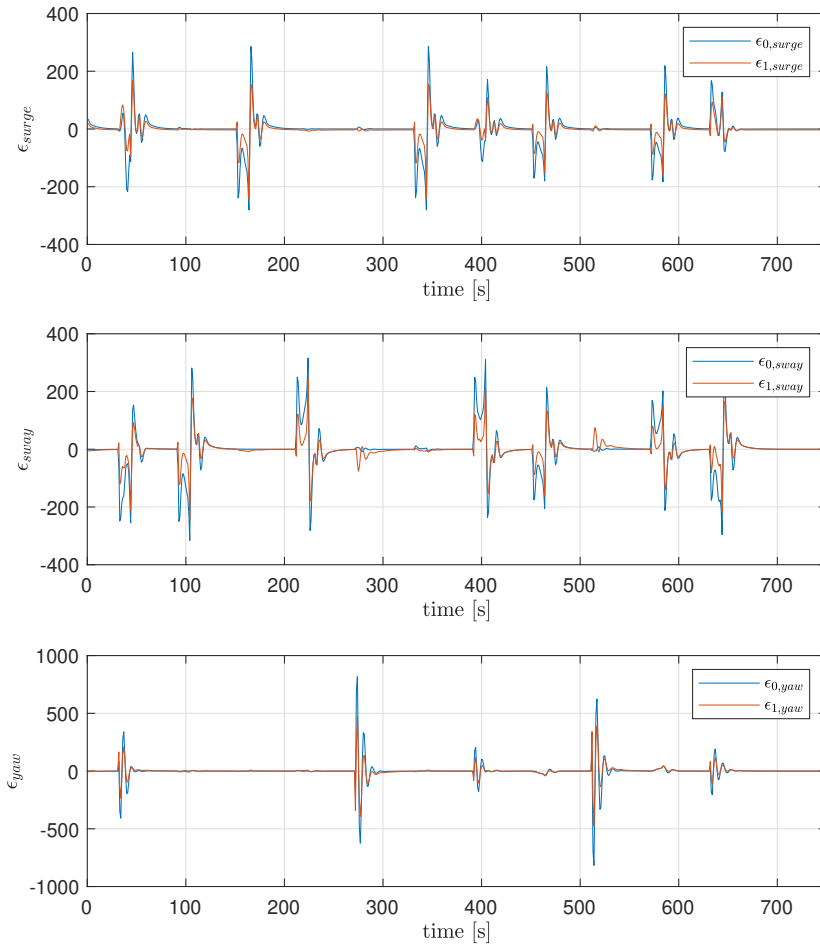
Figure 4.7: The initial residual ϵ_0 and the remaining residual ϵ_1 compared to each other.

4.2.1 Implementation in the controller

The improved PLSR model from analysing the residual ϵ_0 is implemented in the FF as $\boldsymbol{\tau}_{FF_1}$ in (3.24). The same path is tested without the feedback controller to see the improvement of the model, so that the ferry is only controller by the FF. The position of the ferry becomes very inaccurate in following the trajectory, as the instability in yaw makes the ferry go in wrong directions, and needs active control from the FB to be stable. The velocity and acceleration can still be compared to their desired trajectory. This is shown in Figure 4.8, where the improvement of the PLSR model is visualized. In the comparison of the acceleration $\dot{\boldsymbol{\nu}}$ the spikes in the accelerations are closer to the desired trajectory. This effects the velocity by reducing the overshoot from the initial model. Between the large spikes in the acceleration some smaller deviations are caused by error in the terms coupling the states. These are still evident in the simulation. The modeling errors from the PLSR model have created some new deviations caused by the coupling terms. In yaw the coupled terms have been overfitted so even though the spikes in angular acceleration $\dot{r}$ are closer to the desired acceleration $\boldsymbol{\tau}_d$, the improved model has creates new model errors that creates larger deviations from the desired trajectory of r. Yaw is the most complex state to model, and this is shown in this PLSR model. Overall the model for surge and sway has been improved slightly with PLSR model.

By implementing the improved model in the controller the FB should have to compensate less for the model discrepancies in the FF. A plot of how much the feedback controller contributed before and after the improved model is implemented is shown in Figure 4.9. This shows that work from the feedback controller is much less when the FF has the improved model in $\boldsymbol{\tau}_{FF_1}$. The discrepancies which caused large deviations in yaw without FB, is corrected by small adjustments in the control input for yaw τ_ψ. Overall the usage of $\boldsymbol{\tau}_{FB_1}$ is reduced significantly for all states when changing the pose, compared to $\boldsymbol{\tau}_{FB_0}$.
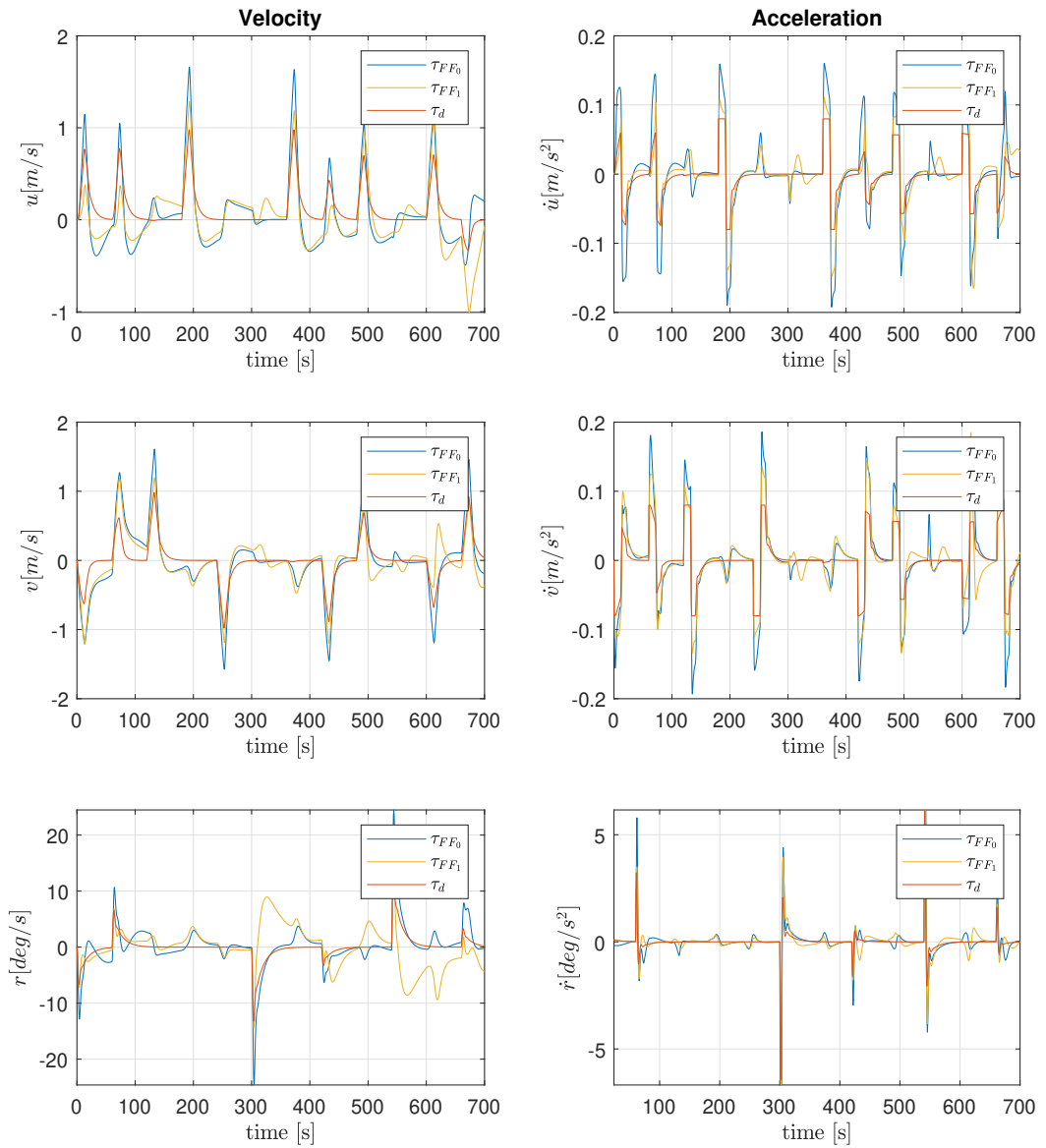
Figure 4.8: trajectory run with initial FF $\boldsymbol{\tau}_{FF_0}$ and the PLSR FF $\boldsymbol{\tau}_{FF_1}$ compared to desired velocity and acceleretion τ_d.
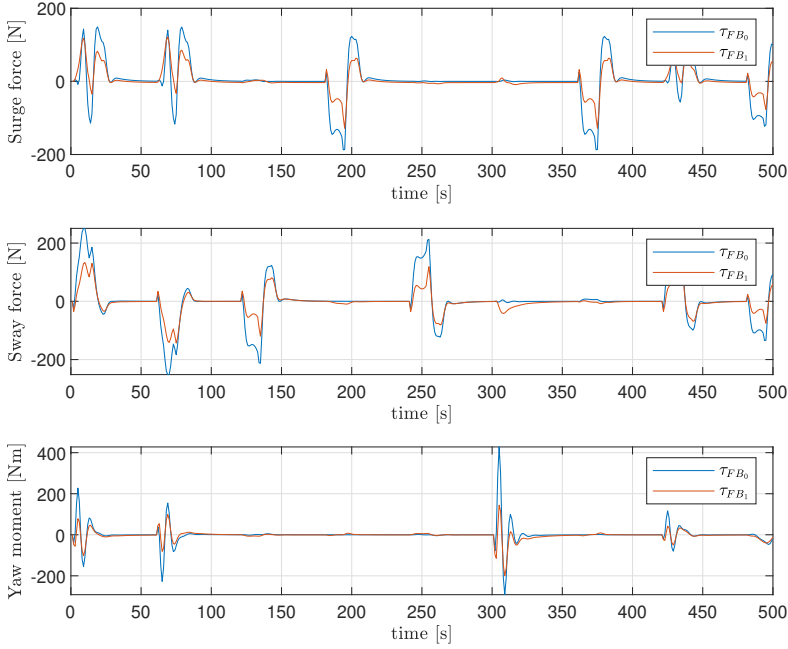
Figure 4.9: The initial FB τ_{FB_0} compared to the FB τ_{FB_1} with PLSR model implemented in the controller.

In Figure 4.10 the magnitude of the control input τ and the FB τ_{FB} with and without the PLSR model is compared. This shows how much of the total output from the controller is contributed by the FB term. With the initial controller the FB term is larger than the total control input for some states, as the corrections that the FB does from the model error is larger than the total control input. The improvement is significant when comparing the usage of initial FB τ_{FB_0} and the improved FB τ_{FB_0}. The magnitude of the FB term is reduced with the PLSR model, as well as the total output from the controller. The difference between the mean usage of τ and τ_{FB} before and after implementation of the improved model is shown in Table 4.3.

Table 4.3: The mean usage of τ and τ_{FB} with and without the PLSR model.

State	Without PLSR model		With PLSR model	
	control input τ	FB τ_{FB}	control input τ	FB τ_{FB}
τ_u	22.2 N	24.0 N	**20.6** N	**14.7** N
τ_v	30.3 N	30.7 N	**28.4** N	**17.6** N
τ_r	19.5 Nm	14.6 Nm	**12.8** Nm	**10.8** Nm
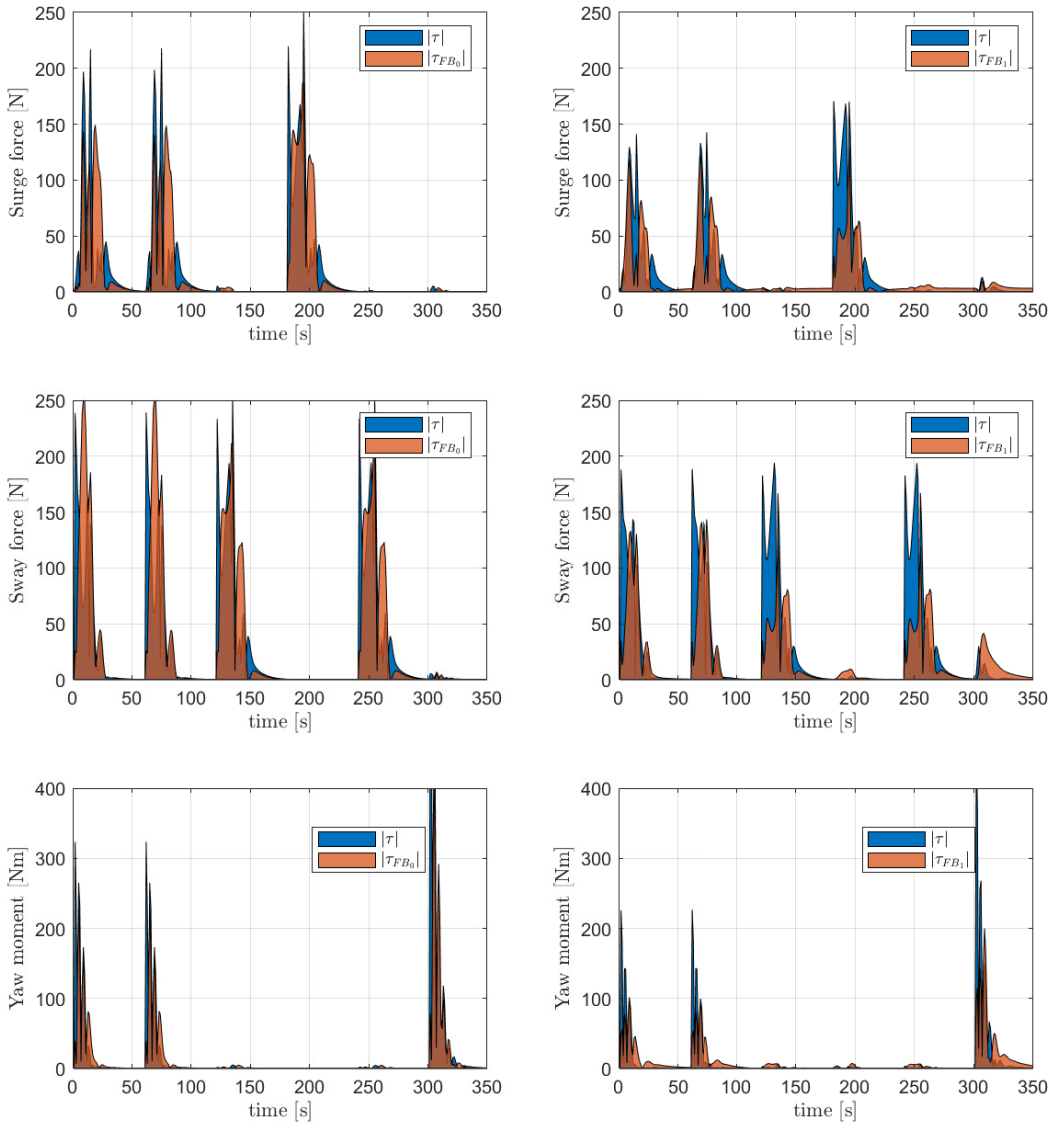
Figure 4.10: The total control input τ compared to the total FB τ_{FB}, without the PLSR model to the right, and with the PLSR model to the left.

To see the improvement of the controller, the positional error between the desired position from the reference filter and the actual position of the ferry is derived. This is found by

$$e_{pos} = \sqrt{(x_d - x)^2 + (y_d - y)^2}, \tag{4.6}$$

and is plotted in Figure 4.11. The positional error is almost halved for most parts of the simulation, showing that the PLSR model has given a significant improvement of performance. The MAE and the MSE is found in Table 4.4. The MSE of e_{pos} is much smaller, as it punishes large deviations more then small. When comparing the MAE of e_{pos} the difference is still evident as the average distance from the desired trajectory has almost been halved. The heading error given by

$$e_{\psi} = \psi_d - \psi, \tag{4.7}$$

is shown in Figure 4.12. The large deviations in heading have been reduced a lot from implementing the PLSR model. There are some model errors from the PLSR model that has created small deviations in between set point changes to heading. This is shown from MAE in heading as the improvement is not the significant. Comparing the MSE for e_{ψ} shows that the large errors have become are much smaller with PLSR.

Table 4.4: Positional and heading error with and without PLSR model.

Model	MAE of e_{pos}	MSE of e_{pos}	MAE of e_{ψ}	MSE of e_{ψ}
Without PLSR model	0.22 m	0.107 m^2	0.80 deg	0.014 deg^2
With case PLSR model	**0.12** m	**0.027** m^2	**0.62** deg	**0.0004** deg^2

Figure 4.11: The positional error with and without the case PLSR model implemented.
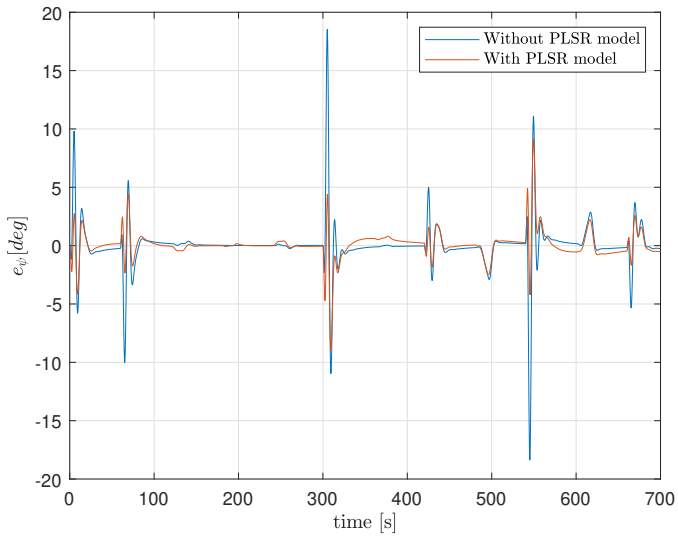
Figure 4.12: The heading error with and without the case PLSR model implemented.

4.3 Basis functions to include in the analysis

The basis functions in section 3.8 shows that there are many possible inputs that can be used in the analysis. This section discusses problems that arise when adding certain basis functions, and which basis functions that are appropriate to include in the analysis.

4.3.1 Magnitude basis functions

The ferry is a dynamic system moving in different directions, where the ferry is both accelerating, decelerating and turning left and right. Hence it makes sense that signed basis functions are included in the analysis. In addition the magnitude of basis functions could give a new aspect to the analysis, where the velocity, independent of the direction, could affect the dynamics. When using the magnitude basis functions, caution must be made for certain basis functions, where they look similar to the signed basis functions. In the trajectory the ferry has very little backwards motion, and a comparison of the signed signal and the magnitude of the signal is shown in Figure 4.13. The signals has almost the same covariance and the analysis rates their contribution to the output signal almost equally. This will result in a large model error when the ferry moves backwards.
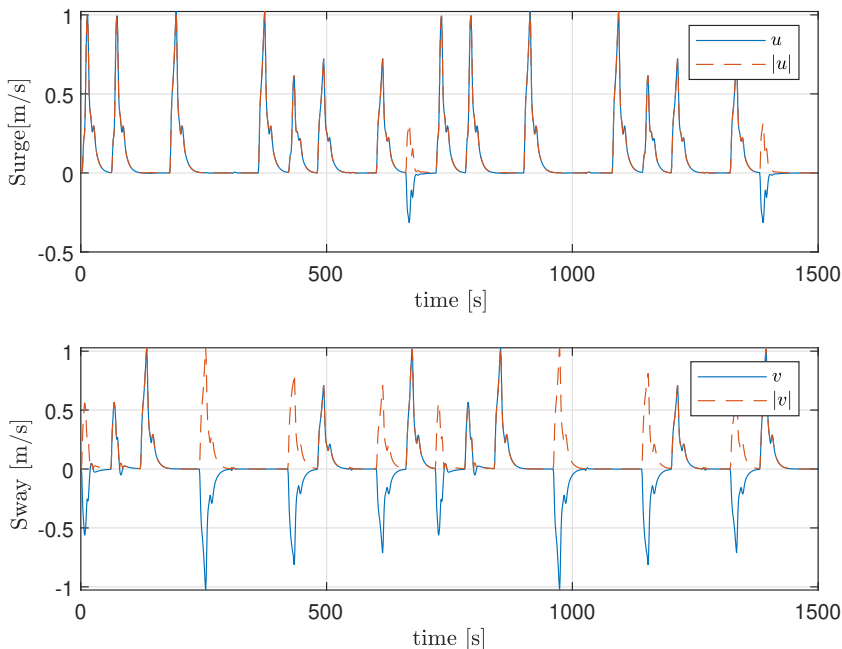
Figure 4.13: The signed data compared to the magnitude of the data, with surge compared above and sway compared below.

To see how the different basis functions are handled by the PLSR the influence from each basis function is compared in $|\mathbf{\Theta}_{pre}|$. This is the magnitude of the regression coefficients for each basis function when the data is scaled to a standard deviation of 1. An analyse with $\mathbf{X} = [\mathbf{\nu}, |\mathbf{\nu}|]$ and $\mathbf{Y} = [\mathbf{\epsilon}_0]$, is done with the NIPALS algorithm for $\epsilon_{o,u}$ and $\epsilon_{o,v}$ in Figure 4.14. In the model the effect of the signed basis functions is much higher than the magnitude basis functions, for both states. In the analysis the effect u and $|u|$ have is regarded as equally when estimating $\epsilon_{o,u}$, while when estimating $\epsilon_{o,v}$ the clear structure difference in v and $|v|$ makes it able to differ the influence of the two signals.
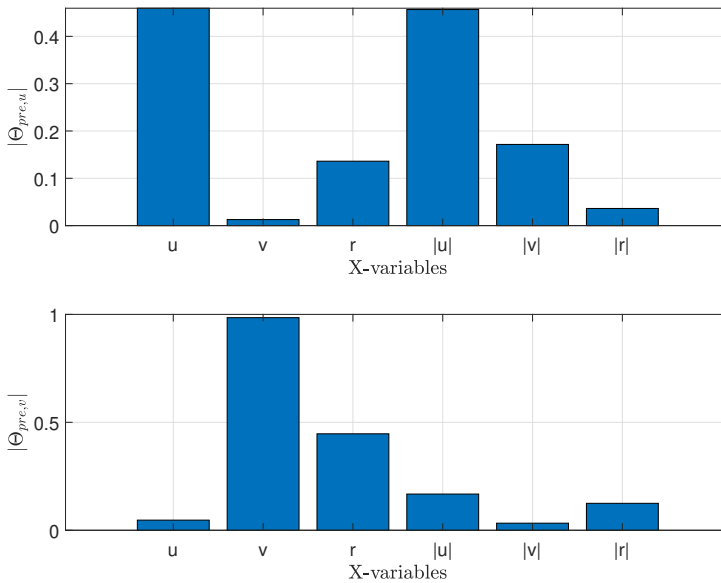
Figure 4.14: $|\mathbf{\Theta}_{pre}|$ showing the influence from each basis function.

Since the algorithm can handle both signed and the magnitude of the basis functions it is interesting to include the magnitude basis functions as well, to see the influence that they might have. If measurements are concentrated of data either above or below zero, as with u, the magnitude of the data will have the same effect. This can create situations where the PLSR model works great while the ferry continues the same operations, but may give large deviations outside the measured region.

4.3.2 Exponential basis functions

The basis functions could be power up to give several basis functions with different exponential. There are some consequences of doing this to the basis functions, as the data becomes very large or small depending if the data is more or less than 1. This causes the highest points to be higher even after scaled to a standard deviation of 1, which makes the difference between the maximum measurement and the minimum measurement more

significant. This is shown for u in Figure 4.15, where all the exponential functions have unit variance. This does so the PLSR analysis gets higher covariance with the higher exponential basis functions, more influenced by the magnitude rather then the change in form. This is seen by looking at $|\mathbf{\Theta}_{pre}|$ with $\mathbf{X} = [\boldsymbol{\nu}, \boldsymbol{\nu}^2, \boldsymbol{\nu}^3, \boldsymbol{\nu}^4, \boldsymbol{\nu}^5, \boldsymbol{\nu}^6]$, in Figure 4.16.
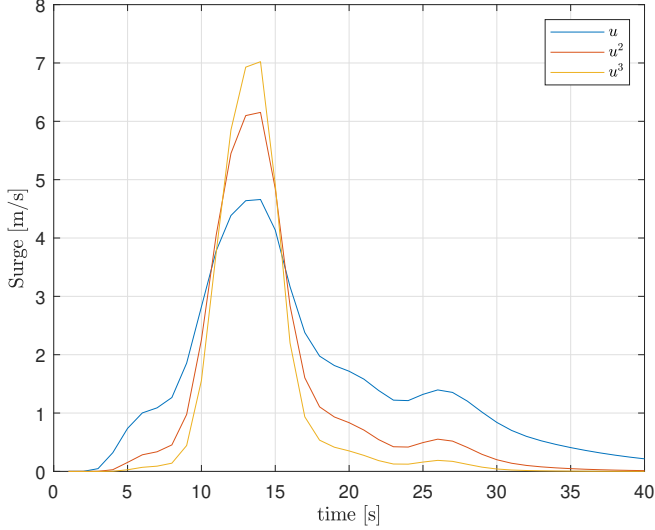
Figure 4.15: Exponential terms of surge compared with standard deviation of 1.

The higher order terms are just as influential as the lower order terms despite the highest term from the true residual model being $\boldsymbol{\nu}^3$. This is a problem when deriving a model, as the model error of an exponential term creates a deviation that increases with the same exponential rate. This can give large modeling errors from small estimation errors. To reduce the influence of higher order terms, the data from these signals are scaled down so that the peaks have less magnitude than the order before. The data are therefore scaled to

$$\mathbf{X}_{exp(\beta)} = \frac{\mathbf{X}^{\beta} - (\bar{\boldsymbol{x}}^{\beta})}{std(\mathbf{X}^{\beta})\beta} \tag{4.8}$$

where β is the order of the exponential. The standard deviation of the exponential terms is then

$$std(\mathbf{X}_{exp(\beta)}) = \frac{1}{\beta}. \tag{4.9}$$

This gives the signals in Figure 4.17, where the peak of the exponential term is lower then the previous order.The influence of the scaled exponential terms is much lower for the higher order term, as shown in Figure 4.18. Hence the scaled exponential terms are used in the PLSR, which helps prevent excess overfitting of the model. In addition to reducing
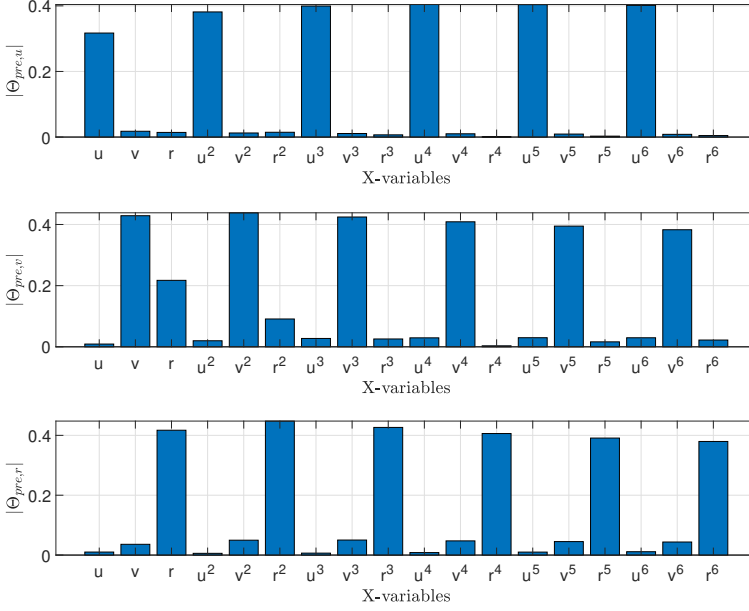
Figure 4.16: The effect of exponential terms in $|\mathbf{\Theta}_{pre}|$ after being scaled.

the effect from the higher order terms, it is important to think about how high exponential order that is desired to include in the analysis. Even though the higher order basis functions are scaled to have less influence in the model, they will still affect the model and the higher the exponential term, the more susceptible the terms are to be overfitted. Therefore terms with an exponential order above three is not included in the analysis. This results in the following exponential terms to be included in the analysis

$$\mathbf{X}_{exp} = [\boldsymbol{\nu}, sgn(\boldsymbol{\nu})\boldsymbol{\nu}^2, \boldsymbol{\nu}^3, |\boldsymbol{\nu}|, |\boldsymbol{\nu}|^2], \tag{4.10}$$

where $sgn(\boldsymbol{\nu})$ is the sign of the elements in $\boldsymbol{\nu}$.
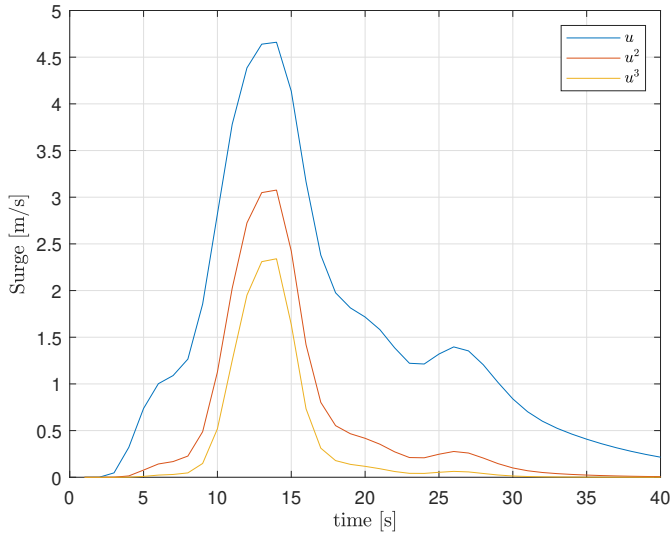
Figure 4.17: Exponential terms of surge compared with standard deviation depending of the order.
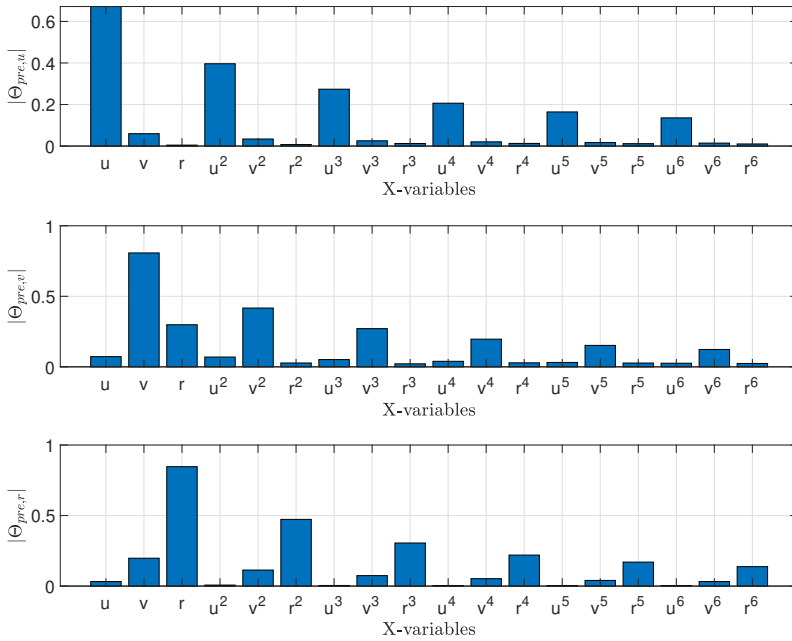
Figure 4.18: The effect of exponential terms in $|\Theta_{pre}|$ after being scaled.

4.3.3 Cross-coupled basis functions

From section 3.8 a combination of two states can give four different signals. With the states $sway$ and yaw these combinations are vr, $|v|r$, $v|r|$ and $|v||r|$. In Figure 4.19 all these signals are plotted, with a time horizon of 20 seconds to follow the first segment. This shows how non of the signals are identical, and although two of the signals follows each other at different parts of the data, they all differ from each other at a point. Hence all of the cross-coupled basis functions are included in the PLSR. This gives the cross-coupled basis functions

$$\boldsymbol{X}_{cc} = [uv, ur, vr, |u|v, |u|r, |v|u, |v|r, |r|u, |r|v, |u||v|, |u||r|, |v||r|]. \tag{4.11}$$
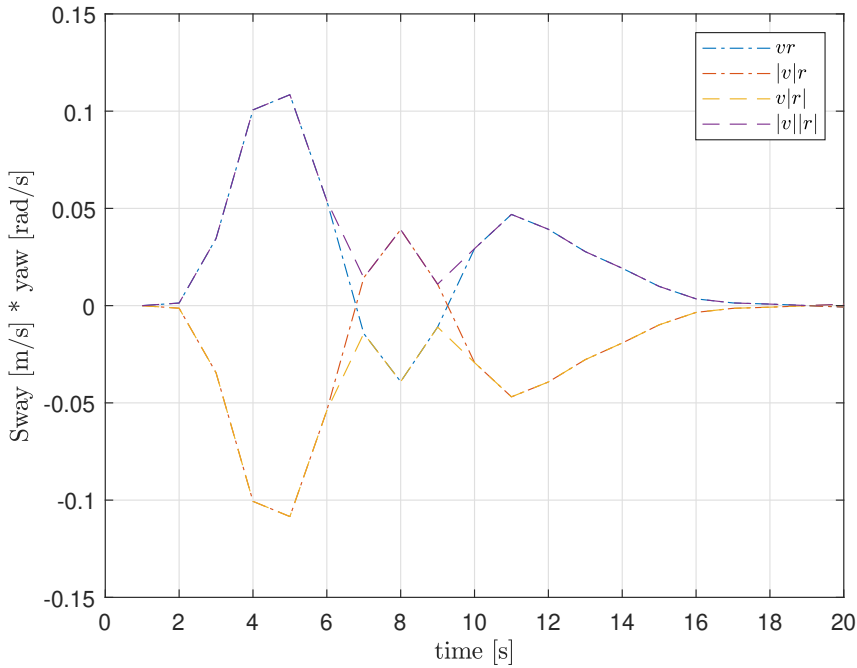
Figure 4.19: plot of the cross-coupled basis functions from sway v and yaw r for the first segment.

4.3.4   Basis functions included in the PLSR

In addition to the cross-coupled basis functions the acceleration $\dot{\boldsymbol{\nu}}$ is also included in the analysis. Since it is uncertain how the quality of the data is, as acceleration measurements usually are not that accurate, post processing of the data may be needed achieve a good signal. Hence no exponential or cross-coupled basis functions are added to acceleration. The input matrix is then given by the acceleration, magnitude, exponential and cross-coupled basis functions. This results in

$$\boldsymbol{X} = [\dot{\boldsymbol{\nu}}, \boldsymbol{X}_{exp}, \boldsymbol{X}_{cc}]. \tag{4.12}$$

To prevent the higher order terms to be weighted more in the analysis, β is chosen depending on the number of variables multiplied together. All the cross-coupled basis functions therefore has $\beta = 2$, as two variables like v and r are multiplied. The exponential basis functions has β equal to the exponential order of the signal. This results in the basis functions included in the PLSR.

4.4 Reduction of basis functions

The NIPALS algorithm is able to deal with a lot of basis functions, but this results in a more complex model depending on how many basis functions are added as an input. Some of the basis functions that has little covariance with the output can also misguide the PLSR, if the basis function does not have any effect in the true model. Hence it can be beneficial to remove this basis function from the analysis all together. There are different ways of reducing the basis functions with the PLSR utilized in the process (Mehmood et al., 2012). When choosing which basis function to remove, the basis function that contributed the least to the output signal in the analysis and therefore has less covariance are removed from the next analysis. With the NIPALS algorithm this can be found from $\mathbf{\Theta}_{pre}$ where all the basis functions are scaled in advance so they are comparable. The magnitude of the parameter in $\mathbf{\Theta}_{pre}$ indicates how much each basis function contributes to the estimate of the output. In Figure 4.20 a plot of $\mathbf{\Theta}_{pre}$ for surge force is shown.
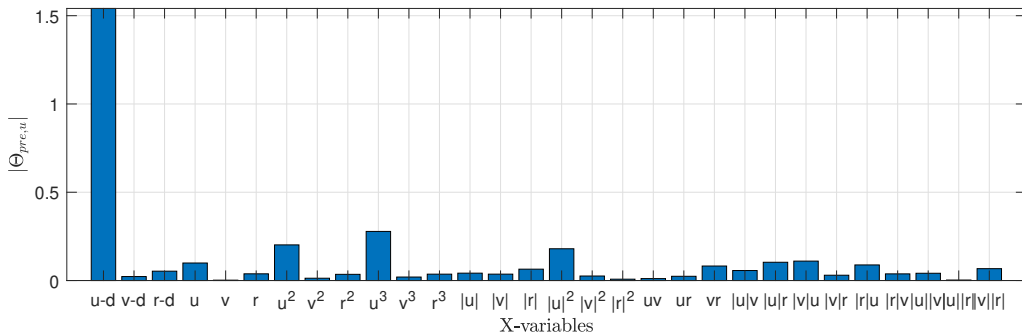
Figure 4.20: $\mathbf{\Theta}_{pre}$ from the PLSR analysis in surge force.

The basis function with the least effect is removed, which in this case is v, and the NIPALS algorithm is run again without this basis function. In addition to the complexity of the model being reduced, the model fit of the next PLSR model may be better or worse, evaluated by cross validation. By removing basis functions with little to no effect the analysis could give better estimation without taking into account data that does not contribute to explaining the output. For each specific model order it is done a PLSR while removing one basis function at the time, until there is only the two most influential basis functions left. Then the next model order is specified and all of the basis functions are reset. This is done for all model orders, and the MSE is logged for all the models created. This gives the opportunity for an interesting plot where the MSE from cross validation for each model order are visualized in a surface plot. From the surface plot the lowest point is given by the lowest MSE, and results in the model with best model fit in the cross validation. A surface plot of surge is shown in Figure 4.21. The minimum of the plot gives the model with best fit, without taking into account other factors. The model order can not be higher than the number of basis functions.

The surface analysis makes it possible to remove the basis functions with the least effect in the model, and see if this gives a better estimation through cross validation. This does not find the optimal selection of basis functions and model order, as that requires much more computational power. To find the optimum the problem becomes exponential depending on the number of inputs, and with 30 inputs this gives $30! = 2.6 \cdot 10^{32}$ possibilities and PLSR models to analyse. The surface analysis uses the knowledge from the previous PLSR model at that specific order to remove a basis function. The same basis functions are not necessarily removed for each model order, as they are weighted differently. Hence there are some model orders that find a more suited combination than other, as seen in the surface plot. The number of PLSR models needed to do the surface analysis is substantially reduced and results in $30^2/2 = 450$ analyses.
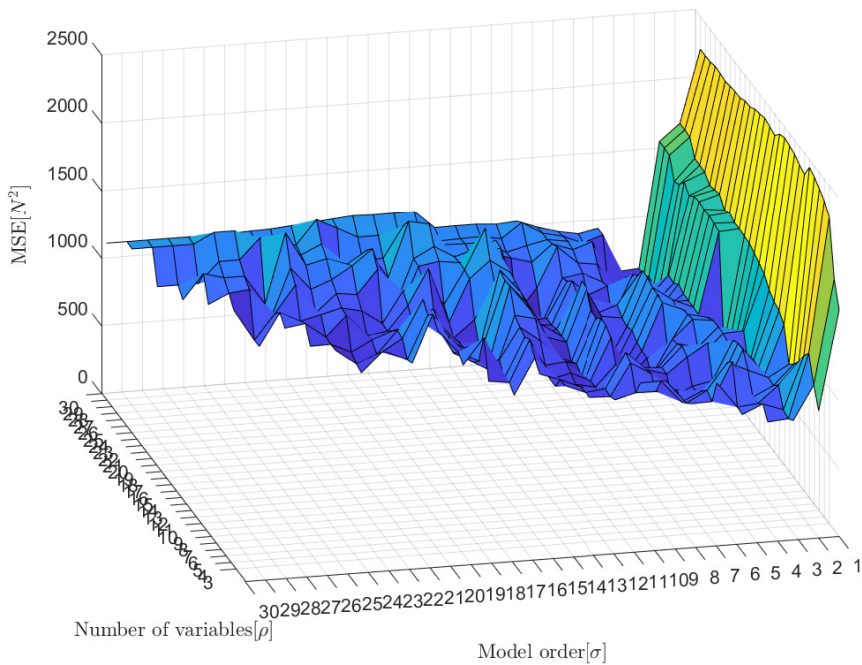
Figure 4.21: Surface plot of the MSE from the different PLSR models for surge.

4.5 Model analysis with PLSR
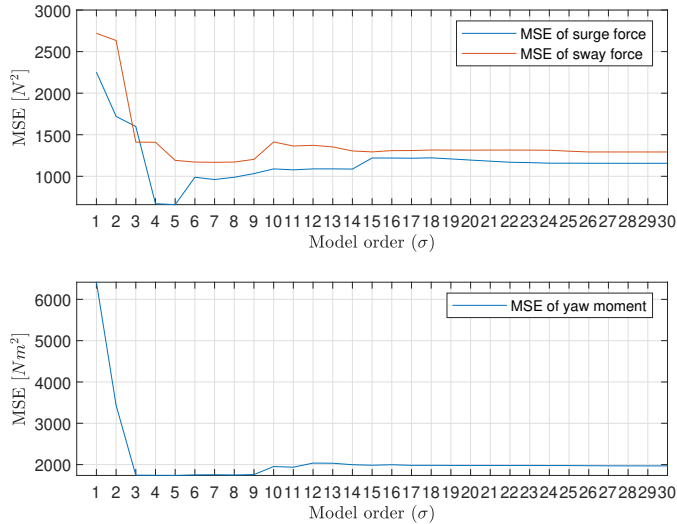
Figure 4.22: The MSE from the different model orders of the PLSR.

The residual between the ferry model and the true model is the output, that is modeled with the basis functions in (4.12). This analysis involves 30 basis functions and gives a much more complex model than the case in section 4.2. The NIPALS algorithm is run to do a PLSR, which gives the MSE for all model orders, shown in Figure 4.22. The optimal model order is a bit different for each state. The MSE from estimating sway force is reduced significantly from order 4 to 5. With $\sigma = 5$ the other states are also well estimated, so this model order is analysed further. In Figure 4.23 the PLSR model giving τ_{ϵ_0} is compared to the residual ϵ_0. The overall fit of the model is pretty accurate, although there are some spikes that is left unmodeled. This becomes more evident when comparing the residual ϵ_0 with the remaining residual after the PLSR model ϵ_1 in Figure 4.24. Big parts of the discrepancies in the ferry model is explained by the PLSR, although it is some of the dynamics that it is not able to capture. The reduction of the residual is seen in Table 4.5, where it also shows how the regular PLSR benefits from the basis functions that was not included in the case.

Table 4.5: The MSE of the residual with and without the PLSR model.

The residual ϵ	MSE of surge force	MSE of sway force	MSE of yaw force
Without PLSR model	2757.4 N^2	4337.7 N^2	7260.8 Nm^2
With case PLSR model	1036.0 N^2	1627.8 N^2	2565.8 Nm^2
With regular PLSR model	**659.2** N^2	**1191.6** N^2	**1737.4** Nm^2

Figure 4.23: The regular PLSR model $\boldsymbol{\tau}_{\epsilon_0}$ compared the residual $\boldsymbol{\epsilon}_0$.
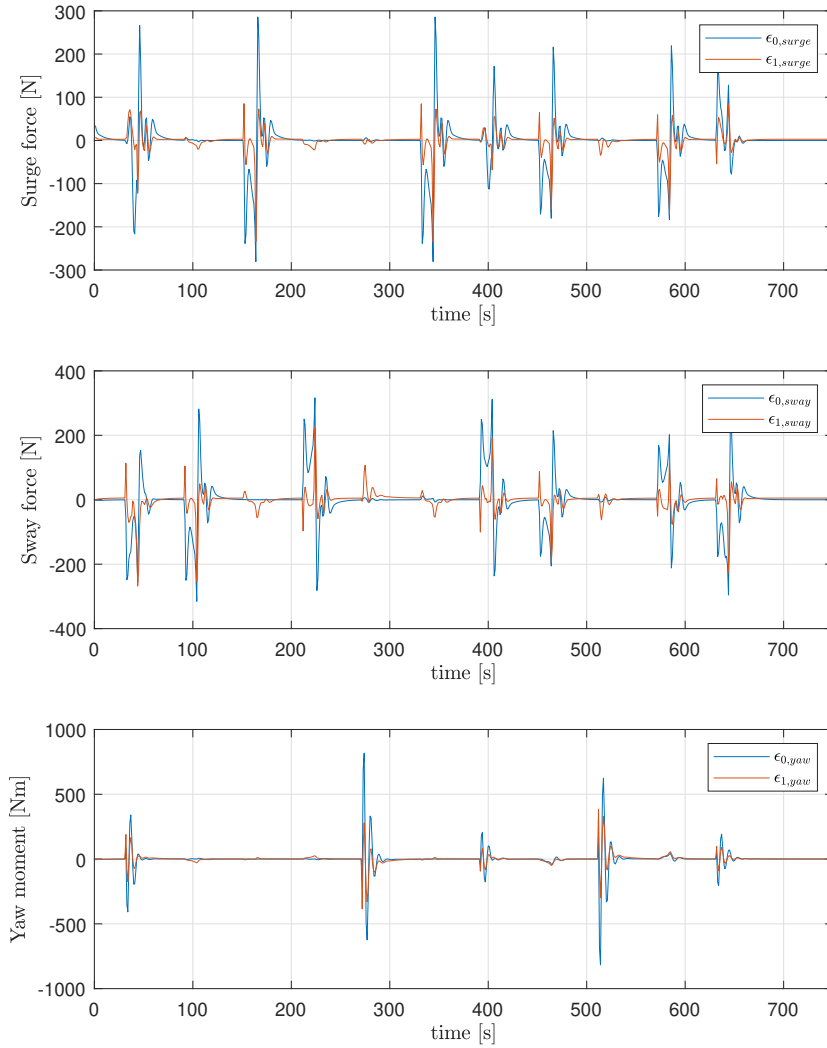
Figure 4.24: The initial residual ϵ_0 and the remaining residual ϵ_1 from the regular PLSR

4.5.1 Surface analysis

In the PLSR model the basis functions is weighted differently in $|\Theta_{pre}|$. In addition the model order deciding how many PC's that is included also effect how each basis function is weighted. Some of the basis functions affects the model less than other, and may be better off if removed from the analysis. From reducing the number of basis functions this gives the surface plot. The plot is shown from two angles for each state, showing the difference between the model orders in Figure 4.25 and the number of variables in Figure 4.26. By finding the minimum of the surface plot this gives the model order and number of basis functions that results in the smallest MSE when compared in the test set. The minimum found in the surface plots with the model order and number of basis functions giving the best model fit, is for each state is surge: $[\sigma, \rho] = [8, 18]$, sway: $[\sigma, \rho] = [22, 22$ and yaw: $[\sigma, \rho] = [18, 20]$. Even more of the residual is explained by these models, and the MSE is improved further as shown in Table 4.6.

Table 4.6: The MSE of the residual to the minimum of the surface plot.

The residual ϵ	MSE of surge force	MSE of sway force	MSE of yaw force
Without PLSR model	2757.4 N^2	4337.7 N^2	7260.8 Nm^2
With case PLSR model	1036.0 N^2	1627.8 N^2	2565.8 Nm^2
With regular PLSR model	659.2 N^2	1191.6 N^2	1737.4 Nm^2
With surface PLSR model	**487.1** N^2	**825.1** N^2	**1372.2** Nm^2

The MSE is very different between the different model orders, as the same basis functions are not necessarily removed for the same model order. The optimum from the surface plot has therefore found a good combination of basis functions and these basis functions are analysed further.
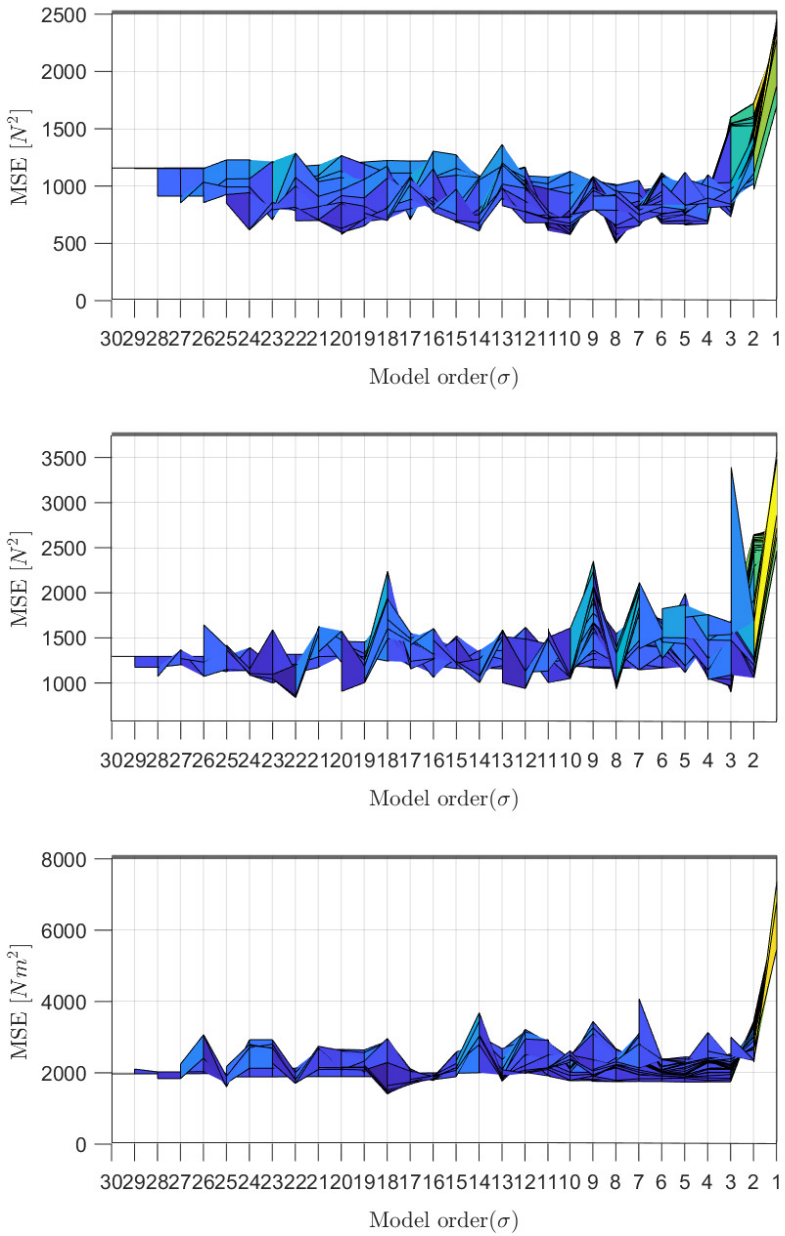
Figure 4.25: Surface plot of the MSE comparing the different model orders. Surge on the top, sway in the middel and yaw at the bottom.
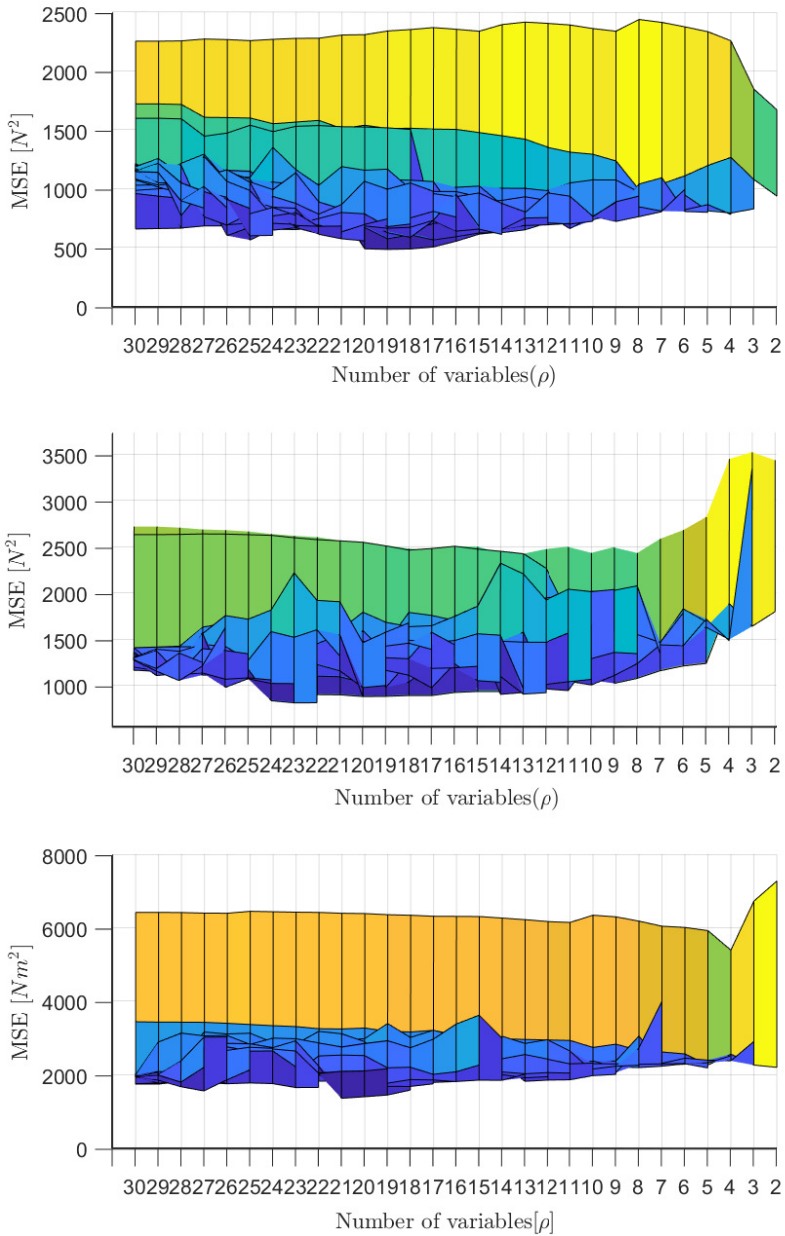
Figure 4.26: Surface plot of the MSE comparing the different number of basis functions. Surge on the top, sway in the middel and yaw at the bottom.

Model selection from surface analysis

When choosing a model order the chance of overfitting the model increases with a higher model order. From the surface analysis the optimal model order for each state is relatively high, and it is beneficial if this can be reduced. A new PLSR is done with the basis functions that correspond to the minimum of the surface plot. The MSE plot in Figure 4.27 shows that with these basis functions most of the residual is explained with model order $\sigma = 2$ for surge and yaw, and $\sigma = 4$ for sway. This reduces the model order considerably at the price of a model fit with slightly higher MSE. The PLSR model for surge and yaw with basis functions from the surface analysis and $\sigma = 2$ gives a MSE that is less than any other points in the surface plot with lower model order than the minimum. This is the selected model for surge and yaw. For sway the MSE of the PLSR models with $\sigma = 4$ is not the best fit when compared with the surface plot. In the surface plot for sway it is a local minimum at $\sigma = 3$ that has a smaller MSE. From visual inspection of the plot this minimum should be further analysed with the basis functions given at this minimum. The MSE is very similar between the minimum and the local minimum with the model order reduced substantially from 22 to 3. This point of the the surface plot for sway is analysed further with these basis functions for different model orders to see if 3 is the optimal model order. The MSE for sway in Figure 4.28 gives an even better result than simply analysing the minimum of the surface plot, and the selected model order for sway is also $\sigma = 2$.

The selected model order for all states is of model order $\sigma = 2$, with the MSE from the selected models shown in Table 4.7. The model fit of the selected PLSR model is shown in Figure 4.29, showing that most of the residual is modeled. In general the model fit is increased when the PLSR is done without basis functions that does not help explain the output. The method of using surface analysis to find how many basis functions to include in the model does result in a model with fewer basis functions and a smaller MSE, with a model order that is significantly lower than from the regular PLSR with all the basis functions or the minimum of the surface plot.

Table 4.7: The MSE of the remaining residual ϵ_1 from the selected model.

The residual ϵ	MSE of surge force	MSE of sway force	MSE of yaw force
Without PLSR model	2757.4 N^2	4337.7 N^2	7260.8 Nm^2
With case PLSR model	1036.0 N^2	1627.8 N^2	2565.8 Nm^2
With regular PLSR model	659.2 N^2	1191.6 N^2	1737.4 Nm^2
With surface PLSR model	**487.1** N^2	**825.1** N^2	**1372.2** Nm^2
With selected PLSR model	634.7 N^2	894.2 N^2	1563.2 Nm^2
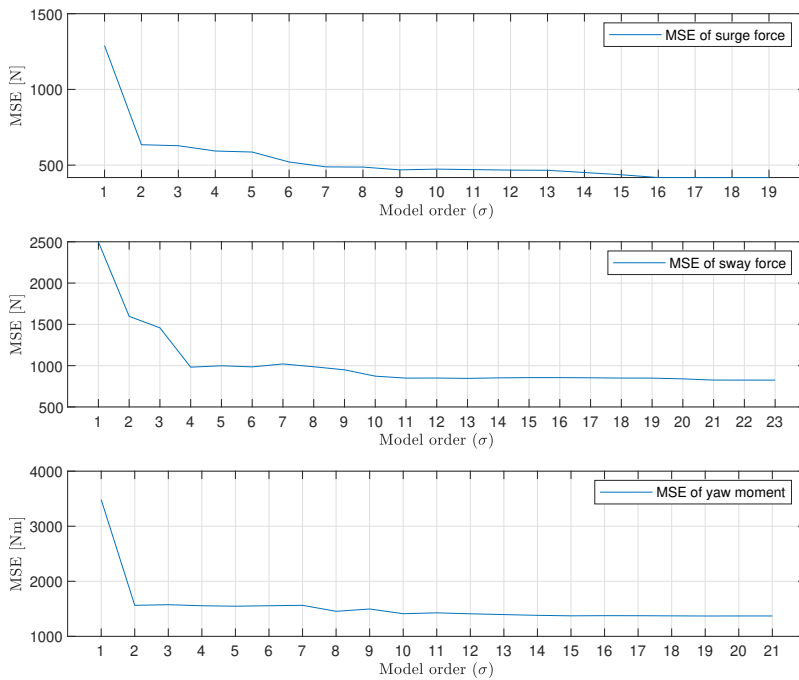
Figure 4.27: The MSE with the basis functions of the minimum in the surface plot. The MSE of the optimal model order of sway does not satisfy, and is reevaluated.
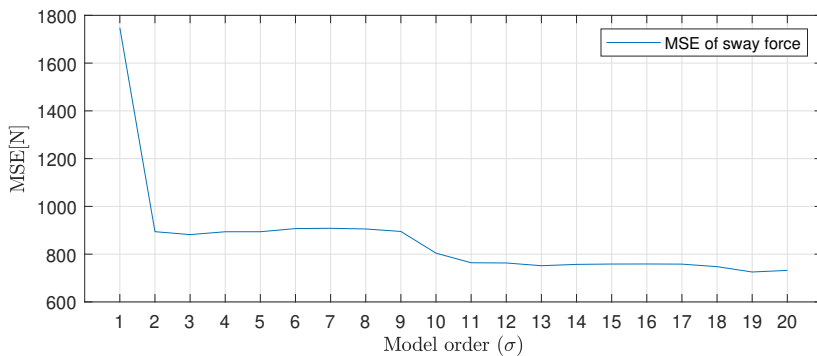
Figure 4.28: The MSE of sway force with the basis functions found from visual inspection of the surface plot. The selected model for sway is found from this selection of basis functions at model order 2.
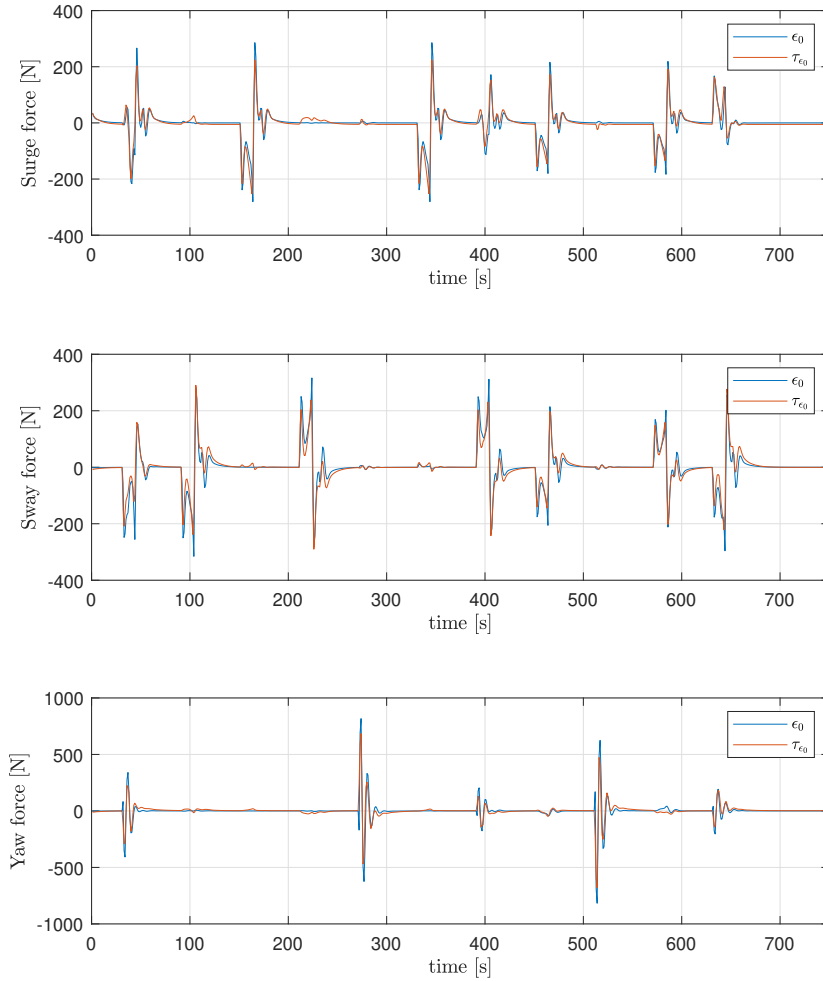
Figure 4.29: Model fit of the selected PLSR model by comparing the estimated residual τ_{ϵ_0} and the residual ϵ_0.

4.5.2 Implementation in the controller

The selected PLSR model is implemented in the FF controller on the form

$$\boldsymbol{F}_1(\dot{\boldsymbol{\nu}}_d, \boldsymbol{\nu}_d) = \boldsymbol{F}_0(\dot{\boldsymbol{\nu}}_d, \boldsymbol{\nu}_d) + \boldsymbol{\Theta}\boldsymbol{\Phi}^T(\dot{\boldsymbol{\nu}}_d, \boldsymbol{\nu}_d), \tag{4.13}$$

where $\boldsymbol{\Phi}^T(\dot{\boldsymbol{\nu}}_d, \boldsymbol{\nu}_d) = [1, \boldsymbol{X}]$ and $\boldsymbol{\Theta} \in \mathbb{R}^{3\times31}$. The regression coefficients in $\boldsymbol{\Theta}$ that correspond to basis functions that are removed from the analysis are set to zero. As in the case, the trajectory is run without the FB term included in the controller to see how the velocity and acceleration follows the desired trajectory. This is shown in Figure 4.30. In general the PLSR model follows the changes of the desired trajectory better, while the model of the coupling between the states are estimated worse. Hence the deviation when the desired trajectory is zero is increased. Comparing the results to the case, the MSE from the trajectory of each state is in Table 4.8. For surge and sway the acceleration has more deviance than in the case, while the velocity is followed better. For yaw the performance for both velocity and accelereation follows the trajectory worse than the case, and also the initial FF. The inclusion of all of the basis functions, where several of them are not included in the model for all states, does so the PLSR also includes more basis functions in the model. The small contribution from some of the terms are hard to identify and this creates the deviance from some of the basis functions. Especially yaw which is affected by the most terms is difficult to estimate accurately. The PLSR model does give a better estimate of the large deviations at the cost of creating other smaller errors when modeling this complex model of the ferry.

Table 4.8: The MSE from the desired trajectory for velocity and acceleration without FB term.

FF model	MSE of u	MSE of v	MSE of r	MSE of $\dot{u}$	MSE of $\dot{v}$	MSE of $\dot{r}$
$\boldsymbol{F}_0$	0.056 m/s	0.060 m/s	**0.001** deg/s	0.0011 m/s^2	0.0009 m/s^2	0.0001 deg/s^2
Case $\boldsymbol{F}_1$	0.060 m/s	0.052 m/s	0.005 deg/s	**0.00053** m/s^2	**0.00058** m/s^2	**0.000054** deg/s^2
$\boldsymbol{F}_1$	**0.046** m/s	**0.050** m/s	0.010 deg/s	0.00087 m/s^2	0.00083 m/s^2	0.000075 deg/s^2

With the FB term contributing, the performance of the controller is improved. How much the FB term is used gives an indication of how much compensation is needed in addition to the FF. This is compared with and without the selected PLSR in Figure 4.31. This shows how much less is needed from the FB term to keep the ferry on the trajectory. The parts where the initial FB is used actively the usage of the FB with the PLSR model has been reduced. The small modeling errors are seen by the FB compensating in places where the initial FB controller is not used. These model descrepancies is still so small that the overall usage of the FB controller is reduced significantly as shown by the mean usage in Table 4.9.
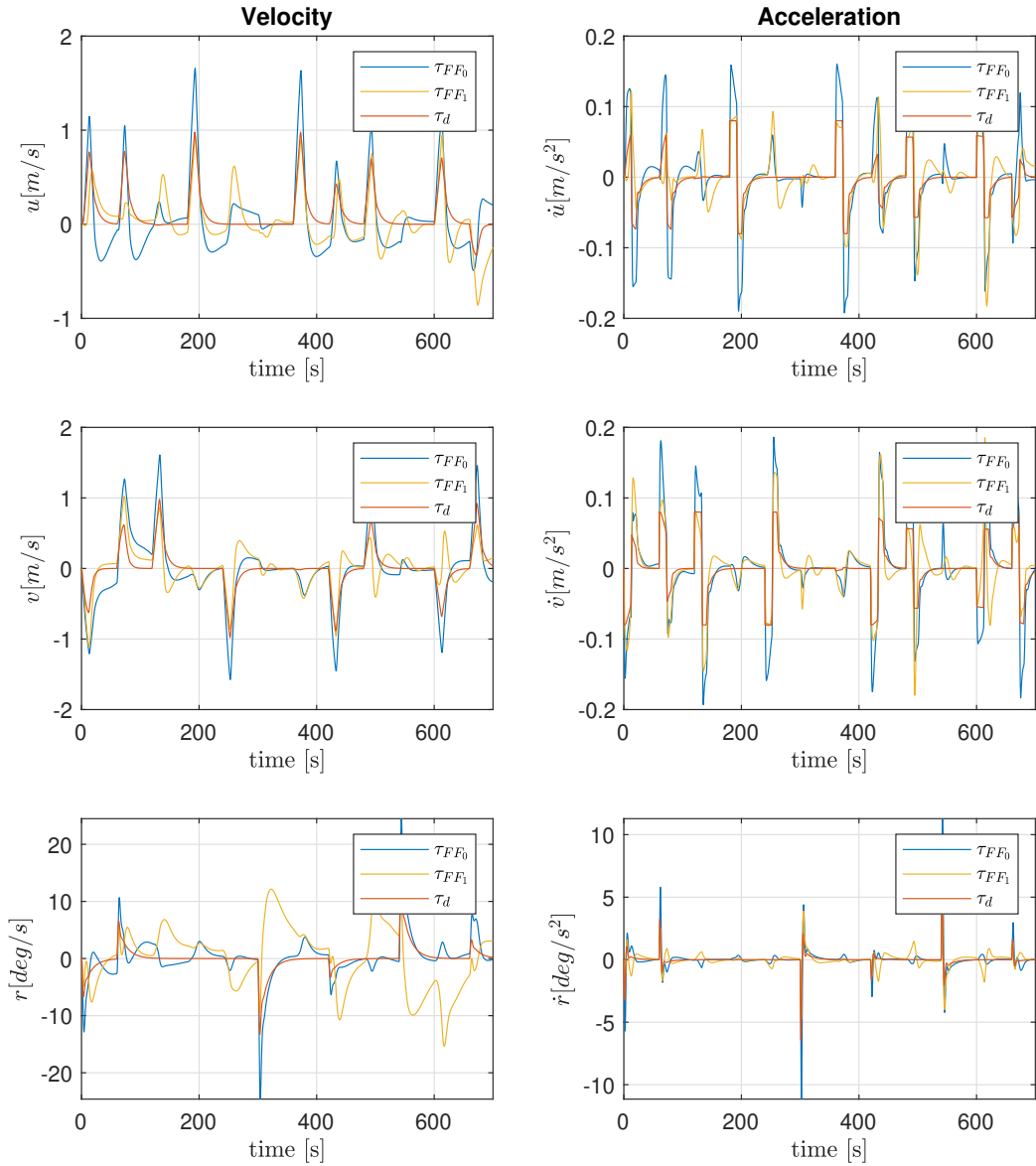
Figure 4.30: The control input without FB term compared with selected PLSR model.
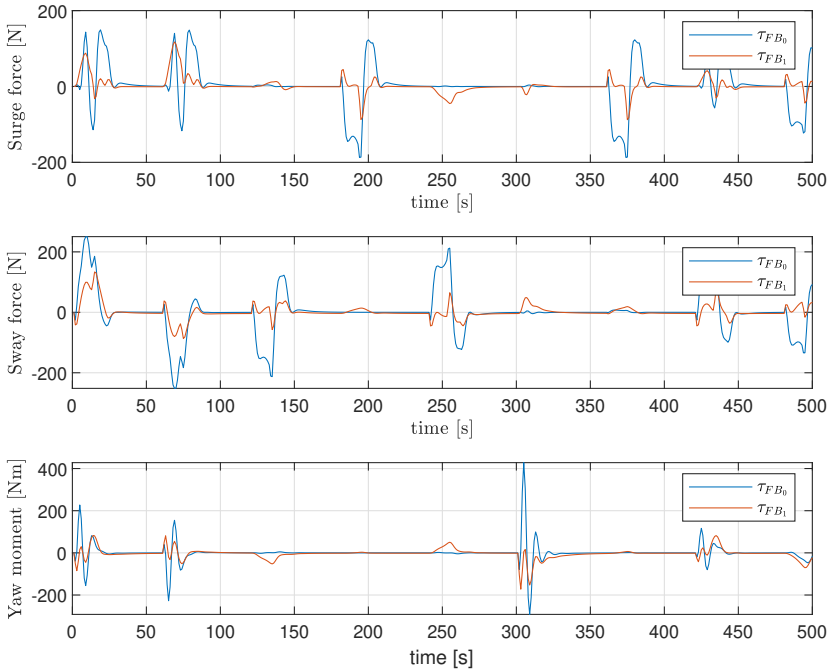
Figure 4.31: The control input of the FB compared where blue line is the original FB and orange is with the selected PLSR model in the controller.

This is further emphasizes in Figure 4.32, where the total usage of the control input is compared to the total usage of the FB term with and without the PLSR model. For surge and sway the FB term contributes much less to the total control input after improving the model in the FF. In yaw the FB term is decreased, however it still contributes to a large part of the control input. This shows the difficulties of modeling yaw as the complexity of this state is higher.

The performance of the ferry is seen by the positional error e_{pos} in Figure 4.33. This shows that the deviations are reduced significantly as most of the error is less than $0.2m$. There are more oscillations around the desired point than with the initial model, however the deviations are much smaller. In addition this increased correction from including the PLSR model does not increase the usage of the control input as seen in Table 4.9. This results in an improved positional performance shown in Table 4.10 with the MSE and the MAE of the positional error. Both have been reduced compared to the initial model and the PLSR model from the case. The implemented PLSR model together with the FB controller gives a much better tracking performance, as the large deviations are handled better by the FF, while the smaller deviations created by the PLSR model is handled easier by the FB term.

Table 4.9: The mean usage of the control input τ and the FB term τ_{FB} with and without the PLSR model.

State	Without PLSR model		With case PLSR model		With PLSR model	
	control input τ	FB τ_{FB}	control input τ	FB τ_{FB}	control input τ	FB τ_{FB}
τ_u	22.2 N	24.0 N	20.6 N	14.7 N	**20.4** N	**9.38** N
τ_v	30.3 N	30.7 N	28.4 N	17.6 N	**27.3** N	**12.5** N
τ_r	19.5 Nm	14.6 Nm	12.8 Nm	**10.8** Nm	**10.2** Nm	12.9 Nm

The heading error in Figure 4.34 is not improved as much as the positional error, due to the complexity and modeling errors in yaw. There are significant errors that do occur in the heading that does not occur without the PLSR model. The largest deviations have been reduces which is why the MSE of the heading error in Table 4.10 is reduced, while the MAE of the heading error has increased slightly.

Table 4.10: Positional and heading error with and without PLSR model.

Model	MAE of e_{pos}	MSE of e_{pos}	MAE of e_ψ	MSE of e_ψ
Without PLSR model	0.22 m	0.107 m^2	0.80 deg	0.014 deg^2
With case PLSR model	0.12 m	0.027 m^2	**0.62** deg	**0.0004** deg^2
With PLSR model	**0.086** m	**0.016** m^2	0.91 deg	0.0007 deg^2
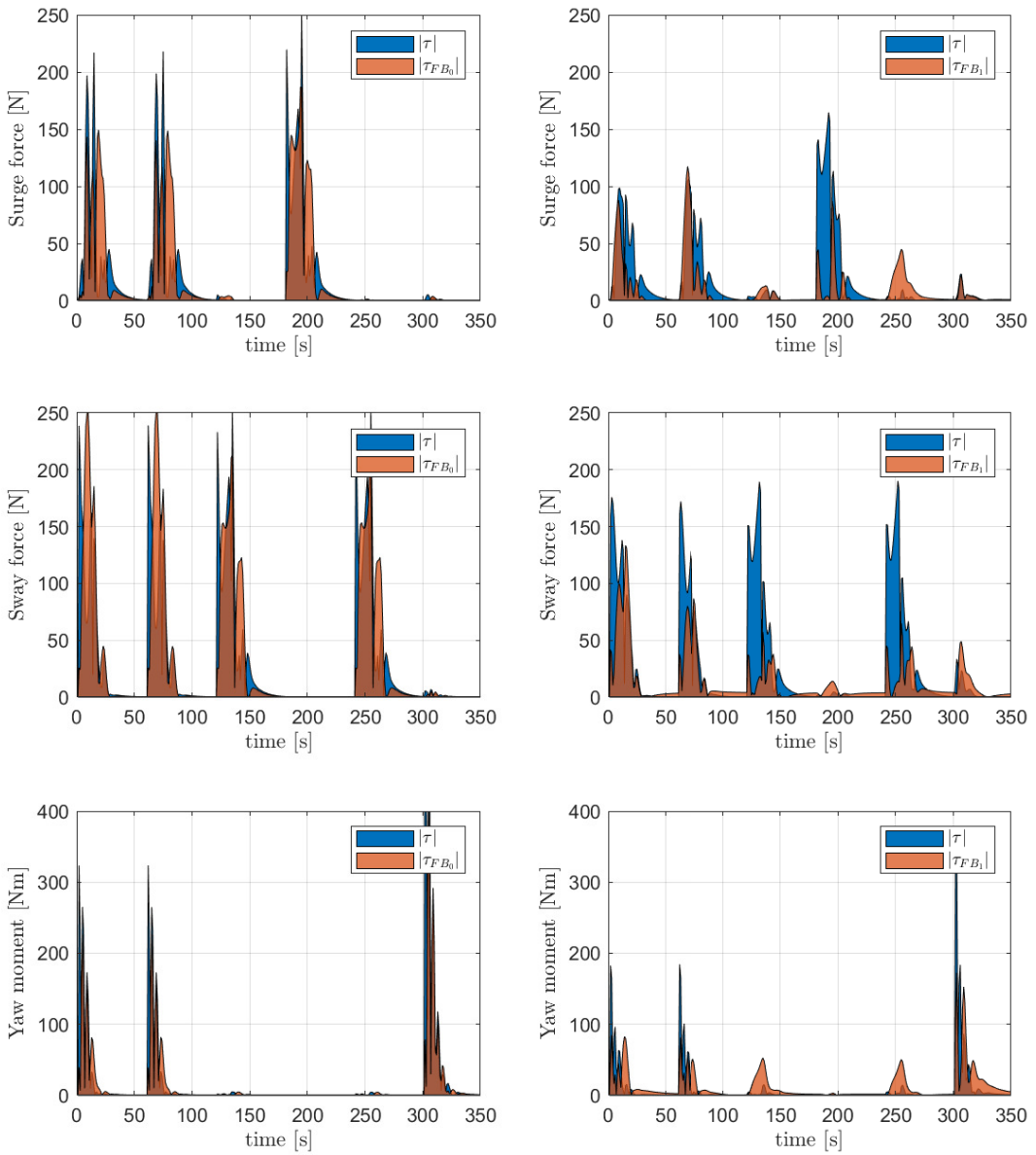
Figure 4.32: The total control input and the total FB compared, without the PLSR model to the left, and with PLSR model to the right.
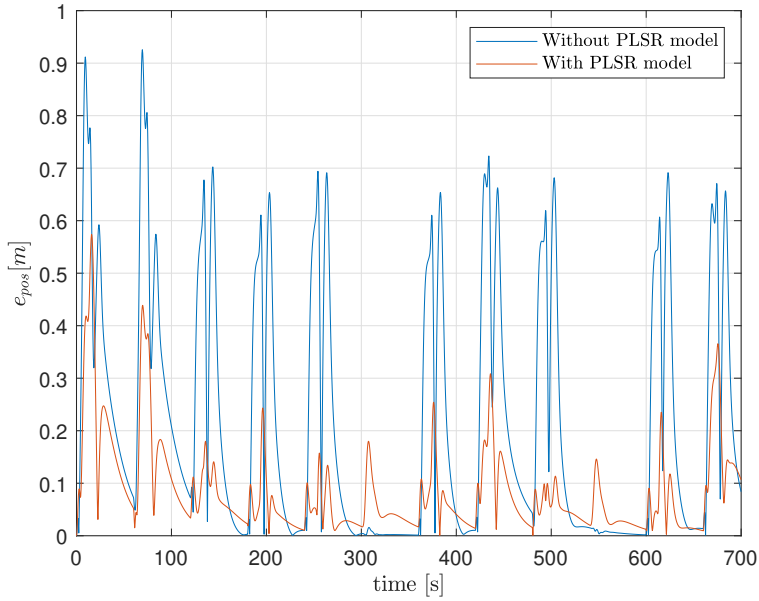
Figure 4.33: The positional error with and without the PLSR model.
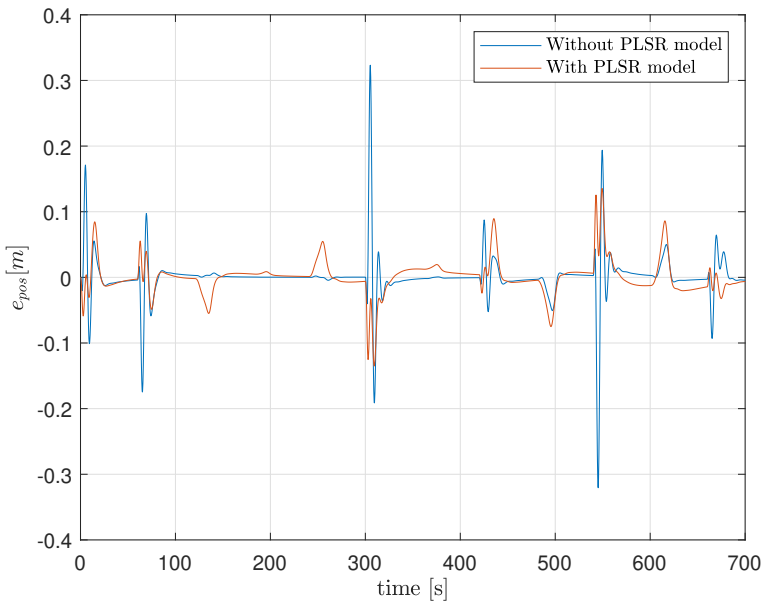
Figure 4.34: The heading error with and without the PLSR model.

4.5.3 Model comparison

The PLSR model is compared to the true model of the residual in Table 4.11. This shows that the acceleration coefficients are close to the true model. These are very dominant in the residual and are captured pretty good by the PLSR model. Other basis functions like $|r|r$ has also been captured to some degree for yaw, while other large parameters that are in the true model has not been captured, as with ur and vr. It does show that there are modeling errors with the PLSR model, and that most of the basis functions that are included in the analysis are fitted in the model, even if the effect is small. It gives a significant improvement when included in the controller, and it does explain the collected data better than the initial model. This shows that it is able to improve the model for the conditions that the data is collected, while the modeling errors will becomes more evident if the ferry is operated outside the limits of the collected data.

Table 4.11: Comparison of the estimated PLSR model and the true model of the residual.

Basis function	Estimated PLSR model			True model of the residual		
	Surge, Θ_u	Sway, Θ_v	Yaw, Θ_r	Surge, Θ_u	Sway, Θ_v	Yaw, Θ_r
1	0.83	5.61	1.57	0	0	0
$\dot{u}$	-1228.96	0	0	-1194.83	0	0
$\dot{v}$	0	-1173.96	0	0	-1266.96	-14.07
$\dot{r}$	0	0	-2469.48	0	-31.19	-2534.45
u	-17.15	0	0	-13.82	0	0
v	-18.39	-61.88	32.23	0	-26.47	1.76
r	0	125.87	-518.30	0	12.37	-61.43
$|u|u$	-14.71	-1.05	-3.95	-55.03	0	0
$|v|v$	-4.59	-29.70	12.03	0	-58.24	-0.42
$|r|r$	0	220.73	-625.80	0	-57.73	-437.21
u^3	-11.04	0	0	-6.98	0	0
v^3	-1.49	-18.32	5.97	0	-12.16	0
r^3	34.83	0	-800.46	0	0	0
$|u|$	-7.83	-22.62	0	0	0	0
$|v|$	15.22	-7.78	0	0	0	0
$|r|$	0	-18.39	0	0	0	0
u^2	-13.45	-4.04	0	0	0	0
v^2	1.59	-3.10	-0.61	0	0	0
r^2	0	-22.46	0	-62.39	0	0
uv	0	-11.50	4.88	0	0	144.25
ur	0	-57.05	57.15	0	2389.66	62.39
vr	100.66	0	16.58	-2533.91	0	0
$|u|v$	-8.14	-26.77	13.52	0	0	0
$|u|r$	-18.53	-132.58	48.39	0	0	0
$|v|u$	-7.77	6.86	-13.47	0	0	0
$|v|r$	0	-257.79	-98.28	0	-572.14	121.96
$|r|u$	0	0	-82.19	0	0	0
$|r|v$	0	-329.13	-21.50	0	-1540.38	336.83
$|u||v|$	-1.09	0	-4.36	0	0	0
$|u||r|$	24.98	-63.21	-78.25	0	0	0
$|v||r|$	99.56	0	-1.55	0	0	0

4.5.4 Controller performance with simulated operation
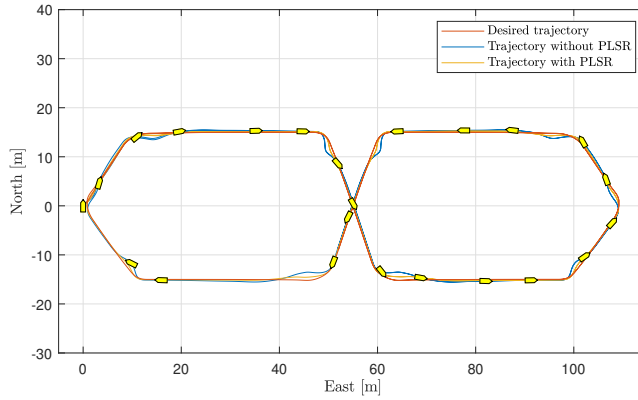
Figure 4.35: The new trajectory simulating operational conditions for the ferry.

The trajectory performed when collecting data is designed to excite all states to get a better system identification. The trajectory does, however, not resemble how the ferry is normally operated. To get an indication of the effect of implementing the PLSR model in the controller when in normal operation, a new trajectory is simulated. The new trajectory simulates operation between two docks with a change of direction that could be needed to avoid an obstacle. This trajectory is continuous by getting new waypoints from the LOS guiding system, and the simulated operation is shown in Figure 4.35. By looking at the positional error in Figure 4.36 it is evident that the improvement still is significant with a new trajectory. The positional error is reduced for all stages of the operation. With the continuous course from the LOS guidance system the reference filter receives a smoother signal, as for the system identification trajectory the movement is more distinct to excite the system. The same is seen for the heading error in Figure 4.37, as the controller keeps the desired heading much better with the PLSR model. This shows that most of the lack-of-fit residual is modeled by the PLSR. Even with the new trajectory the model still gives a significant improvement, and the model discrepancies does not affect the performance very much. The difference with and without the PLSR model is shown by the MAE and MSE for positional and heading error in Table 4.12.

Table 4.12: Positional and heading error with and without PLSR model for the simulated operation.

Model	MAE of e_{pos}	MSE of e_{pos}	MAE of e_ψ	MSE of e_ψ
Without PLSR model	0.42 m	0.30 m^2	1.13 deg	3.84 deg^2
With selected PLSR model	**0.20** m	**0.07** m^2	**0.62** deg	**0.66** deg^2
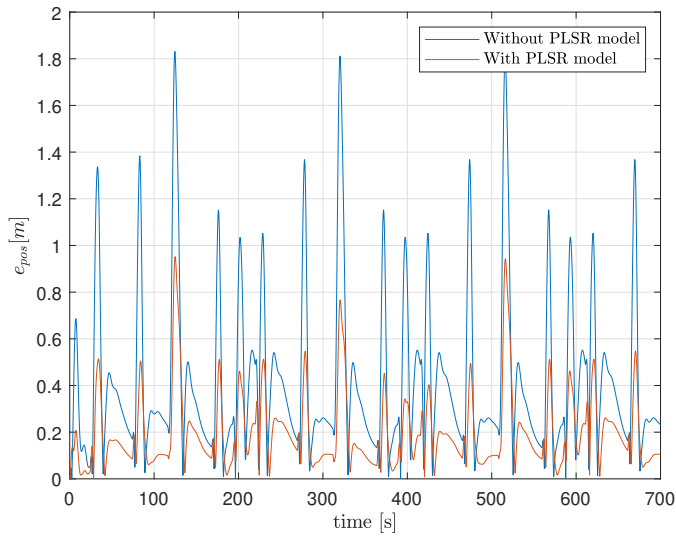
Figure 4.36: The positional error from the simulated operation.
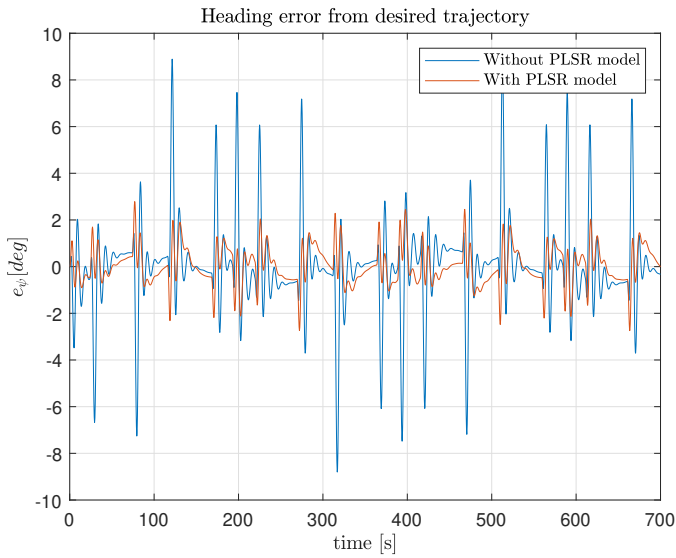
Figure 4.37: The heading error from the simulated operation.

Another way to compare the controllers is by looking at the energy consumption. This shows if the use of control input is increased to keep a more accurate trajectory. For a fully electric ferry this could make a big difference to how long the ferry is able to operate before charging. A small error reduction may not be beneficial if it requires much extra energy. The difference in energy consumption is shown in Table 4.13. To compare the evident difference between the controllers the cumulative error and work is combined with the IAEW metric. The implementation of the PLSR model also makes the ferry run more efficiently. The positional error and work is shown in Figure 4.38 and the heading error and work is shown in Figure 4.39. This shows that the implementation of the PLSR model is superior to the initial controller.

Table 4.13: The average work done for keeping the position and heading in the simulated operation.

Measurement	Without PLSR model		With PLSR model	
	Position	**Heading**	**Position**	**Heading**
Energy consumption	53.5 W	1.93 W	**45.9** W	**0.94** W
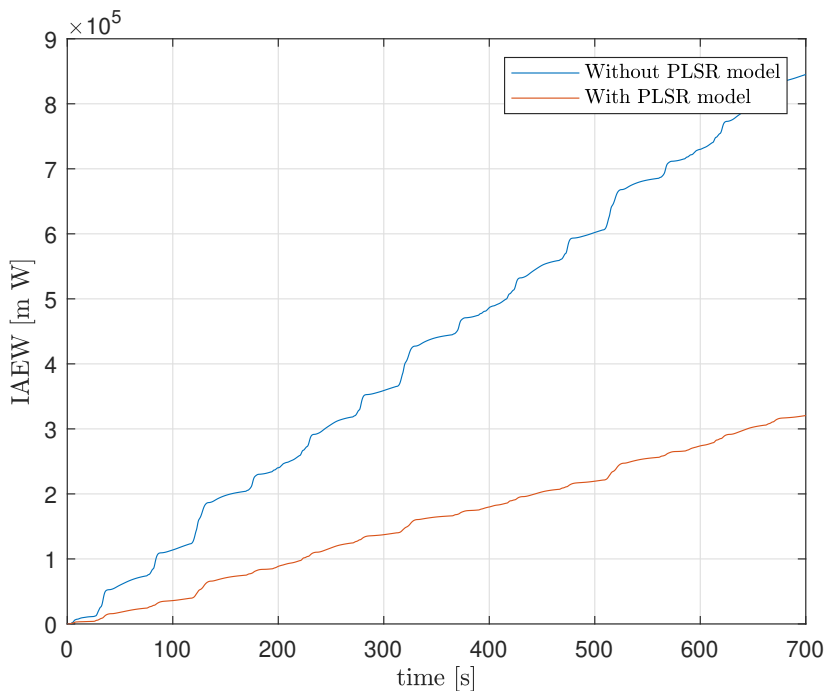
Figure 4.38: The cumulative error and work shown with the IAEW for the position.
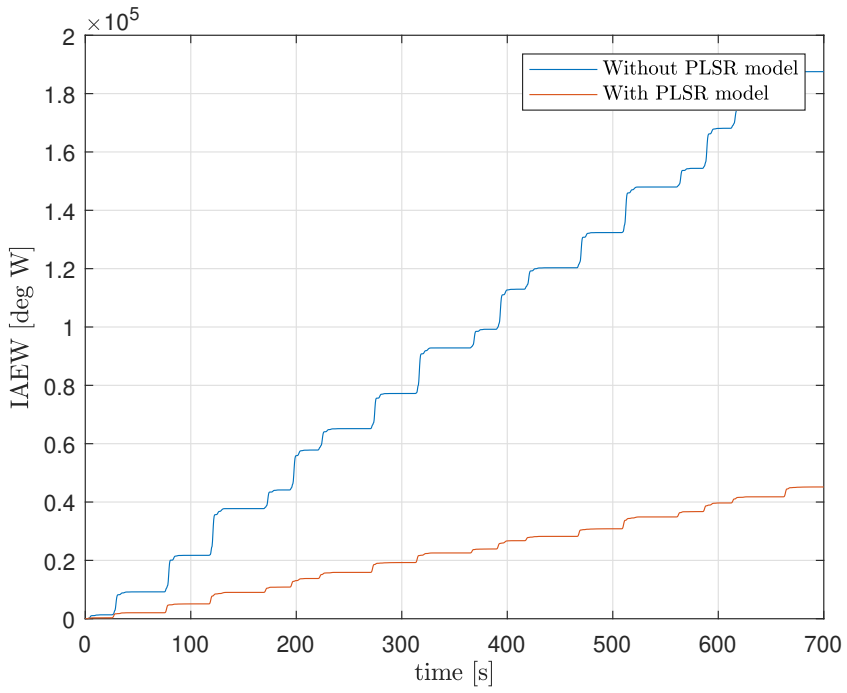
Figure 4.39: The cumulative error and work shown with the IAEW for the heading.

4.6 Simulation with noise

The measurements are affected by noise in different ways. All the equipment that does measurements are inflicted with a variance in the estimation, from the GNSS to the IMU. In addition the signals contains white noise from the cables and electricity on board. Hence the system identification is tested with added noise to the different states. Previously the signals are filtered on the ferry with an error state kalman filter (ESKF), and noise from the different states are plotted in (Sæther, 2019). This gives an approximation of the amplitude of the noise each state is subject to. The measurement noise is simulated as a Gaussian process with zero mean. The standard deviation for each state is shown in Table 4.14.

Table 4.14: Standard deviation of the noise added to each state.

States	Standard deviation
x	0.02 m
y	0.02 m
ψ	0.2 deg
u	0.05 m/s
v	0.05 m/s
r	0.2 deg/s
$\dot{u}$	0.01 m/s^2
$\dot{v}$	0.01 m/s^2
$\dot{r}$	0.1 deg/s^2

The noise influences the input signal to the thrusters. The thrusters are not able to follow all the rapid movement caused by the noisy signals, so this is prevented by the dynamics of the thrusters given in subsection 4.1.2. If the noise added to the output states are transferred through the feedback controller and directly into the ferry, the noise in the control input will cause movement. This correlation between the noise and the movement gives more accurate system identification, through exciting each state more. This is not how the noise would act on real measurements, hence the implementation of the lowpass filter results in more realistic simulations. The surge force from the controller is compared before and after the thruster dynamics in Figure 4.41. The time horizon is reduced to better see the changes. The state measurements are subject to substantial noise as shown in Figure 4.40, with the same trajectory as in Figure 4.1.
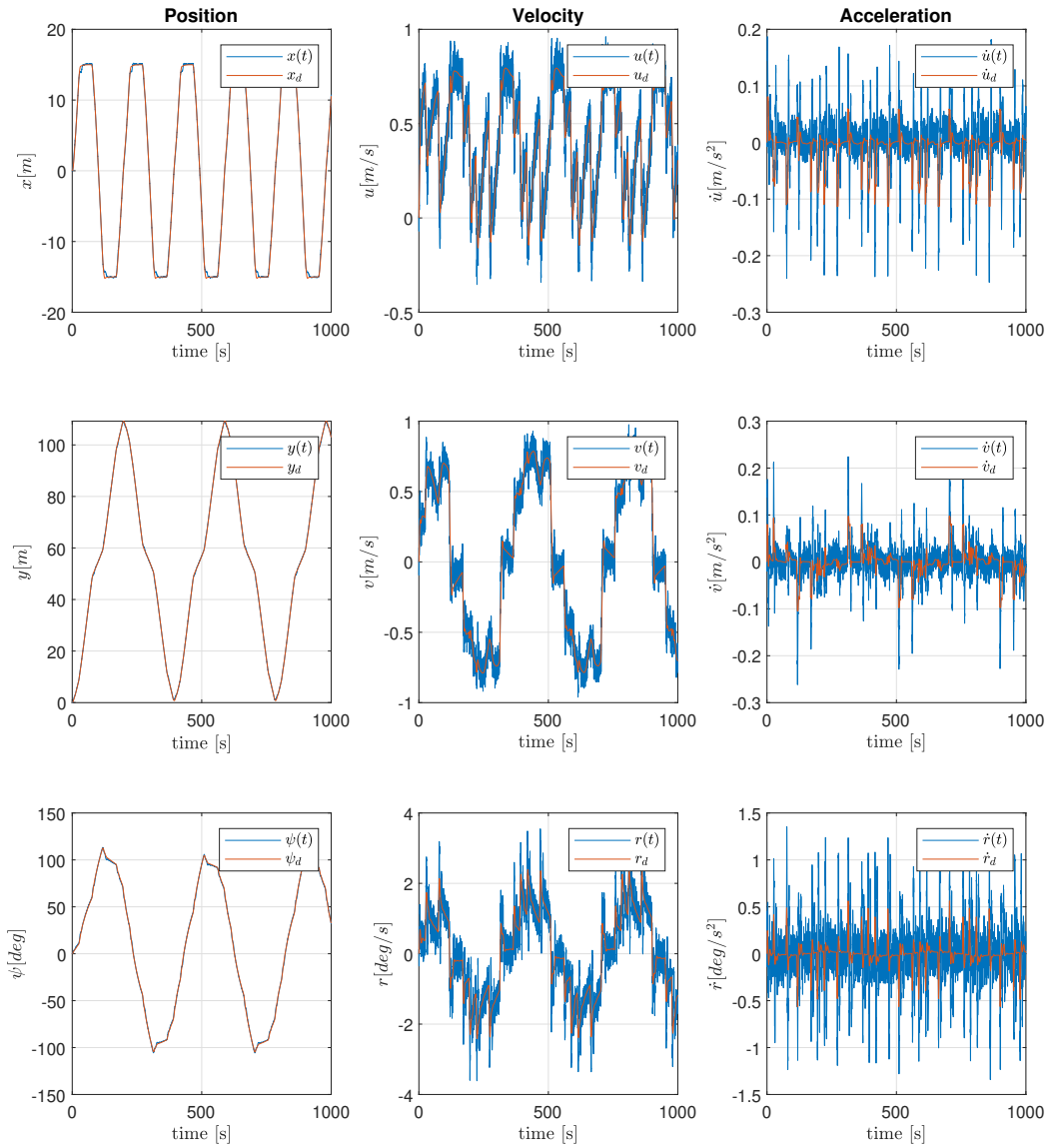
Figure 4.40: The measurements of each state inflicted with noise.
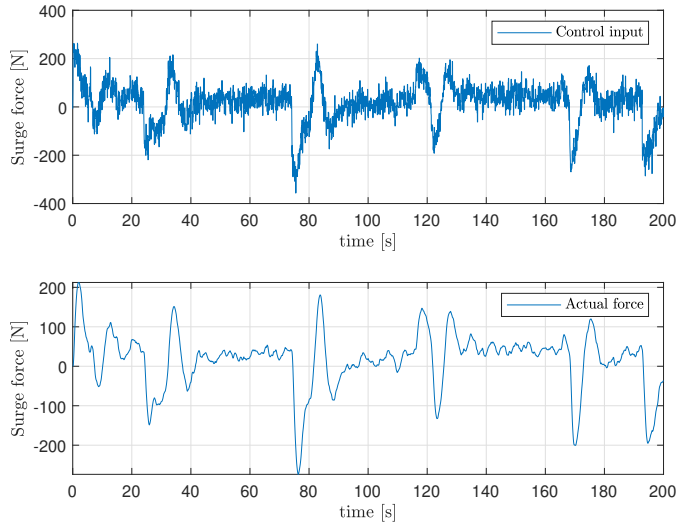
Figure 4.41: The difference between the control input and the actual force with noise.

The MSE from the PLSR models is shown in Figure 4.42. The MSE for the estimations has increased overall, which is expected. With noise it should not be possible for the PLSR to explain all the data, as the noise is uncorrelated with any of the basis functions. In addition the models with higher order and more basis functions is more easily overfitted. The model then tries to explain the noise in the data, which is different in the test set. This gives an increased MSE when comparing the models to the test data.

Even with a substantial noise the PLSR is able to find a model improving the fit. A model is chosen from the model order that gives least MSE for each state, without taking into consideration complexity and overfitting in this analysis. In Figure 4.43 the estimated residual τ_{ϵ_0} is compared to the residual ϵ_0. The plot shows half of the test set to make it easier to compare. The model tracks the residual, and most of the large changes are explained. The small oscillations in the residual ϵ_0 caused by the noise is almost filtered out by the model, but with the same structure, as shown in Figure 4.43 from 20 to 60 seconds in the surge force.

By adding the model of τ_{ϵ_0} to the initial model, the improved residual ϵ_1 is given. In Figure 4.44 the improvement of the residual from ϵ_0 to ϵ_1 is shown. Ideally the residual should only consist of a white, zero mean noise that is left unmodeled, and ϵ_1 in the plot comes very close to this. Hence the estimated model for τ_{ϵ_0} was still pretty accurate despite the noise added to the signals. The MSE of the signals in Table 4.15 shows that the error is reduced substantially.
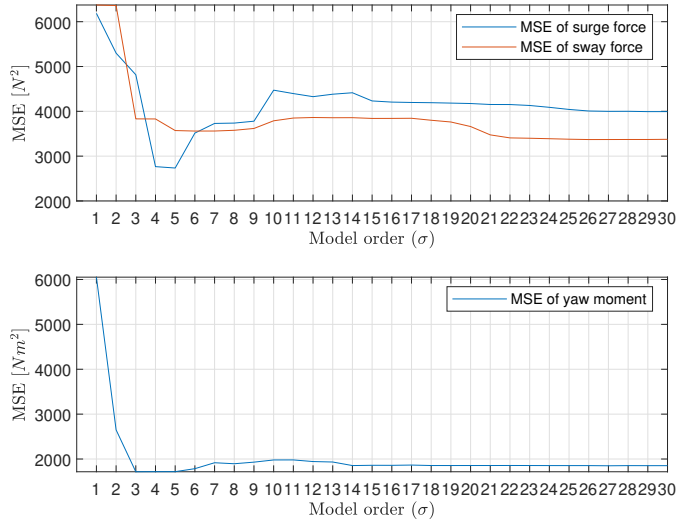
Figure 4.42: The MSE of the different model orders with noise.

Table 4.15: The MSE of the residual with and without the PLSR model with noise.

The residual ϵ	MSE of surge force	MSE of sway force	MSE of yaw force
Without PLSR model	6986 N^2	8878 N^2	7538 Nm^2
With PLSR model	**2766** N^2	**3830** N^2	**1718** Nm^2
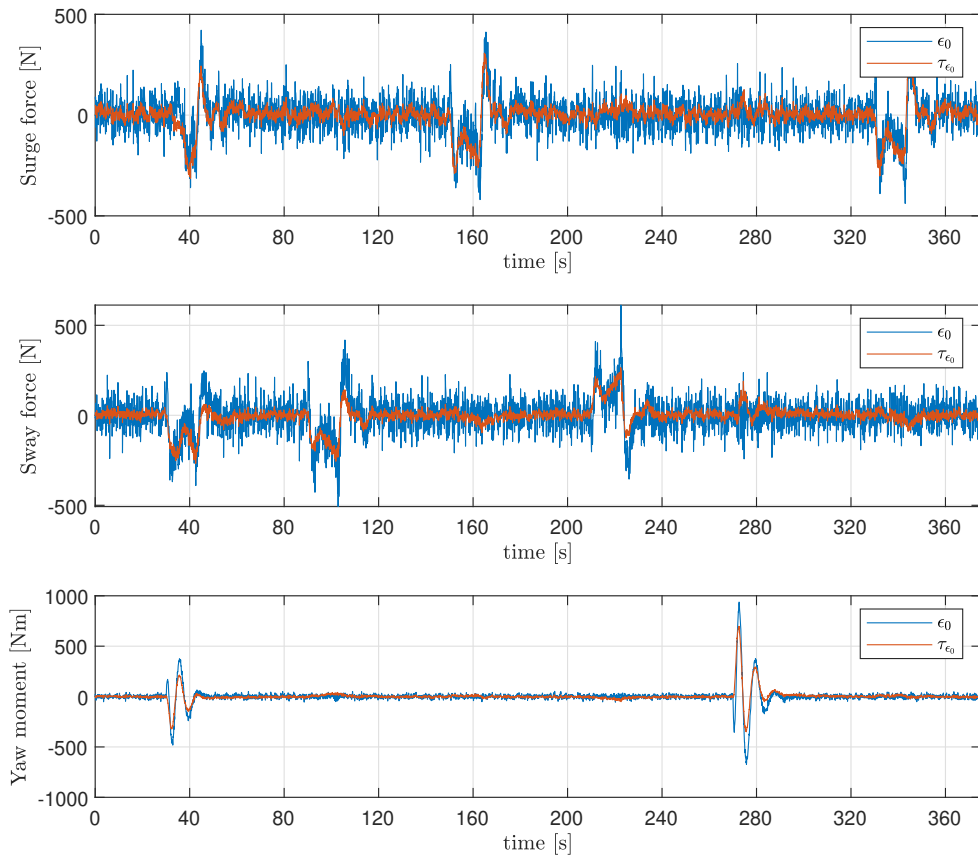
Figure 4.43: Estimation of the control input with PLSR subject to noise.
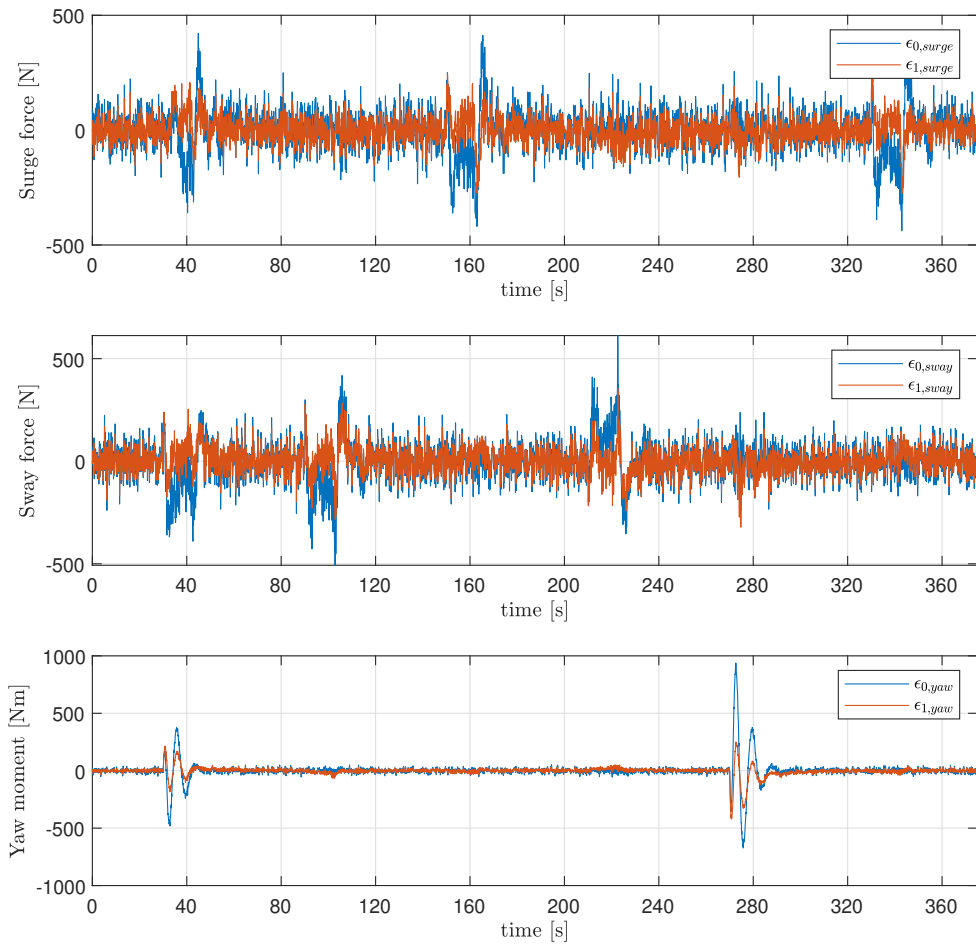
Figure 4.44: Remaining residual after implementation of PLSR model.

4.7   Constant disturbance

The ferry is subject to external disturbances when operating in the ocean. This can come from sea currents and wind force, which is not measured. A constant disturbance is added to the simulation to test how it effects the analysis. The constant disturbance is implemented in the NED frame. This gives a disturbance force working in the same direction for the whole simulation, independent of which direction the ferry is moving or heading. Since the ferry is moving in both directions when simulating, the disturbance is not neglected as the data is scaled to zero mean before analysed. The disturbance force is implemented as shown in Table 4.16. No constant disturbance is implemented to the heading as it is not likely for any external forces to apply such a force, as a wind force is dependent of the heading of the ferry. A constant yaw moment results in a constant error which the NIPALS algorithm would scale to zero mean, and add to the constant term of the model afterwards.

Table 4.16: External force implemented as a constant disturbance in NED

State	Disturbance
x	200 N
y	100 N
ψ	0 Nm
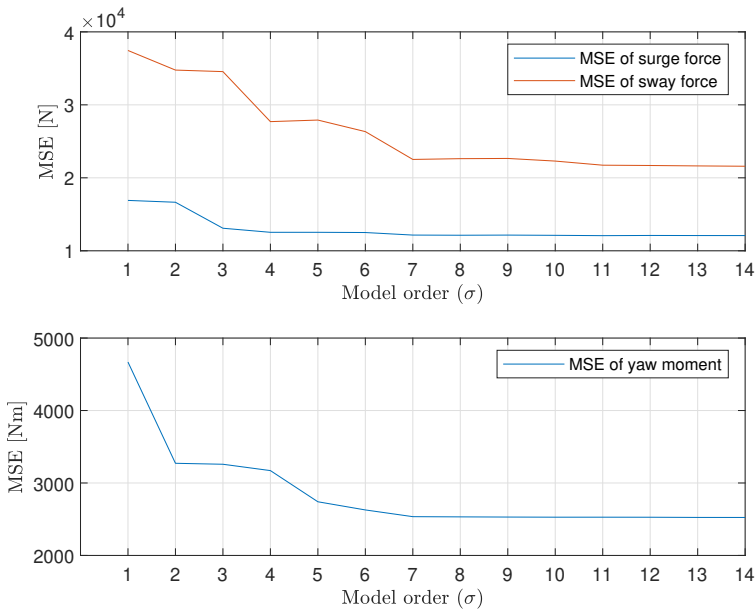
Figure 4.45: The MSE for the different model orders with constant disturbance.

The MSE from the PLSR with the selected basis functions is shown in Figure 4.45. The goal of this simulation is to see how the algorithm deals with the constant disturbance, so for simplicity reduction of basis functions and surface analysis is not done. The MSE indicates that a model of order $\sigma = 7$ gives the best fit without complicating the model more then necessary. A comparison of τ_{ϵ_0} and ϵ_0 is done in Figure 4.46. In surge and sway force it is a deviation between the signals that is caused be the disturbance, and as the ferry changes direction this matches with the deviations changing direction as well. The form of τ_{ϵ_0} and ϵ_0 are very similar as they almost have the same oscillations. There is nothing in the data that can explain the constant disturbance, and it is positive that the analysis does not try to use the data to get the output to fit the disturbance. Instead it analyses which basis functions that has a variance that can explain the variance in the output.
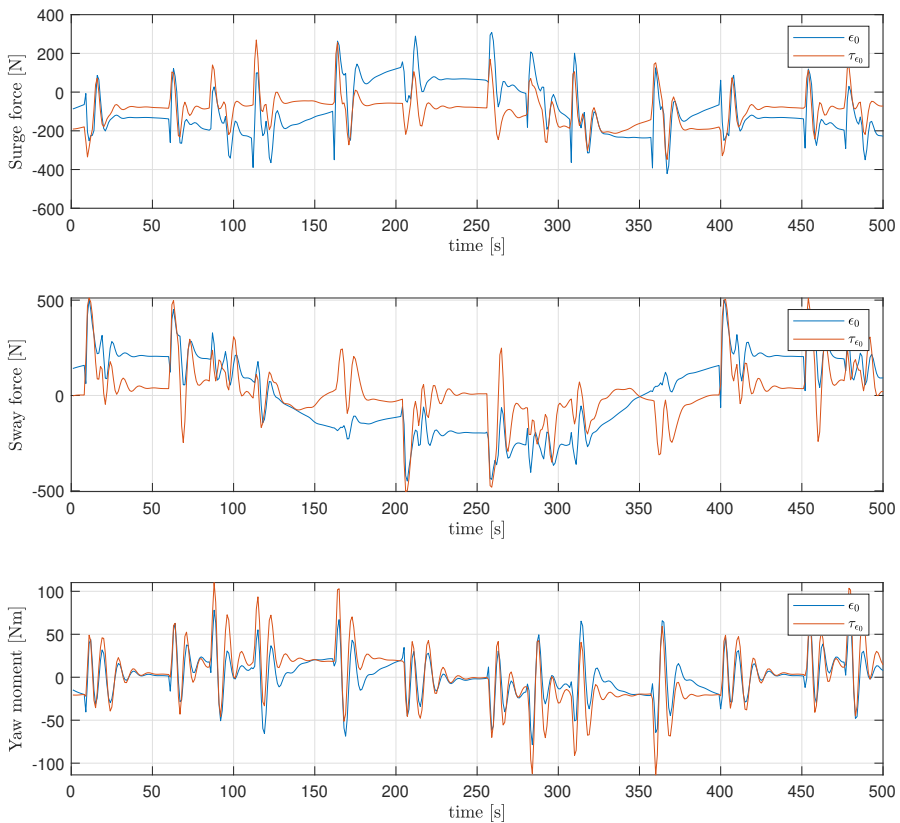
Figure 4.46: The residual compared to the estimated residual with constant disturbance.

The magnitude of the estimation error between τ_{ϵ_0} and ϵ_0 is compared to the magnitude of the constant disturbance in Figure 4.47. The estimation model for τ_{ϵ_0} has fitted the data so that the peaks of some of the oscillations coincide with residual. This causes the magnitude of the error to have large variance, but the mean of the error matches closely to the magnitude of the disturbance. Ideally the disturbance error, which can not be explained with the data, should be unmodeled. The NIPALS model does in general avoid modeling the unexplained error, although it is subject to some overfitting of the model, seen by the variance in Figure 4.47.
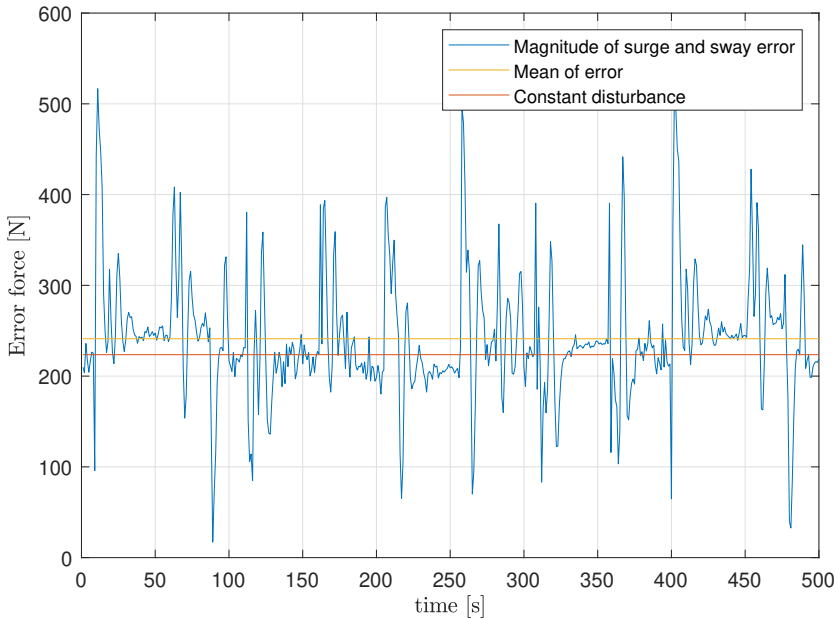
Figure 4.47: Magnitude of surge and sway compared to the constant disturbance.

4.8   Discussion

In the simulations the PLSR is able to give a good estimate of the residual under different conditions. The case shows that even without many of the basis functions that explains the output, it derives a model that can improve the estimations. Since it looks for covariance between the input and output, it is not able to model something that can not be explained by any of the basis functions. The comparison of the residual and the case PLSR model in Figure 4.5 shows that general movement is captured by the model, however the more complex spikes in the residual are left unmodeled, as they can not be explained by the selected inputs. This will likely be the case when analysing the ferry, as there are other factors than the measurements and basis functions available that can affect the ferry dynamics. This could be dynamics based on further derivatives of the acceleration, weight distribution or other external forces. The PLSR may find covariances that are only valid in the training data caused by other factors, and this is why the the cross validation must be done to prevent large modeling errors. The higher the model order the more of the variance in the residual is explained. The higher order PC's are easier overfitted as the small variance can match some of the variance in the input. Through cross validation these modeling errors may become evident as the model does not fit the data in the test set. This causes the MSE for higher model orders to increase, as shown in the case by Figure 4.4. With a very small improvement by choosing a higher order, a trade off between the chance of overfitting and better model fit must be done.

The PLSR model derived with noise gave satisfying results as the main variance of the residual was modeled. The noise is white and uncorrelated, which benefits the PLSR as it is more or less ignored, although some of the more rapid changes in the residual also becomes uncorrelated and unmodeled. When inflicting a constant disturbance to the ferry the PLSR also handled this very well. There was found little covariance with the constant disturbance and this resulted in an almost stationary deviation, with a magnitude that was close to the constant disturbance, as shown in Figure 4.47. It did cause some model discrepancies which is evident when comparing the residual and the modeled residual, however the fact that it is able to keep most of the external disturbance unmodeled is beneficial. This could be interesting to investigate further and see how accurate external forces can be estimated through PLSR. Such information could be valuable when collecting data, and contribute to more insight in the data before performing different analyses.

The basis functions selected gave a wide range of combinations. All of the basis function differs from each other, even though they could be similar for large parts of the data. The main reason for including many of the variations is that they have different covariance that can match with the output. The acceleration measurement were not altered into other basis functions as the data is acquired with IMU measurements and/or through derivation of the velocity and the accuracy of the data is more unreliable. A problem with including numerous basis functions is that they all become a part of the model to some degree, even if the effect is very small. In the simulations the reduction of basis functions through surface analysis did prove to find combinations of the basis functions that gave better a model fit than including all of the basis functions. This results in a method that is more computational efficient than trying all combinations of the basis functions. With the surface

analysis the MSE of the selected models were lowered compared to the regular PLSR. In addition by using more suitable basis functions the model order is lowered as well, compared to the initial model order.

By including the model in the controller the performance did improve overall. When following the trajectory without the FB term the deviations from the desired acceleration are lowered for all states. The deviations from the desired velocity were slightly improved and for yaw the complexity and instability caused an increase in the error. With the FB term helping, the inclusion of the model improved the controller substantially. The FB term is needed much less with the more accurate model, and is only need for small corrections. In addition this lowered the total control input, which reduces the wear and tear of the thrusters, and is more energy efficient. With the improvement of the FF this resulted in a more accurate path following, with much smaller deviations. The positional error is reduced significantly shown by the MAE, and the large errors are also improved a lot as the MSE is reduced to a tenth of before. The performance of the heading error has been improved by large errors being reduced, however this has caused other smaller deviations that makes the MAE go slightly up.

The model comparison between the actual model of the residual and the PLSR model shows that there are discrepancies. One of the main things is that the PLSR model is dependent of more basis functions, as all of the basis functions included in the analysis effects the model. However some of the regression coefficients are estimated accurately, and does give a good approximation of the residual. When the controller with the PLSR model was tested on a different trajectory more similar to operating conditions the improvement is evident. The implementation of the PLSR model reduced the positional and heading error significantly, and when taking the work into account with the IAEW the ferry followed the trajectory more efficiently.

Chapter 5

Experimental results

The experimental results are presented in this chapter. An overview of the exprimental platform and area is given, and the data post processing is shown. The MVA is performed on the lack-of-fit residual found from the experimental data, resulting in an improved model for implementation in the controller and a model for simulation purposes.

5.1 Experimental platform and environment

The experiments are performed on the ferry milliAmpere. It is a fully electric powered ferry, with a propulsion system consisting of two azimuth thrusters. The thrusters are located along the center of the ferry with one in the front and one in the back. The vessel has a flat bottom hull, with a length of $5m$ and a width of $2.8m$. An overview of the ferry from the front and the side is seen in Figure 5.1. The navigation system of the ferry is based on a Vector$^{\text{TM}}$ VS330 GNSS Receiver and an Xsens MTi20 IMU. An ESKF described in (Sæther, 2019) is used for sensor fusion between the GNSS and the IMU for the measurements of the position and velocity. The acceleration data is received directly from the IMU. The ferry has an onboard computer with Ubuntu OS and ROS kinetic that connects the system. It is implemented a model reference adaptive controller that is able to receive waypoints and follow the desired trajectory.

The test environment is placed in the harbour of Pirkaia in Trondheim. The harbour is well shielded from current and waves, and is a good test location with little disturbances. The trajectory from Figure 4.1 is run on milliAmpere as shown in Figure 5.2, with the figure lined with north straight upwards. The segments of the path are done with the same length and rotations as in the simulations, however the coordinates have been rotated to fit inside the harbour. The starting point is indicated by the ferry in the figure. The test day was 29. april 2020, with little to no wind and the weather forecast showing $0-3m/s$ wind speed during the tests were done.
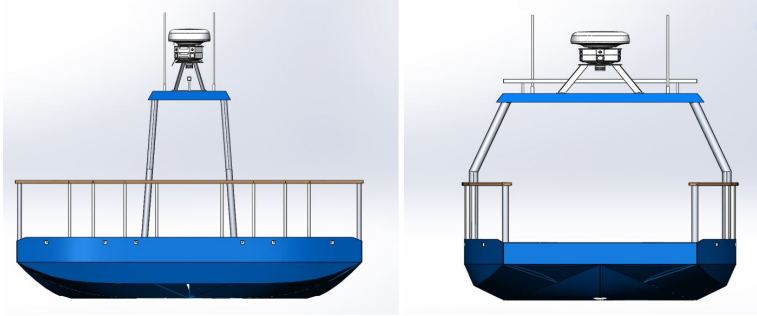
Figure 5.1: CAD drawing of milliAmpere, courtesy of Glenn Angell. Side view of the ferry to the left. Front view of the ferry to the right.

Figure 5.2: Path of the experiment in the test area. The starting position of the ferry indicated by the green point. Courtesy of Google Maps.

5.2 Data post processing

The trajectory is run four times, with each trip taking around 1000 seconds, with all of the data collected. The data that is needed for the MVA is the control input, velocity and acceleration. The control input is logged directly from the output of the controller and the velocity and acceleration is logged from the measurements of the sensors. The measurement has been run through the ESKF and is not subject to much noise. There are some outliers in the data that must be removed. This is done by filtering out points that are more than 3 standard deviations away from a moving average of 10 samples. The 10 samples are selected as the few samples give a high standard deviation and tolerance for what to remove, so that nothing of the real signal is filtered out. The points that have been filtered out are replaced with a new point found by interpolation of the previous and next sample. The different data is logged as they are sampled, and this causes the data to have different sampling time. Each message containing data has a timestamp that tells when it is sent. The PLSR need the data to have a common sampling rate, so that each row in X is a new time step. The common sampling rate is chosen by the slowest sampling rate, which is the control input at $10Hz$. All of the measurements are then down sampled to a fixed sampling rate of $10Hz$ through linear interpolation to fit data points at the desired sample time.
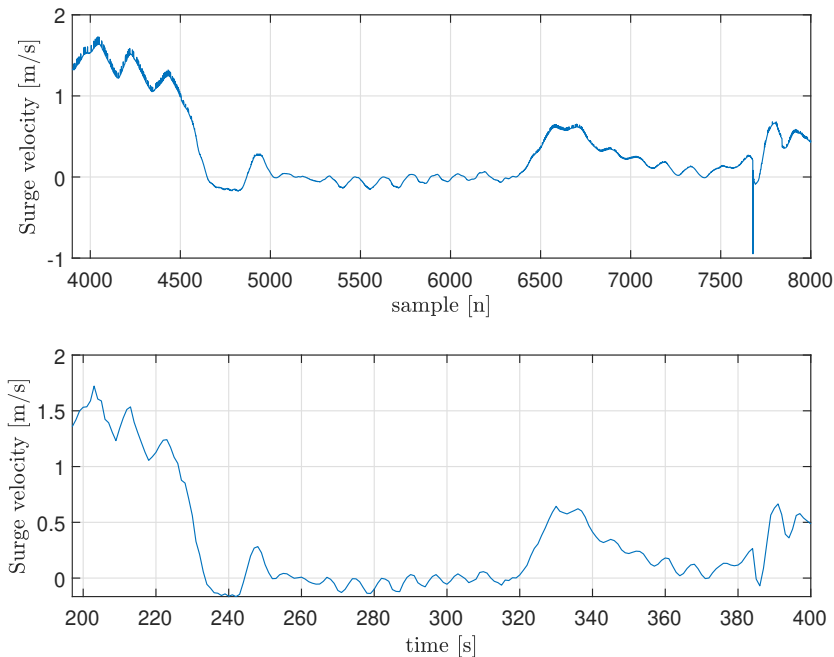
Figure 5.3: The data of surge velocity before processing above, and after processing the data below.

The data from the control input, velocity and linear acceleration has outliers removed and are down sampled to $10Hz$. An example of the post processing of surge velocity is shown in Figure 5.3. The outlier between sample 7500 and 8000 is removed and the data is now sampled at the desired frequency. The data is also made smoother and some of the noise is removed by the down sampling. The linear acceleration in surge has a problem of not being zero when no surge force is applied, as it should be in this experiment. The IMU measurement and the derivative of the velocity is compared in Figure 5.4, and shows that the acceleration should be calibrated to zero mean. The derivative of the velocity is not as accurate for estimating the acceleration, as the noise is amplified when finding the derivative. Hence the IMU measurements give more accurate date. However by filtering the velocity and finding the derivative it does give a indication of what the acceleration should be, and shows that the mean of the IMU data must be moved to zero. The change of mean in the IMU occurs before any of the path following is initiated, so the data that is analysed is not affected by any changes in the middle of a test.
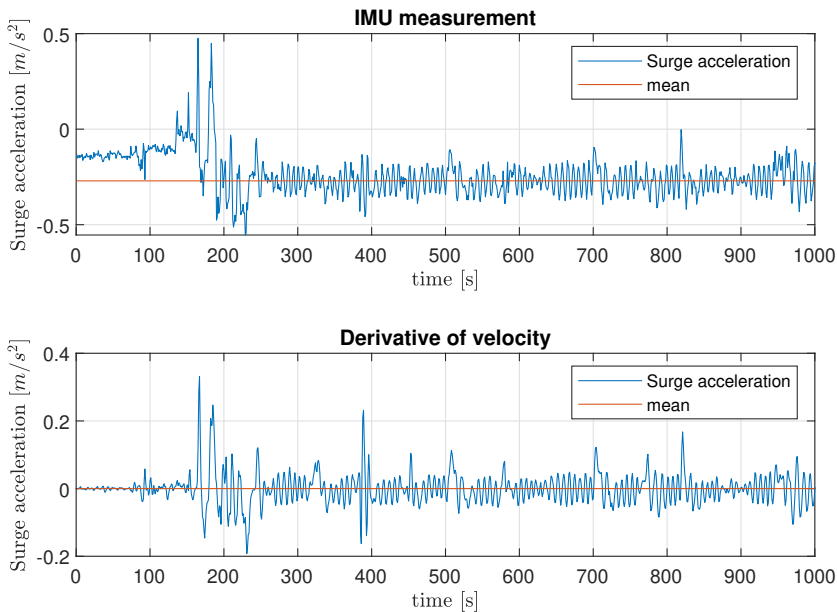
Figure 5.4: Surge acceleration with problems calibration to zero mean.

The angular acceleration for yaw $\dot{r}$ is not measured and must be estimated. It is found from the derivative of the angular velocity. The angular velocity is not subject to excess noise, so that the estimated angular acceleration is accurate and can be used in the MVA.

In addition to the control input the actual force from each thruster is found. The control input gives the desired force, and the thruster allocation algorithm converts that to an angle and motor speed for the thruster. Hence the actual force is slightly different than the control input. Which signal that is used in the MVA depends on what the goal of the analysis is. In the simulations the goal is to improve the model in the controller, so that the estimated control input from the FF predicts the control input needed to follow the trajectory. In this case the control input is included in the MVA, as that is the signal to be optimized. This PLSR model will then explain parts of the thruster dynamics as well. When selecting the actual force of the thrusters for the MVA, this gives a more accurate model of the ferry. The thruster dynamics are not included in this PLSR model, and only the ferry dynamics are explained. The initial model is made from the actual force from the thrusters, and is suited for simulations, where the ferry and thruster dynamics are modeled separately.

The actual force is derived from the motor speed χ and angle α. The force from the motor speed is found by a mapping of the thruster data (Pedersen, 2019). In Figure 5.5 the data is plotted and a 5th order model is fitted to convert the motor speed to force. A 5th order model is chosen to give a better estimation of the data than a cubic model. Since the model only is valid from $[-5400rpm, 5300rpm]$ the deviations from the nonlinearities outside the measurements does not affect the conversion. The conversion is given by

$$\tau_\chi = -1.31e - 16\chi^5 - 1.78e - 13\chi^4 + 6.16e - 09\chi^3$$
$$+ 8.7e - 06\chi^2 + 0.00478\chi - 1.07 \quad (5.1)$$

where τ_χ is the force produced of the thruster. The actual force $\boldsymbol{\tau}_A$ is found by combining the angle of the thruster and calculate the force that is produced for each state. When deriving the yaw moment each thruster is located with a distance of $l = 1.8$ from the center. This gives the actual force

$$\tau_{A,u} = cos(\alpha_1)\tau_{\chi_1} + cos(\alpha_2)\tau_{\chi_2} \quad (5.2a)$$
$$\tau_{A,v} = sin(\alpha_1)\tau_{\chi_1} + sin(\alpha_2)\tau_{\chi_2} \quad (5.2b)$$
$$\tau_{A,r} = sin(\alpha_1)\tau_{\chi_1}l - sin(\alpha_2)\tau_{\chi_2}l \quad (5.2c)$$

where the subscript differentiates between thruster 1 and 2, and $\boldsymbol{\tau}_A = [\tau_{A,u}, \tau_{A,v}, \tau_{A,r}]^T$. This results in the actual force affecting the ferry by the thrusters.
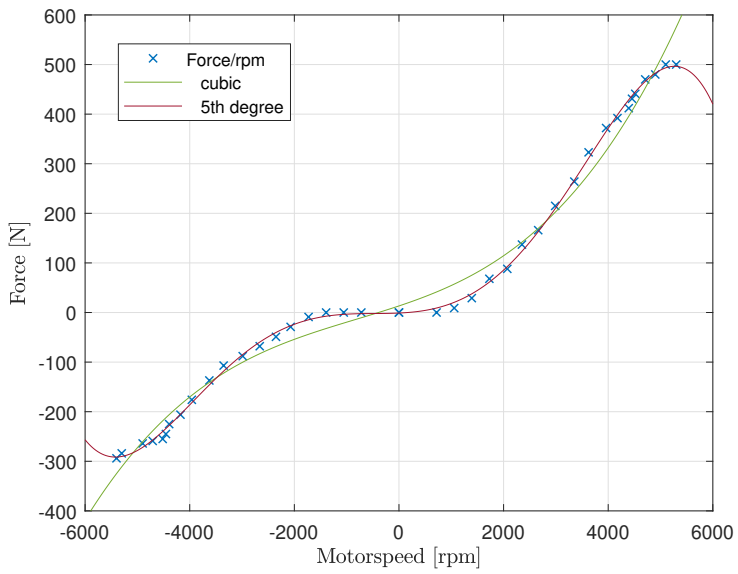
Figure 5.5: Fitted model to convert motor speed to force.

5.3 Multivariate modeling and analysis

The four sets of data are divided into a training set and a test set. The effect from external disturbances, like the weather, may have changed during the tests were performed. To minimize the possibility of this creating a bias in the data the training set contains trip 1 and 3, while the test set contains trip 2 and 4. The velocity and acceleration from the data is used to estimate the control input from the initial model in (3.19). The Control input τ and the actual force τ_A is compared with the estimated force τ_{m_0} in Figure 5.6. The initial model is based on the actual force, so the estimated force is closer to the actual force compared to the control input. The time horizon of the figure is decreased to see the difference between them. It shows that the initial model is overestimating the needed control input and actual force, as the oscillations has higher amplitude than the control input. The residual between these signals is the goal of the PLSR model to explain. If the model explains this residual exactly the estimated force follows the other signals perfectly depending on which data is analysed.
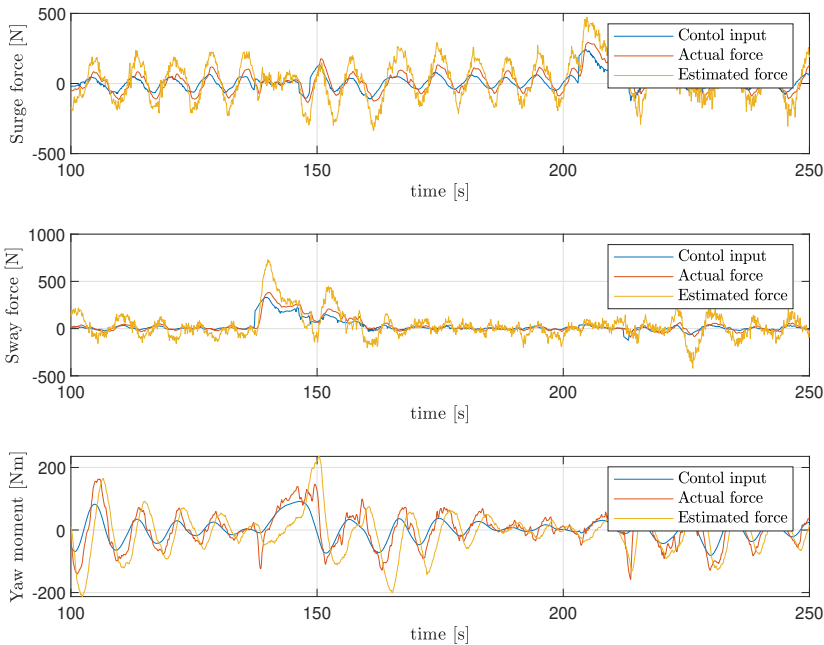
Figure 5.6: The control input, actual force and estimated force compared.

5.3.1 PLSR model for control

This analysis is to improve the model in the FF, so that the estimated control input needed is more accurate. The residual ϵ_0 is estimated through a PLSR with the basis functions in (4.12). Figure 5.7 shows the model fit for each model order by the MSE between the PLSR models and the test set. The MSE is significantly reduced for all states with the PLSR model. Model order $\sigma = 5$ is selected for this analysis, as the MSE is among the smallest for all states and the MSE does not drop significantly for any of the higher model orders. The improvement from implementing the PLSR model is showed in Table 5.1, by the difference between the MSE from the original residual and the remaining residual. The difference is quite significant as the improved model has reduced the MSE with more than four times for surge and sway, and nearly three times for yaw. With surface analysis this model is improved further, by removing the basis functions that does not contribute.

Table 5.1: The MSE of the residual with and without the PLSR model for the experimental data.

The residual ϵ	MSE of surge force	MSE of sway force	MSE of yaw force
Without PLSR model	10546 N^2	21177 N^2	5585 Nm^2
Regular PLSR model	**2497** N^2	**4506** N^2	**2065** Nm^2
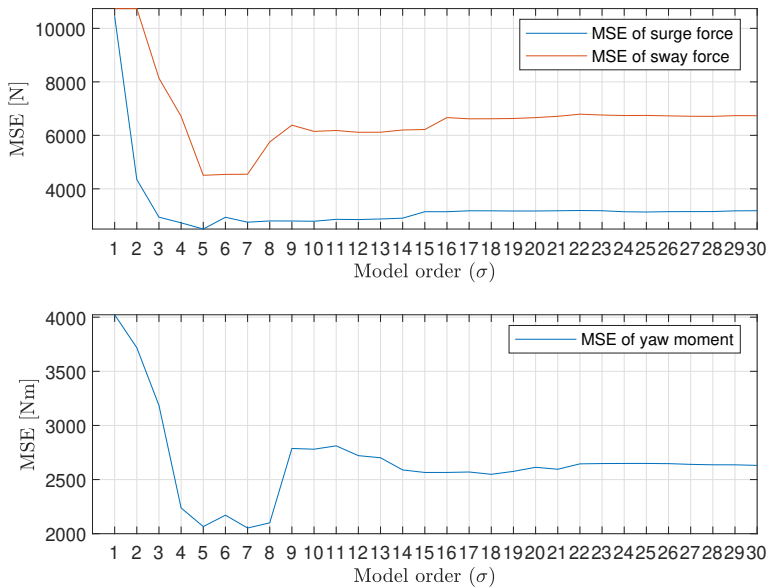
Figure 5.7: The MSE for each model order of the PLSR.

Surface analysis of control input

With the surface analysis the aim is to see if there are better PLSR models for explaining the residual if basis functions that contribute little to nothing in the model is removed from the PLSR. This gives a way of selecting the basis functions that give the optimal PLSR model and chosen them. In Figure 5.8 and Figure 5.9 the surface plot for surge, sway and yaw is shown depending on the model order and the variable number. The minimum for each state is surge: $[\sigma, \rho] = [5, 30]$, sway: $[\sigma, \rho] = [4, 27]$ and yaw: $[\sigma, \rho] = [14, 16]$. The minimum for surge is found without removing any basis functions, and is therefore the same PLSR model as before the surface analysis. For the other states the minimum of the surface plot is from removing a number of basis functions. A new PLSR is done with the basis functions from the minimum of the surface plot to see if it is beneficial to reduce the model order. The MSE with these basis functions is shown in Figure 5.10. For sway the optimal model order remains the same as the minimum from the surface plot, giving $\sigma = 4$. For yaw the MSE is almost unchanged between model order 3 and the minimum of the surface plot, which is 14. Hence model order $\sigma = 3$ is selected for yaw. This results in a significantly lower model order than initially found in the surface plot, and reduces the chance of overfitting the model substantially. In addition this PLSR model for yaw has a lower MSE than the local minimum of the surface plot at $[\sigma, \rho] = [6, 27]$, which is close to the MSE of the minimum.

The selected PLSR model is compared to the residual of the test set in Figure 5.11. It shows that most of the residual is explained with this model, however there are spikes in the residual that the model is not able to capture, like at around 100 seconds for surge force and at 340 seconds for yaw moment. The residual and the remaining residual is shown in Figure 5.12. Much of the oscillations in the original residual is removed, and the remaining residual is closer to zero for large parts of the estimation. The selected models for each state is given in Table 5.3, with a zero as regression coefficient if the basis function is not included for the model of that state. The residual is estimated with these regression coefficients from (3.15). This model has a model fit resulting in the MSE in Table 5.2. The selected model is proposed to be implemented in the FF for a more accurate estimation of the needed control input.

Table 5.2: The MSE of the residual with and without the different PLSR model for improving the control input.

The residual ϵ	MSE of surge force	MSE of sway force	MSE of yaw force
Without PLSR model	10546 N^2	21177 N^2	5585 Nm^2
Regular PLSR model	2497 N^2	4506 N^2	2065 Nm^2
Surface PLSR model	2497 N^2	4252 N^2	**1649** Nm^2
Selected PLSR model	**2497** N^2	**4252** N^2	1663 Nm^2
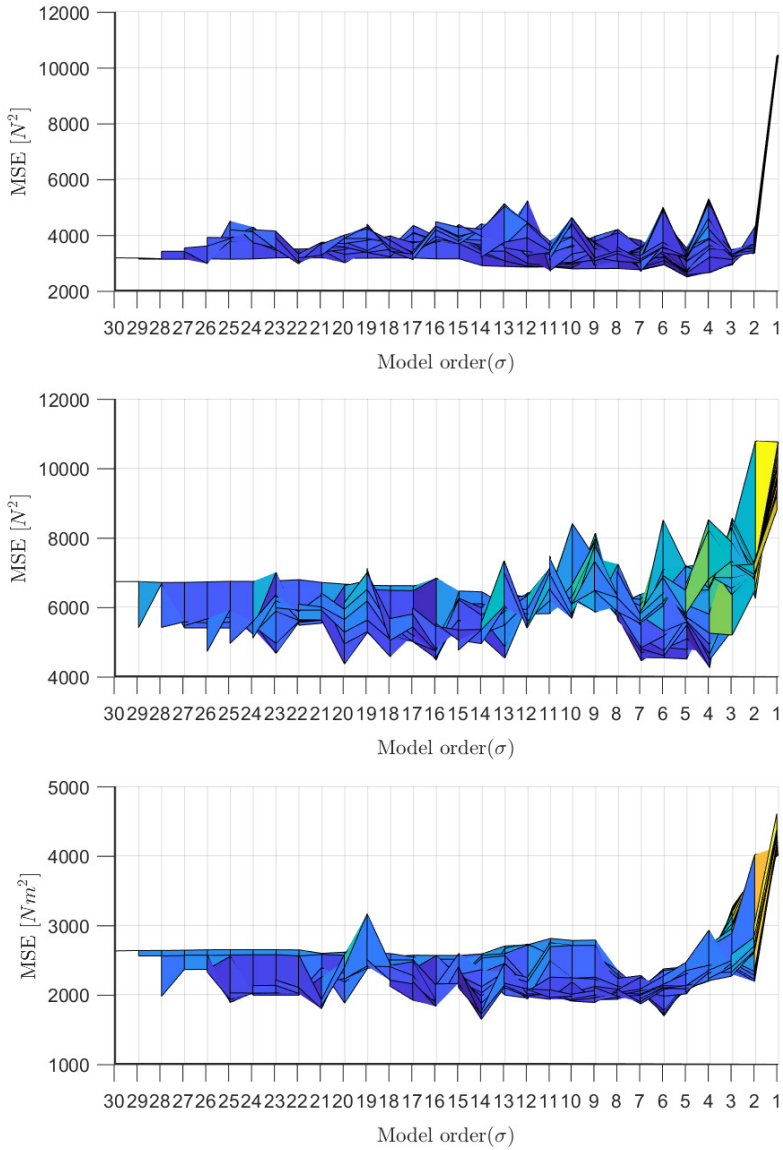
Figure 5.8: Surface plot of the MSE comparing the different model orders for the control input. Surge on the top, sway in the middel and yaw at the bottom.
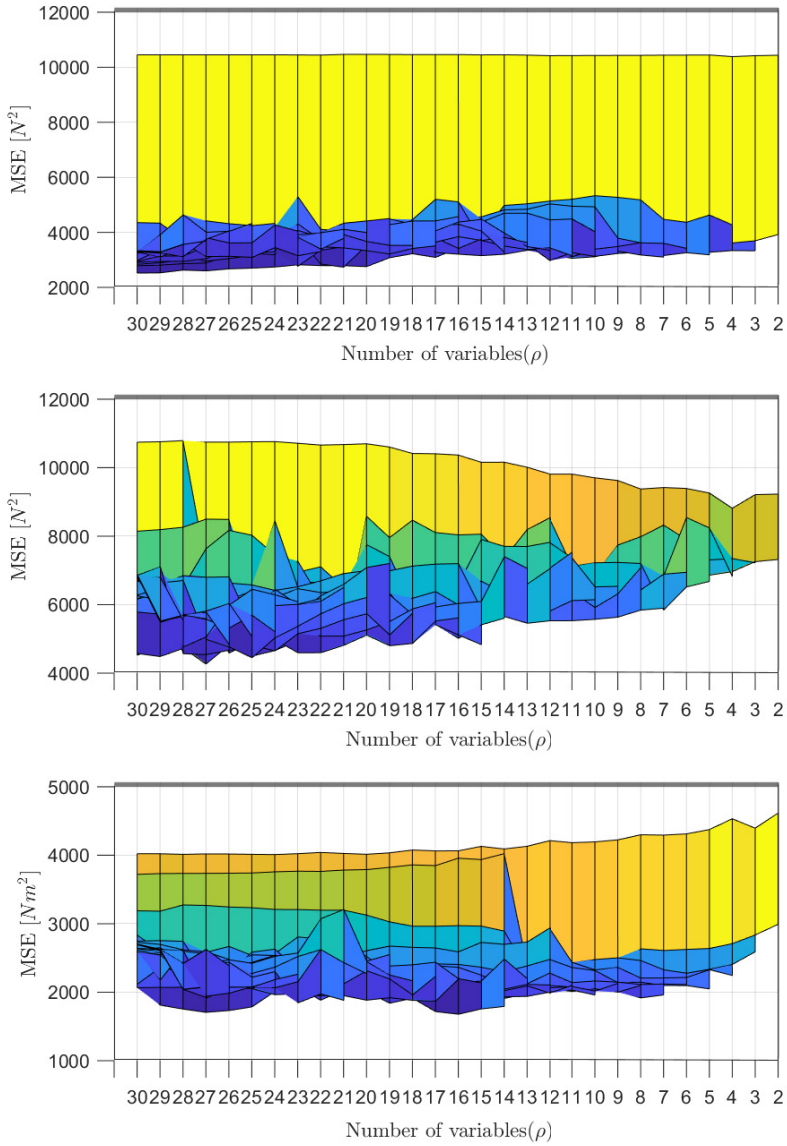
Figure 5.9: Surface plot of the MSE comparing the different number of basis functions for the control input. Surge on the top, sway in the middel and yaw at the bottom.
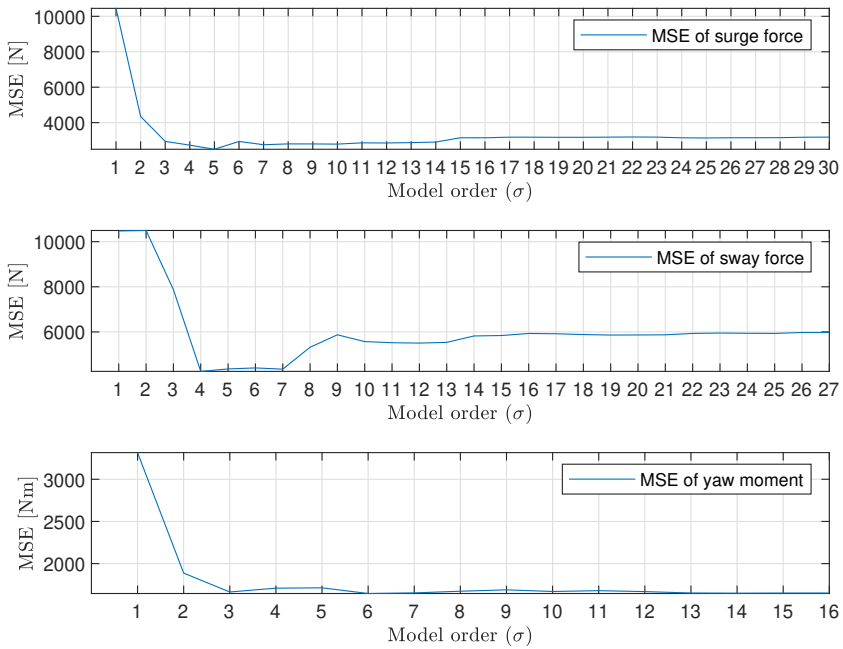
Figure 5.10: The MSE of the the model orders with the basis functions found in the surface analysis.
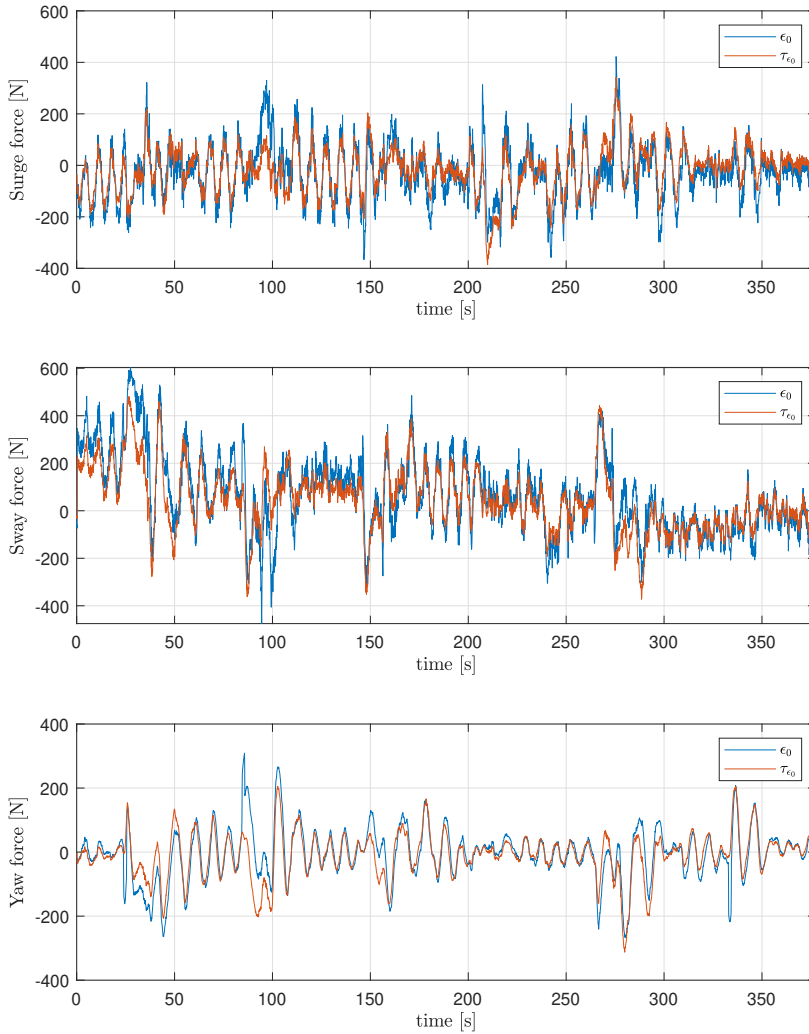
Figure 5.11: The residual compared to the selected model for the control input.
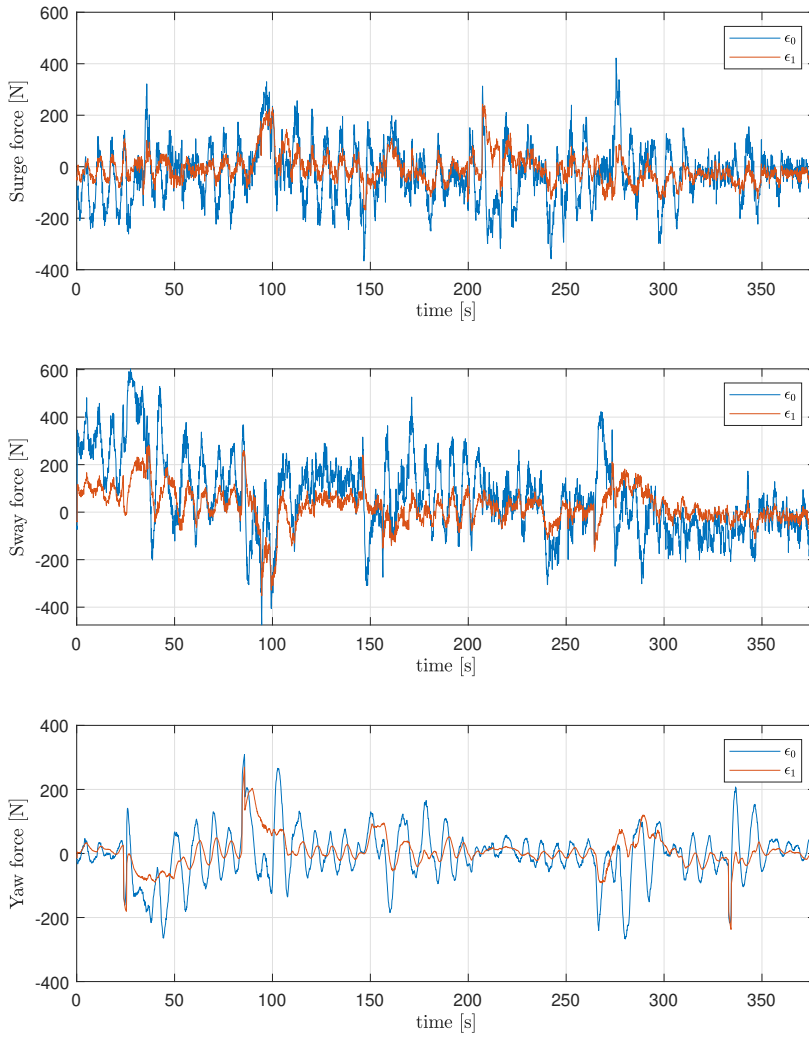
Figure 5.12: The original residual and the remaining residual with the selected PLSR model for the control input.

Table 5.3: Regression coefficients of the selected PLSR model for improving the controller model.

Basis function	Surge, Θ_u	Sway, Θ_v	Yaw, Θ_r
1	-1.10	4.85	3.43
$\dot{u}$	-1407.75	20.41	0
$\dot{v}$	120.42	-1420.09	0
$\dot{r}$	-905.24	-602.24	-4166.66
u	-33.15	16.88	0
v	-13.37	-3.39	34.21
r	-114.54	-161.05	-519.45
$|u|u$	-24.54	11.44	0
$|v|v$	-4.34	-1.65	5.85
$|r|r$	-673.91	-200.46	-1122.40
u^3	-18.98	10.57	0
v^3	-2.64	-1.37	-0.18
r^3	-4185.92	277.86	-1981.69
$|u|$	-45.14	14.43	0
$|v|$	25.93	55.18	0
$|r|$	351.29	-632.05	0
u^2	-23.99	8.66	0
v^2	18.61	21.65	-101.56
r^2	1128.95	-1711.34	0
uv	-0.91	24.60	75.64
ur	-245.11	6.71	597.74
vr	601.89	-151.81	-1496.41
$|u|v$	-4.29	9.31	48.25
$|u|r$	-173.86	-174.59	122.62
$|v|u$	-19.17	0	-41.27
$|v|r$	-168.73	-113.00	-43.68
$|r|u$	-47.04	0	0
$|r|v$	-139.64	-5.97	224.52
$|u||v|$	-9.67	-11.15	0
$|u||r|$	-11.74	-151.31	0
$|v||r|$	319.54	0	0

5.3.2   PLSR model for system identification

This PLSR model uses the actual force from the thrusters and compares it to the estimated force. The residual between these signals is estimated through PLSR. The difference with this model is that the dynamics of the thrusters does not affect the actual force, as it is derived directly from the motor speed and angle. This model is a more accurate description of the dynamics of the ferry and how a force applied to the ferry affects it. In simulations where the ferry and the thrusters are model separately this model gives a better estimation of the movement of the ferry. The MSE from the regular PLSR is shown in Figure 5.13. The selected model order is chosen to $\sigma = 4$ for surge and sway, and $\sigma = 7$ for yaw. With these models the MSE is shown in Table 5.4. To see if the model can be improved further, surface analysis is utilized to check for a better choice of basis functions in the PLSR

Table 5.4: The MSE of the residual with and without the regular PLSR model for improving the ferry model.

| The residual ϵ	MSE of surge force	MSE of sway force	MSE of yaw force
Without PLSR model	6306 N^2	16829 N^2	4478 Nm^2
Regular PLSR model	**1346** N^2	**3323** N^2	**2270** Nm^2
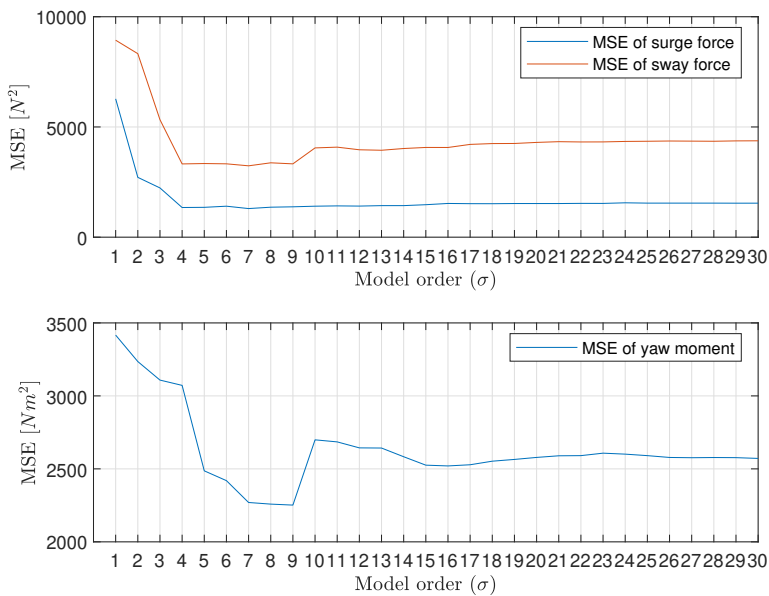
**Figure 5.13:** The MSE for each model order of the PLSR.

Surface analysis for system identification

The surface plot is shown in Figure 5.14 and Figure 5.15 dependent of model order and number of variables. The minimum of the surface analysis for each state is given at, surge: $[\sigma, \rho] = [14, 20]$, sway: $[\sigma, \rho] = [9, 29]$ and yaw: $[\sigma, \rho] = [14, 16]$. A PLSR is done with the basis functions used at the minimum of the surface plot, which results in the MSE shown in Figure 5.16. For surge it is seen that the model order can be reduced from 14 without increasing the MSE of the model fit to much. It is a local minimum for surge at $\sigma = 3$, which results in a low model order, however the MSE is further lowered significantly until it flattens out at model order $\sigma = 8$. Hence the model order for surge is selected to $\sigma = 8$. The same characteristics yield for the MSE of sway, giving the model order $\sigma = 8$ selected for sway. An other valid selection for the model order of sway is $\sigma = 4$, as this does reduce the model order further. This will come at the cost of a model with a MSE that is increased by more than $600 N^2$. For yaw it is a more difficult selection of model order, as there are mainly three model orders that could be a good choice. These are $\sigma = 4, 6, 9$, where the MSE is improved by $72 Nm^2$ and $68 Nm^2$ respectively. The improvements are not that significant, so $\sigma = 4$ is selected as the safest option to reduce overfitting.

The MSE for the selected models is shown in Table 5.5. The surface analysis does improve the PLSR model further than the regular PLSR including all of the basis functions. The estimated residual with the selected model is compared to the residual in Figure 5.17. The model has captured most of the dynamics for surge and sway, while there are more deviations for yaw. This is seen better in Figure 5.18, where the remaining residual after the model is implemented is shown. The model for surge and sway keeps the remaining residual close to zero with little oscillations. For yaw the model does not capture all of the oscillations in the residual, however some of the largest deviations have been reduced. The regression coefficients that are proposed for the model to improve the ferry model is given in Table 5.6.

Table 5.5: The MSE of the residual with and without the different PLSR model for improving the ferry model.

The residual ϵ	MSE of surge force	MSE of sway force	MSE of yaw force
Without PLSR model	6306 N^2	16829 N^2	4478 Nm^2
Regular PLSR model	1346 N^2	3323 N^2	2270 Nm^2
Surface PLSR model	**1263** N^2	2786 N^2	**1942** Nm^2
Selected PLSR model	1268 N^2	**2771** N^2	2077 Nm^2
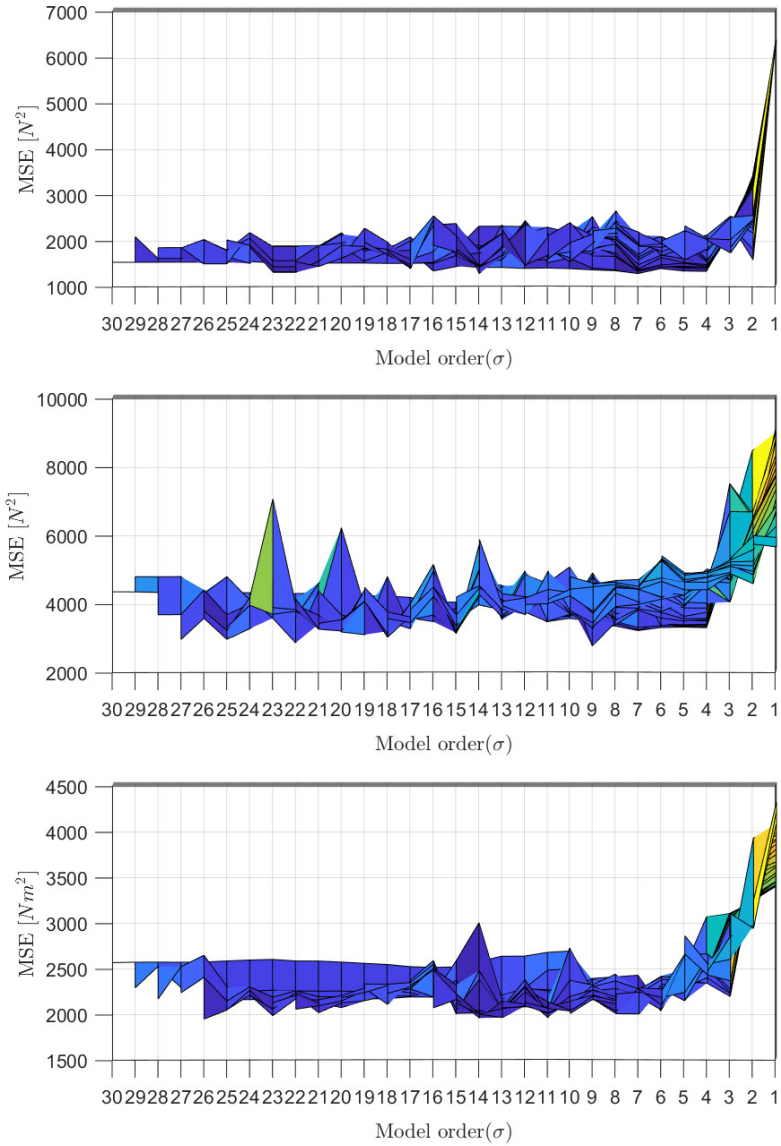
Figure 5.14: Surface plot of the MSE comparing the different model orders for the actual force. Surge on the top, sway in the middel and yaw at the bottom.
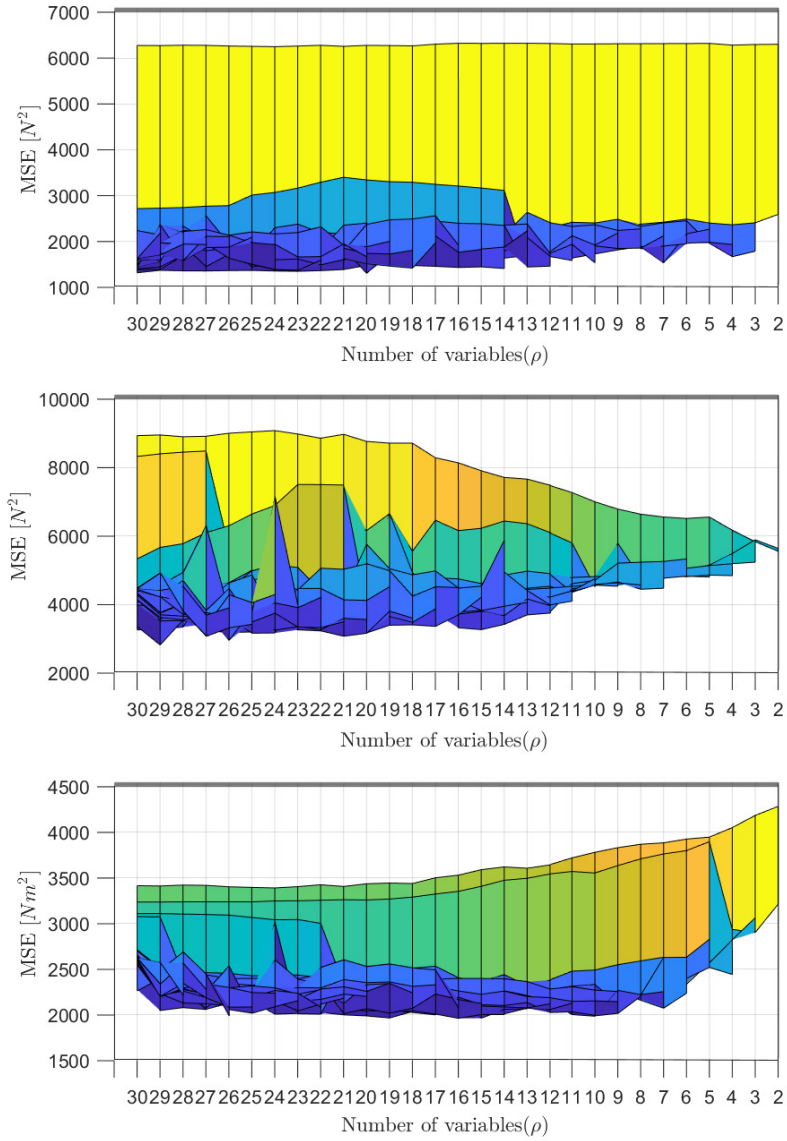
Figure 5.15: Surface plot of the MSE comparing the different number of basis functions for the actual force. Surge on the top, sway in the middel and yaw at the bottom.
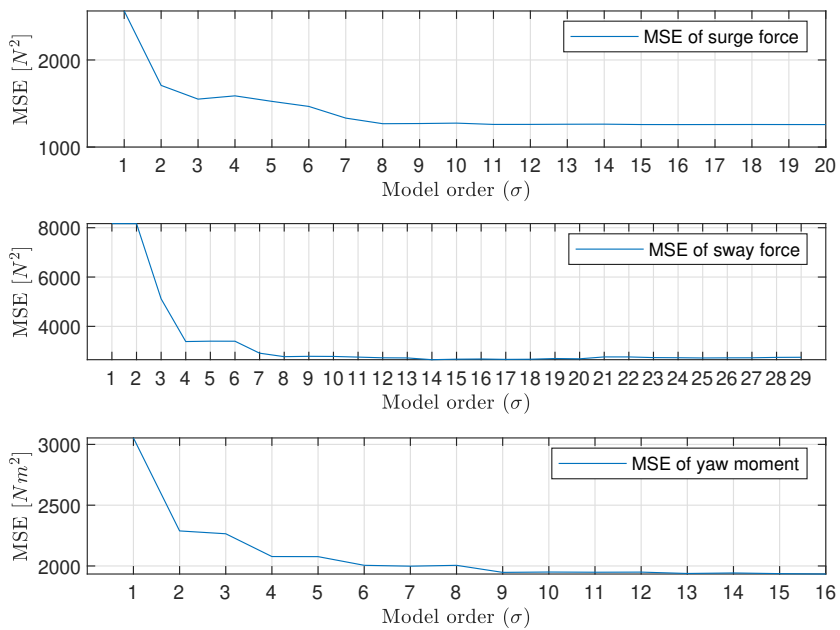
Figure 5.16: The MSE for each model order of PLSR with basis functions from surf analysis.
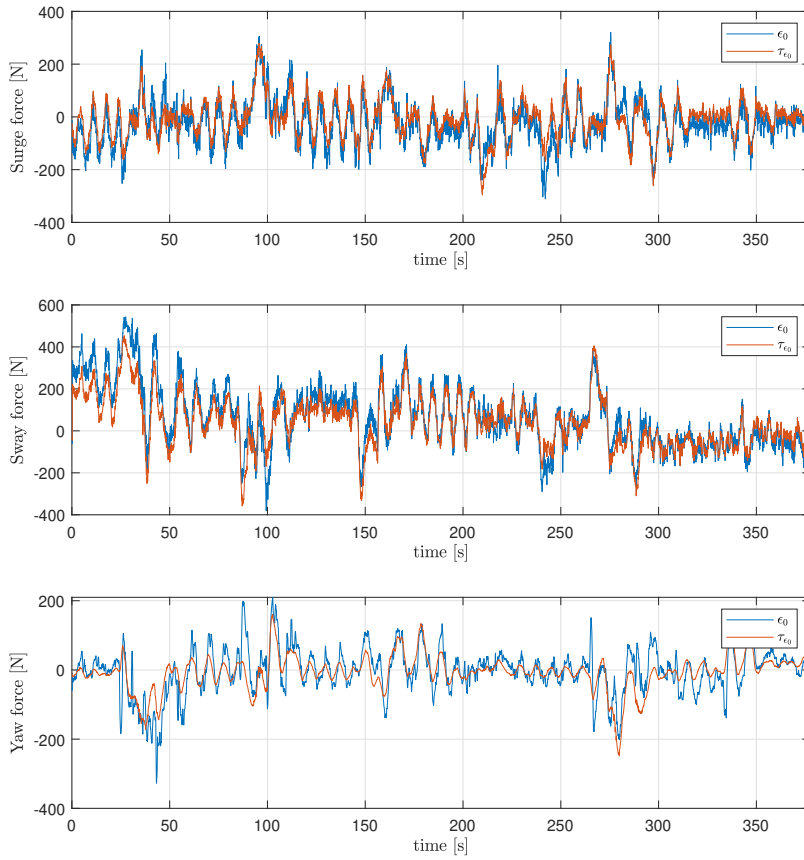
Figure 5.17: The residual compared to the selected model for the actual force.
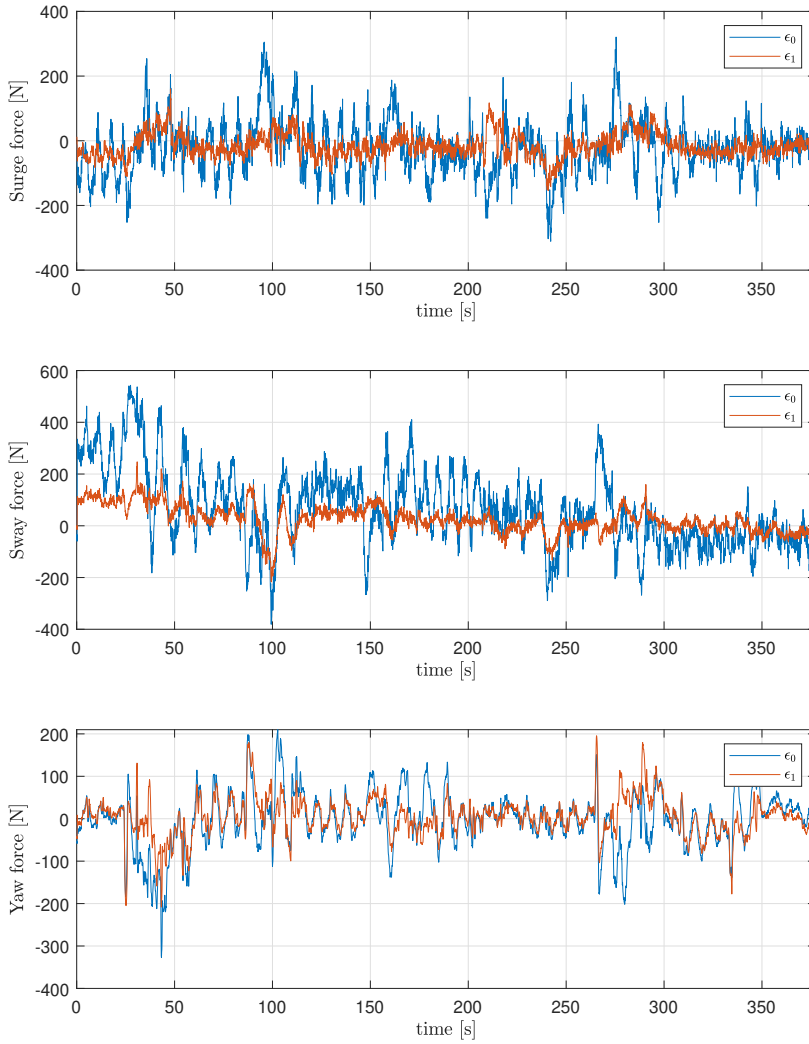
Figure 5.18: The original residual and the remaining residual with the selected PLSR model for the actual force.

Table 5.6: Regression coefficients of the selected PLSR model for improving the ferry model.

Basis functions	Surge, Θ_u	Sway, Θ_v	Yaw, Θ_r
1	23.58	7.10	-1.56
$\dot{u}$	-1184.01	-34.35	0
$\dot{v}$	0	-1501.86	0
$\dot{r}$	0	-483.17	-1663.46
u	25.00	-7.70	0
v	-7.43	31.61	0
r	0	328.60	-717.43
$|u|u$	0	8.90	0
$|v|v$	32.66	17.89	0
$|r|r$	-584.56	663.66	-1880.54
u^3	-45.76	13.50	0
v^3	19.57	13.15	46.32
r^3	-4963.25	508.38	-6012.59
$|u|$	-44.50	34.88	0
$|v|$	-65.43	-8.22	0
$|r|$	-379.40	-117.66	0
u^2	-41.02	16.43	0
v^2	0	9.87	-48.54
r^2	0	620.48	0
uv	27.93	-27.77	190.59
ur	0	-1146.03	1079.00
vr	3102.22	0	-1290.29
$|u|v$	0	6.54	155.50
$|u|r$	0	-741.18	395.21
$|v|u$	77.62	-113.83	0
$|v|r$	-266.55	-158.48	314.11
$|r|u$	-438.13	-157.74	606.93
$|r|v$	216.32	-64.01	747.74
$|u||v|$	0	-78.99	62.19
$|u||r|$	-534.29	226.42	0
$|v||r|$	681.59	189.34	-825.90

5.3.3   Improvement with the PLSR model

It was not enough time to test the PLSR model on the ferry, and see the results. However the model is compared to the data that is collected. This gives an indication of how the estimation is improved. By using the selected PLSR model together with the initial model the estimated control input and actual force is closer to the collected data. In Figure 5.19 the actual force is compared to the estimated actual force with and without the PLSR model. This shows that the accuracy of the estimations have increased from only using the initial model.
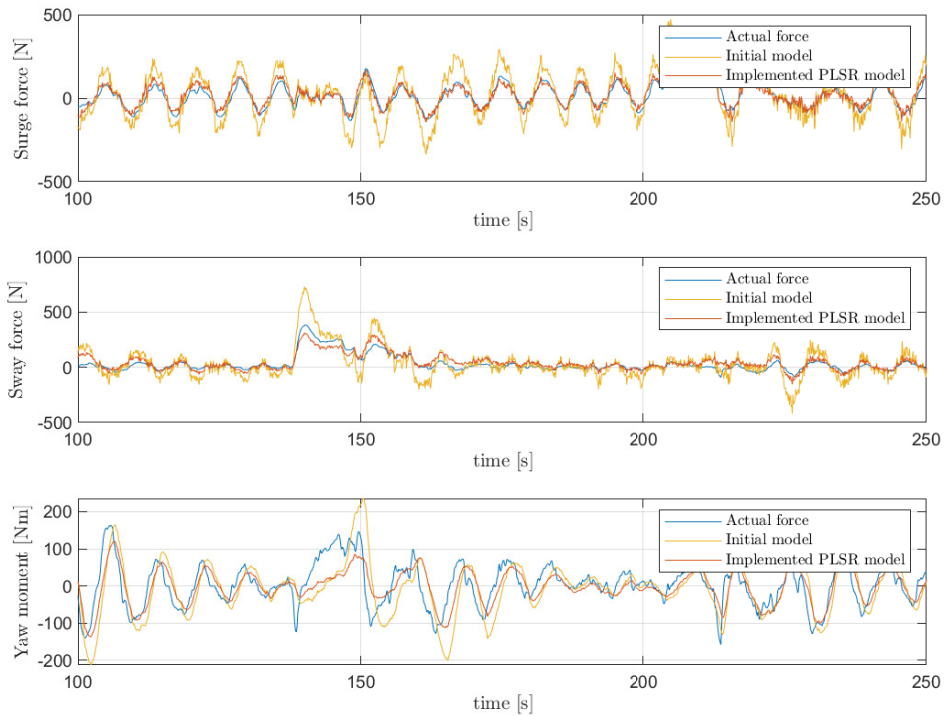
Figure 5.19: The actual force compared to the estimated actual force with the initial model and with the selected PLSR model implemented.

This visualizes how the reduction of the MSE of the model improves the estimation of the control input and actual force. If the implementation of the PLSR model in the FF will improve the estimation in the same way as with the collected data, the FF will gives a much more accurate control input to follow the desired trajectory.

5.4   Discussion

The model to be included in the controller is improved by the regular PLSR, and shows that the accuracy of the model is increased with these basis function. The surface analysis did not find better suited input combinations for surge, and the best model for surge is obtained with all of the basis functions in the PLSR. For sway and yaw the surface analysis found combinations of the basis functions that was better suited and resulted in a lower MSE. The minimum for sway was also the selected model, which both has lower MSE and model order than the original model found by the regular PLSR. The surface analysis for yaw showed that the minimum MSE was found at model order 14, however this basis function combinations was investigated further to find that model order 3 resulted in almost the same model fit. Hence the surface analysis did provide more insight for sway and yaw to derive a better model of the residual.

The PLSR model with the resiudal based of the actual force, intended to improve the ferry model, resulted in a good approxiamtion of the residual. The model is further improved with the surface analysis. The model order is selected higher than in the regular PLSR, however the the MSE from cross validation was improved significantly up to the selected model order. This resulted in a more accurate model than for any of the model orders found with the regular PLSR.

The derived PLSR model on the experimental data does reduce the lack-of-fit residual and gives a more precise estimation. It was not enough time to test the proposed model for the FF in the controller. When comparing the results of the experimental data to the simulations, the MSE of the estimation error from the initial model is reduced almost as much as in the simulations with the PLSR model. If the effects are close to the results in the simulations when implementing the improved model in the controller, the derived model for the FF should give a more accurate estimation of the control input. This would result in an increased tracking performance and a more energy efficient controller.

There is a quite visible residual when comparing the estimated force with the control input and actual force, which seems like the initial model is not as accurate as it could be. This results in a significant error to model with the MVA, where some of the deviations could have been modeled by the initial model. It would be interesting to perform a new fitting of the parameters in the initial model, to achieve a more exact estimation, before utilizing the PLSR.

The basis functions are based on measurements of speed and acceleration, however there are other factors that affect the dynamics that could be measured. By implementing sensors for e.g. wind speed and direction and/or depth gauge, this can contribute to estimation of wind force and load weight. These measurements could be included in the MVA to further improve the ferry model.

Chapter 6

Conclusion and future work

In this thesis, an approach for improving a first-principal-based initial model of an autonomous passenger ferry using methods from multivariate analysis (MVA) is presented. A lack-of-fit residual between the initial model and the ferry system is modeled with multivariate methods to improve the performance of the control system. Through simulations, it is shown that it is possible to approximate a model of the residual with partial least squares regression (PLSR) and improve the existing initial model. A selection of basis functions is presented that can have an effect on the model. The PLSR is able to find correlations between the selected basis functions and the residual, to derive a model that explains large parts of the lack-of-fit residual. This results in a significant reduction of the estimation error between the model and the true system. The benefits of PLSR for identifying ship dynamics are further emphasized from the simulations with inflicted noise and constant disturbance, where the errors from the constant disturbance remains mostly unmodeled.

A new method including surface analysis is used in both the simulations and for the experimental data. The method did find a more suitable combinations of the basis functions to include in the analysis. The selection of basis functions from the surface analysis is beneficial as it removes basis functions that have little correlation with the output. This results in a better model fit and a reduction of dependent basis functions in the model. Without these basis functions included in the multivariate model the chance of overfitting is also reduced.

From the simulations, the controller of the ferry was improved by including the PLSR-based model. This increased the tracking accuracy as the feedforward (FF) controller gives a better estimation of the required control input for following the reference. In addition, the usage of the control input is reduced, for both the total control input and the the feedback (FB) usage, since less correction of the FF is needed. A model comparison of the simulation results showed that there are model discrepancies in the PLSR model, however the model still is able to explain large parts of the residual. The controller with the PLSR model is tested on a trajectory simulating more realistic operational conditions. This

shows that the improvement is significant and the accuracy from following the trajectory is increased substantially. The model discrepancies of the multivariate model does not affect the performance too much, and since the model discrepancies are sufficiently small compared to the initial lack-of-fit residual they are easier to correct with the FB controller. In addition to a better tracking of the trajectory, the inclusion of the multivariate model in the FF also results in an increased energy efficiency.

The MVA of the experimental data resulted in two models that are proposed to reduce the estimation error of the initial model. The first model is proposed for implementation in the controller to give a more accurate estimation of the needed control input to follow the desired trajectory. The other model improves the initial model of the ferry to explains the dynamics with less error.

The results of this thesis shows that MVA can be used to model a lack-of-fit residual of dynamical systems and improve an initial model. The possibilities for future work include:

- Implement the proposed PLSR model in the actual motion controller of the ferry, and evaluate the performance.

- Investigate the possibilities of automating the process of improving the ferry model to compensate for long term changes in the dynamics. In particular, two things must be solved to be able to do this.

  - There must be an update condition that detects when the current model does not represent the dynamics of the ferry accurately any more and needs improvement.

  - In addition there must be an automated model selection that finds the optimal model, which is not necessarily the model with the least mean squared error (MSE) in cross validation.

- Include more sensors that can that can contribute with measurements of other factors affecting the ferry, e.g. wind force and load weight, and implement them in the MVA for a more accurate model.

- Explore if external disturbances can be estimated from the deviations of the PLSR model. The simulations showed that the PLSR was able to distinguish most of the constant disturbance and this could give valuable information about collected data.

Bibliography

J. Antony. *Design of Experiments for Engineers and Scientists (Second Edition)*. Elsevier, Oxford, second edition edition, 2014. ISBN 978-0-08-099417-8. doi: https://doi.org/10.1016/C2012-0-03558-2.

A.-L. Boulesteix and K. Strimmer. Partial least squares: a versatile tool for the analysis of high-dimensional genomic data. *Briefings in Bioinformatics*, 8(1):32–44, 05 2006. ISSN 1467-5463. doi: 10.1093/bib/bbl016.

R. Bro, K. Kjeldahl, A. Smilde, and H. Kiers. Cross-validation of component models: A critical look at current methods. *Analytical and bioanalytical chemistry*, 390:1241–51, 04 2008. doi: 10.1007/s00216-007-1790-1.

K. H. Esbensen, B. Swarbrick, and F. Westad. *Multivariate Data Analysis, An introduction to multivariate analysis*. CAMO, Inc, 01 2018.

T. I. Fossen. *Handbook of Marine Craft Hydrodynamics and Motion Control*. John Wiley and Sons, 2011.

S. Gale, H. Rahmati, J. T. Gravdahl, and H. Martens. Improvement of a robotic manipulator model based on multivariate residual modeling. *Frontiers in Robotics and AI*, 4:28, 2017. ISSN 2296-9144. doi: https://doi.org/10.3389/frobt.2017.00028.

T. Hastie, R. Tibshirani, and J. Friedman. *The Elements of Statistical Learning: Data Mining, Inference, and Prediction, Second Edition*. Springer, 02 2009. ISBN 0387848576.

M. Jervan. Parameter identification for adaptive control of autonomous passenger ferry. Specialization project report. Norwegian University of Science and Technology (NTNU), Trondheim, Norway. 2019.

H. Martens. The informative converse paradox: Windows into the unknown. *Chemometrics and Intelligent Laboratory Systems*, 107(1):124 – 138, 2011. ISSN 0169-7439. doi: https://doi.org/10.1016/j.chemolab.2011.02.007.

T. Mehmood, K. H. Liland, L. Snipen, and S. Sæbø. A review of variable selection methods in partial least squares regression. *Chemometrics and Intelligent Laboratory Systems*, 118:62 – 69, 2012. ISSN 0169-7439. doi: https://doi.org/10.1016/j.chemolab.2012.07.010.

A. A. Pedersen. Optimization based system identification for the milliampere ferry. Master's thesis, Norwegian University of Science and Technology (NTNU), Trondheim, Norway, 2019.

R. Skjetne, M. Sørensen, M. Breivik, S. Værnø, A. Brodtkorb, A. J. Sørensen, Ø. K. Kjerstad, V. Calabrò, and B. Vinje. Amos DP research cruise 2016: Academic full-scale testing of experimental dynamic positioning control algorithms onboard R/V Gunnerus. 06 2017. doi: 10.1115/OMAE2017-62045.

P. Stoica and Y. Selen. Model-order selection: a review of information criterion rules. *IEEE Signal Processing Magazine*, 21(4):36–47, 2004.

B. Sæther. Development and testing of navigation and motion control systems for milliampere. Master's thesis, Norwegian University of Science and Technology (NTNU), Trondheim, Norway, 2019.

M. E. N. Sørensen and M. Breivik. Comparing nonlinear adaptive motion controllers for marine surface vessels. *IFAC-PapersOnLine*, 48(16):291 – 298, 2015. ISSN 2405-8963. doi: https://doi.org/10.1016/j.ifacol.2015.10.295. 10th IFAC Conference on Manoeuvring and Control of Marine Craft MCMC 2015, Copenhagen, Denmark.

Tekna. Big data cybernetics, 2019, 2019. URL https://www.tekna.no/fag-og-nettverk/IKT/ikt-bloggen/stordata-kybernetikk/.

Yara. Yara Birkeland, 2020, 2020. URL https://www.yara.com/news-and-media/press-kits/yara-birkeland-press-kit/.

J. Yin, Z. Zou, and F. Xu. Parametric identification of Abkowitz model for ship manoeuvring motion by using partial least squares regression. *Journal of Offshore Mechanics and Arctic Engineering*, 137:3–11, 06 2015. doi: https://doi.org/10.1115/1.4029827.

Appendices

Appendix A

Parameters of the initial model

Table A.1: Estimated parameter values for the initial model of ferry (Pedersen, 2019).

Parameter	Estimated Value	Unit
m_{11}	2389.657	kg
m_{12}	0	kg
m_{13}	0	kg
m_{21}	0	kg
m_{22}	2533.911	kg
m_{23}	62.386	kg
m_{31}	0	kg
m_{32}	28.141	kg
m_{33}	5068.910	kgm^2
X_u	-27.632	kg/s
$X_{|u|u}$	-110.064	kg/s
X_{uuu}	-13.965	kg/s
Y_v	-52.947	kg/s
$Y_{|v|v}$	-116.486	kg/s
Y_{vvv}	-24.313	kg/s
$Y_{|r|v}$	-1540.383	kg/s
Y_r	24.732	kg/s
$Y_{|v|r}$	572.141	kg/s
$Y_{|r|r}$	-115.457	kg/s
N_v	3.524	kg/s
$N_{|v|v}$	-0.832	kg/s
$N_{|r|v}$	336.827	kg/s
N_r	-122.860	kg/s
$N_{|r|r}$	-874.428	kg/s
N_{rrr}	0.000	kg/s
$N_{|v|r}$	-121.957	kg/s

Magnus Jervan

Improvement of an Autonomous Passenger Ferry Model Based on Multivariate Residual Modeling

NTNU
Norwegian University of
Science and Technology